

AN ABSTRACT OF THE DISSERTATION OF

Adam Mate for the degree of Doctor of Philosophy in Electrical and Computer Engineering presented on May 5, 2020.

Title: A Generation Prioritization Method for Power System Restoration with Renewable Resources

Abstract approved: _____

Eduardo J. Cotilla-Sanchez

The electrical grid is a key component of the Nation's critical infrastructure. Its continuous and reliable operation is of vital importance; any system-wide disruption would have a debilitating impact on crucial services, public health and safety, the economy, and the national security of the United States. High-impact low-frequency events pose the greatest threat to the grid due to their severity and unpredictability; these may be caused by naturally occurring hazards (e.g., earthquakes, solar storms, extreme weather conditions) or acts of human volition (e.g., malicious cyber-, or coordinated set of physical attacks). To improve the resilience of the grid against such threats and enhance the protection of the critical infrastructure, this research examines ways in which power system restoration processes are considerably accelerated. A new generation prioritization method is proposed for time-sensitive system restorations, which significantly shortens the total restoration times. To achieve this, available renewable generation is leveraged and an algorithm is developed that plans the optimal operational schedule of the system close to real time. Benchmarking and validation experiments are performed on test systems modeled after the electrical grid of the U.S. Pacific Northwest, and prove that this convenient toolset supports a quick recovery, faster than other common approaches.

©Copyright by Adam Mate
May 5, 2020
All Rights Reserved

A Generation Prioritization Method for Power System Restoration
with Renewable Resources

by

Adam Mate

A DISSERTATION

submitted to

Oregon State University

in partial fulfillment of
the requirements for the
degree of

Doctor of Philosophy

Presented May 5, 2020
Commencement June 2020

Doctor of Philosophy dissertation of Adam Mate presented on May 5, 2020.

APPROVED:

Major Professor, representing Electrical and Computer Engineering

Head of the School of Electrical Engineering and Computer Science

Dean of the Graduate School

I understand that my dissertation will become part of the permanent collection of Oregon State University libraries. My signature below authorizes release of my dissertation to any reader upon request.

Adam Mate, Author

ACKNOWLEDGEMENTS

I express sincere appreciation to all those who helped the making of this dissertation. This includes advisor, mentors, colleagues, family, and friends. Special recognitions to:

Advisor Dr. Eduardo J. Cotilla-Sanchez, for his guidance and support throughout the past years. I am grateful for the opportunity that I got to learn from and work together with him on solving challenging engineering problems. And I am thankful for his many advice in both personal and professional areas of my life.

Mentor Dr. Arthur K. Barnes, at Los Alamos National Laboratory, for his professional guidance and assistance in the creation of the RTS-GMLC-GIC test system and the performance of GMD studies using PowerModelsGMD.jl.

Colleagues Dr. Adam Schultz and Dr. Naoto Imamura, in the College of Earth, Ocean, and Atmospheric Sciences at Oregon State University, for their assistance in the induced dc voltage calculations of the Halloween GMD event.

Mother Eva Matene Kovacs, father Zsolt Mate, and brother David Mate, for their love, support, and constant encouragement throughout the years.

Los Alamos National Laboratory mentors and colleagues, for the Curricular Practical Training internship opportunity. I am grateful for the seven months I got to spend in Los Alamos NM with learning, exploring, and being professionally inspired.

CONTRIBUTION OF AUTHORS

Materials from this dissertation have been published in the following form:

[1]: A. Mate, T. Hagan, E. Cotilla-Sanchez, T. K. A. Brekken, and A. von Joanne, “Impacts of Earthquakes on Electrical Grid Resilience,” Proceedings of the 2021 IEEE/IAS 57th Industrial and Commercial Power Systems Technical Conference, pp. 1–5, Apr. 2021.

and

[2]: A. Mate, A. K. Barnes, R. W. Bent, and E. Cotilla-Sanchez, “Analyzing and Mitigating the Impacts of GMD and EMP Events on the Electrical Grid with PowerModelsGMD.jl,” Technical Report, arXiv:2101.05042 [eess.SY], pp. 1–9, Apr. 2021. LA-UR-19-29623.

and

[3]: P. Cicilio, D. Glennon, A. Mate, A. Barnes, V. Chalishazar, E. Cotilla-Sanchez, B. Vaagensmith, J. Gentle, C. Rieger, and R. Wies, M. H. Kapourchali, “Resilience in an Evolving Electrical Grid,” Multidisciplinary Digital Publishing Institute – Energies – Special Issue: Advances in Methods and Metrics for Power Systems, from Reliability to Resilience, vol. 14, no. .3, pp. 1–25, Jan. 2021. LA-UR-20-29808.

and

[4]: A. Schultz, S. Murphy, E. Cotilla-Sanchez, N. Imamura, A. Mate, and A. Barnes, “Fusing Magnetotelluric, Magnetic Observatory and Power Grid Sensor Data with Real-Time Power Flow Analysis,” Technical Presentation at the American Geophysical Union 2019 Fall Meeting, Dec. 2019.

and

[5]: A. Mate and E. Cotilla-Sanchez, “Rapid Method for Generation Prioritization during System Restoration with Renewable Resources,” Proceedings of the 2019 IEEE/IAS 55th Industrial and Commercial Power Systems Technical Conference, pp. 1–8, Jun. 2019.

TABLE OF CONTENTS

	<u>Page</u>
1 General Introduction	1
1.1 Motivation	1
1.2 Background	4
1.3 Formed Hypotheses	8
2 Case Study Datasets	9
2.1 RTS-GMLC	10
2.2 RTS-GMLC-GIC	12
3 Dataset Customization	17
3.1 Identification Numbers	17
3.2 Asset States	18
3.3 Power Demand Profiles	19
3.4 Energy Portfolio	20
3.5 Reactive Power Generation	24
3.6 System Topology	27
3.7 Operational Details	28
4 Prioritization of System Assets	30
4.1 Demand Prioritization	30
4.2 Generation Prioritization	31
4.3 Priority List Unit Commitment	33
4.4 Mixed-Integer Linear Programming Unit Commitment	37
5 Proposed Generation Prioritization Method	38
5.1 Generation Participation Weight	38
5.2 Universal Selection Scheme	42
6 Properties of Case Studies	45
6.1 Simulation Process Structure	45
6.2 Testing Environment	50
6.3 Priority List Comparison	51
6.4 Benchmarking Case Studies	52
7 Method Validation Experiments	58
7.1 Ranking Generating Units	58
7.2 Normal System Operation	61

TABLE OF CONTENTS (Continued)

	<u>Page</u>
7.3 Cascadia Subduction Zone Event	63
7.4 Geomagnetic Disturbance Event	65
8 Conclusion	67
8.1 Evaluation of Results	67
8.2 Performance Scalability	67
Bibliography	69
Appendices	84

LIST OF FIGURES

Figure		Page
1.1	Schematic view of the tectonic plates in the CSZ area [6]	4
1.2	The space weather environment [7]	7
2.1	Network layout of RTS-GMLC, annotated with the relative size and location of generation capacity [8]	11
2.2	One-line diagram of RTS-GMLC	12
2.3	Formulation of equivalent dc network [9]	14
2.4	Modified location of generating units in RTS-GMLC-GIC	15
2.5	Characteristics of the RTS-GMLC-GIC test case [10]	16
5.1	Block diagram of the two-level USS method	42
5.2	USS method decision making – conventional generating units	43
5.3	Second level of the USS method – <i>Step I</i>	43
5.4	Second level of the USS method – <i>Step II</i>	44
5.5	Second level of the USS method – <i>Step III</i>	44
6.1	Improved power demand profiles of RTS-GMLC on May 5th	46
6.2	Improved reactive power demand of each system area on May 5th	47
6.3	Energy portfolio of RTS-GMLC	47
6.4	Energy portfolio of RTS-GMLC on May 8th, 12pm	48
6.5	Modified energy portfolio of RTS-GMLC	49
6.6	One-line diagram of RTS-GMLC – CSZ event restoration timeline	54
6.7	One-line diagram of RTS-GMLC-GIC – Most intense hour of the Halloween storm GMD event	56
6.8	One-line diagram of RTS-GMLC-GIC – Intensified evening of the Halloween storm GMD event	57
7.1	Ranked lists of conventional generating units	58
7.2	Comparison of PL methods – <i>Option 1</i> . renewable portfolio	59

LIST OF FIGURES (Continued)

<u>Figure</u>		<u>Page</u>
7.3	Comparison of PL methods – <i>Option 2.</i> renewable portfolio	60
7.4	Comparison of generation prioritization methods – normal operation, <i>Option 2.</i> renewable portfolio	62
7.5	Comparison of MILP UC and USS methods – normal operation, variable renewable portfolio	63
7.6	Comparison of generation prioritization methods – CSZ event, <i>Option 2.</i> renewable portfolio	64
7.7	Comparison of MILP UC and USS methods – CSZ event, <i>Option 4.</i> renewable portfolio	65
7.8	Comparison of generation prioritization methods – Most intense hour of the Halloween storm GMD event, <i>Option 2.</i> renewable portfolio	66
7.9	Comparison of generation prioritization methods – Intensified evening of the Halloween storm GMD event, <i>Option 2.</i> renewable portfolio	66
8.1	Performance of the USS method depending on the number of generating units	68
8.2	Performance scalability of the USS method	68

LIST OF TABLES

<u>Table</u>		<u>Page</u>
3.1	Predicted 2020 energy portfolio of the PNW	23
3.2	Implemented renewable portfolio options	23
4.1	Attributes of PL approaches	33
4.2	Attributes of MILP UC approaches	37
5.1	Attributes of the GPW index based USS method	38
5.2	Determination of $MP-P$ and $MP-Q$ values	41

NOMENCLATURE

ANN: artificial neural networks based UC
ANSI: Advanced Network Science Initiative at LANL
APF: Area Participation Factor factor
ARPA-E: Advanced Research Projects Agency - Energy of the U.S. DOE
CEOAS: the College of Earth, Ocean, and Atmospheric Sciences at OSU
COE: the College of Engineering at OSU
CSV: comma-separated values file
CSZ: Cascadia Subduction Zone
DOE: the U.S. Department of Energy
DP: dynamic programming based UC
EE: exhaustive enumeration based UC
EIA: Energy Information Administration of the U.S. DOE
ES: expert systems based UC
EP: evolutionary programming based UC
FL: fuzzy logic based UC
GA: genetic algorithm based UC
GEF: geoelectric field
GIC: geomagnetically induced current
GMD: geomagnetic disturbance
GMI: Grid Modernization Initiative of the U.S. DOE
GMLC: Grid Modernization Laboratory Consortium of the U.S. DOE
GPW: Generation Participation Weight index
GRID DATA: Generating Realistic Information for the Development of Distribution and Transmission Algorithms program of the U.S. DOE ARPA-E
GSU: generator step-up transformers
HILF: High-impact low-frequency event
IEEE: Institute of Electrical and Electronics Engineers
IEEE PES: IEEE Power Energy Society
IPL: Improved Priority List
LANL: Los Alamos National Laboratory
LR: Lagrangian relaxation based UC
MIP: mixed-integer programming
MILP: mixed-integer linear programming based UC
MP: Maximum Power factor
MPL: Modified Priority List

NOMENCLATURE (Continued)

NPCC: Northwest Power and Conservation Council

NPL: New Priority List

NREL: National Renewable Energy Laboratory

OPF: optimal power flow study

OSU: Oregon State University

PF: power flow study

PL: priority list based UC

PMsGMD: PowerModelsGMD.jl software

PNW: the U.S. Pacific Northwest region

PS: Previous State factor

PSO: particle swarm optimization based UC

RPS: Renewable Portfolio Standards

RTS-79: 1979 IEEE Reliability Test System

RTS-96: 1996 IEEE Reliability Test System

RTS-GMLC: IEEE Reliability Test System of the Grid Modernization Laboratory Consortium

SOC: Simplified Operating Cost factor

sync-cond: synchronous condenser

UC: unit commitment

US: the United States

USS: Universal Selection Scheme method

xfmr: transformer

Chapter 1: General Introduction

High-impact low-frequency (HILF) events [11] present the greatest threat to the bulk power system, a key component of the United States' (US) critical infrastructures [12]. Even though such events rarely occur – or, in some cases, have never occurred – they have the potential to cause catastrophic impacts: unpredictable system-wide disruptions and severe long-term damage in generation, transmission and distribution networks; endangering the continuous and reliable operation of the entire electrical grid [11,13]. Examples of HILF risks include major natural disasters (e.g., earthquakes, tsunamis, extreme weather conditions, pandemics, geomagnetic disturbances) and acts of human volition (e.g., coordinated cyber-, physical-, and blended attacks, and high-altitude detonation of nuclear weapons). HILF events transcend other risks to the electrical sector due to their magnitude of impact and the relatively limited operational experience in addressing them [11,14,15].

The U.S. Pacific Northwest (PNW) region faces complex and devastating HILF disaster scenarios (see Section 1.2). An imminent Cascadia Subduction Zone (CSZ) megathrust earthquake [16], yielding the creation of a powerful tsunami, hundreds of aftershocks and increased volcanic activity. A severe geomagnetic disturbance (GMD) caused by intense solar activity [17] – due to the high latitude geographical location of the region – resulting in extreme stress on the transmission network and its numerous assets.

In order to prepare for these events, and later be able to successfully cope with their consequences, the resilience of the electrical grid must be improved [18,19]. One way to do that is through shortening recovery times; quick (but also reliable) restoration is important, not just following HILF events, as it results in prevented life-loss and avoided economic-loss. This research, consequently, examines ways to considerably accelerate power system restoration processes, focusing on the operational schedule determination sub-task. After discussing the motivations (see Section 1.1) and relevant backgrounds (see Section 1.2) of this work, a new generation prioritization method is proposed for time-sensitive system restorations; this serves as the basis of the two dissertation hypotheses (see Section 1.3).

1.1 Motivation

Power system restoration is one of the five stages of power system operation. The system is in an abnormal status, and characterizable with: partial or complete collapse of the electrical grid, widespread unserved loads and disconnected assets (including generating units, transformers, transmission and distribution lines, and protection devices), severely

disrupted communication network, and many more [20–22]. It is a complex process, in which the objective is to restore the system to normal operation as quickly as it may be consistent with system-security, while at the same time minimizing the amount of unserved demand and diminishing adverse impacts on the society [21, 23].

Prepared restoration strategies determine the manner in which various tasks are coordinated, and the sequence in which they are executed. These are designed as general guidelines, i.e., to be flexible in application and adaptable to anticipated scenarios. The exact group of tasks depend on the system involved and the exact circumstances; not all tasks are always carried out, or not necessarily in the same sequence [24, 25]. A number of tools have been developed over the years to support planning and decision making [26–29].

The major tasks throughout the restorative stage of power system operation are the following [30–33]:

- status identification: information gathering; assessment of the system and the statuses of its assets
- communication and coordination (with affected transmission operators, balancing authorities, generation operators, reliability coordinators)
- determination of a restoration plan (tailored to prevailing conditions): definition of the *target power system*
- preparation of system (generating units for startup, and network for re-energization)
- implementation of the restoration plan: re-energize network; coordinate power generation and demand; synchronize sub-networks (existing islands); establish interconnections with neighboring networks
- return to normal operation: restoration is complete when the *target power system* configuration is reached

A key step in any restoration process is the determination of an operational schedule for all available generating units – those that, during and following a HILF event, remained intact or are already restored – to enable the execution of prepared system restoration plans. HILF events present a unique, particularly challenging threat, which requires special considerations throughout this step [34–36].

By nature, HILF events affect vast areas and result in extensive destruction: probable damage in all levels of power systems (i.e., generation, transmission, and distribution levels), in the supporting infrastructure (such as operation centers, access roads, power supply, etc.), and in the communication system. Reduced visibility greatly limits available information: data about the system-state (online parts of the system, or the exact status of certain assets) is often unavailable or not accurate; in case of malicious attacks, straight-up untrustable. The restoration process itself is extremely time-sensitive: it is critical to be completed in a minimal amount of time, as quick action results in prevented life-loss and

avoided economic-loss; any delay may result in tragic consequences. However, due to the degraded system-state, many resources are unavailable to quickly restore the system.

Common unit commitment approaches (see Section 4.2), which determine operational schedules during normal system operation, are not adequate in these situations. Depending on integrated modeling details and solution technique, they might take an extended amount of time to find realistic and/or optimal schedules. The data required for decision-making is often unavailable, presenting a barrier in their usability. In addition, they are not necessarily suitable for modern power systems with significant renewable penetrations, and likely under-perform or simply fail in such environment. Consequently it is unequivocal that a novel approach is needed to tackle prevailing challenges: a generation prioritization method designed for power system restorations.

Most renewable generating units – hereinafter *hydro*, *wind*, and *solar* energy resource categorizes are differentiated [37] – are able to withstand HILF threats quite well; remarkably better than traditional ones [38]. Early efforts have been made to take advantage of their ability to quickly respond to and recover from an extreme event: a handful of works explored and discuss the application possibilities of renewables as blackstart units during restoration, and – in general – their increased use in system restoration processes [39–45]. Nevertheless, this advancement in power system operation is not a common practice today; shortening system recovery times, however, would not only result in saved expenses, but importantly in saved lives as well.

To sum up the desired goal to achieve: A way to determine an operational schedule for all generating units, in each moment of a power system restoration process, which is

- fast (faster than alternative approaches) yet simple enough to be a prudent choice
 - relies on less and more simple data, which can be collected quicker, especially when computational capability is limited or temporarily non-existent
 - simple, so easy to understand and use, even for those unfamiliar folk
- takes advantage of readily available renewable generation, which – by itself – accelerate restoration time-frames and thus improve system resilience
 - due to the fact that renewables withstand HILF events quite well
 - nowadays - with appropriate planning – renewables are forecastable

HILF events are inevitable: it is just a matter of time when the next occurs, such as disaster scenarios presented in Section 1.2. It is time to get ready, to educate our communities, and to prepare protocols and useful toolsets aimed to mitigate expected consequences. Increasing the resilience of the bulk power system, via shortening recovery times after an occurred catastrophe, is of the utmost importance; summary of relevant knowledge and a proposed elegant solution to the discussed problem is one way to do that.

1.2 Background

The Cascadia Subduction Zone

The CSZ is an approximately 600 miles long offshore fault, which lies in the coastal region of the PNW, stretching from Cape Mendocino in northern California – through the States of Oregon and Washington – to the Brooks Peninsula in southern British Columbia, Canada [6,16,46–48]. The fault is part of a great arc of subduction zones that surrounds the Pacific Ocean, creating a formation called the “Ring of Fire,” and is a geologic mirror image of the subduction zone lying east of Japan. Since the 1980s, when researchers recognized it as an active fault, the scientific community has been aware of the major geological hazard that the region faces: the possibility of a tremendous earthquake and tsunami caused by this fault, which can strike at any moment and can cause enormous destruction [16].

In the CSZ, three denser oceanic tectonic plates (namely the Explorer, Juan de Fuca, and Gorda plates) are sliding from west to east and subducting beneath the less dense continental plate (North American plate) that moves in a general southwest direction, overriding the oceanic plates. The movement of these plates is neither constant nor smooth: the plates stick, building stress until the fault suddenly breaks and releases the accumulated energy in the form of an earthquake(s) [47]. Thereafter, the plates start moving again, and continue to move, until getting stuck again.

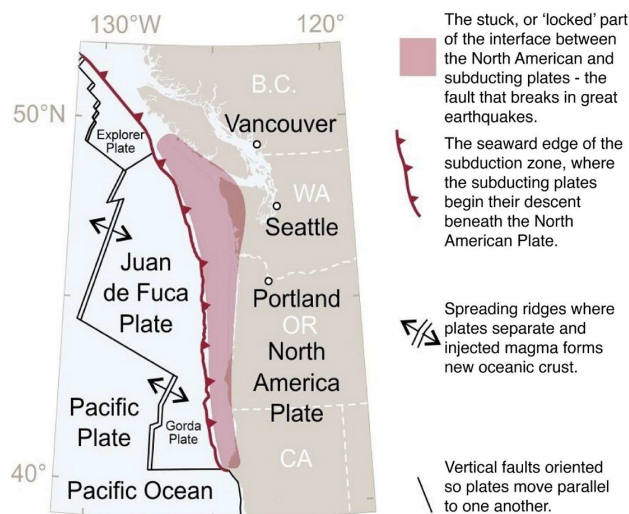


Figure 1.1: Schematic view of the tectonic plates in the CSZ area [6]

There is no doubt that another subduction earthquake will strike the PNW in the future. In the last decade, research has confirmed that the CSZ has a long history of great earthquakes. The most recent happened on January 26, 1700, creating a magnitude 9.0

earthquake followed within minutes by a large tsunami. Energy for the next earthquake is currently building up along the fault, and has been since the last earthquake [6,16,47]. The time interval between previous CSZ events varied from a few decades to many centuries, but most intervals were shorter than the time elapsed since the last event in 1700 [16]. The calculated odds that the next earthquake will occur in the next 50 years range from 7-15% for a “great” earthquake affecting the entire PNW to about 37% for a “very large” earthquake affecting southern Oregon and northern California [6,16,46–48].

Geologists assembled a ten-thousand-year record of past events, by studying sediments in coastal marshes and on the ocean floor. This shows that half of the past earthquakes have been “very large” (estimated magnitude of 8.3 to 8.6) and centered on the southern Oregon coast, while the other half have been “great” (estimated magnitude 8.7 to 9.3) and extended along the full length of the fault [16]. Although it is possible that the next earthquake(s) will be a partial rupture of the fault, section by section, in a series of large events over a period of years, it is strongly anticipated by many scientists that it will be similar to the last event in 1700, and will be the result of the entire fault rupturing, causing one great earthquake measuring magnitude 9.0, with ground shaking lasting 4-6 minutes [6,47].

Earthquake Resilience in Oregon

After the discovery of the major threat, the rate of change to increase Oregon’s resilience has been slow. The first-time that explicit seismic provisions were adopted in Oregon’s building codes was in 1993 [16,49]. Only following the 2011 Tohoku, Japan earthquake and tsunami disaster, was special attention given to the CSZ threat at the state governmental level. The Oregon Seismic Safety Policy Advisory Commission, with the help of more than 150 volunteer professionals, prepared the Oregon Resilience Plan in 2013 [16]. This plan was the first comprehensive study and had the following goals: assess the state of resilience in Oregon, plan for the impacts of a CSZ event, and map a path of policy and investment priorities for the next fifty years. Up until today, two CSZ earthquake scenario documents have been created, [47] and [6] (with multiple versions), with the goal to provide information for the public on the hazards the PNW faces.

These three studies [6,16,47] identified the following key findings on the current state of resilience of Oregon’s electrical grid:

- Electrical facilities and network components – including power plants, substations, transmission lines – are seismically vulnerable to damage and have significant risk due to ground shaking and ground failure, especially landslides, soil liquefaction, lateral spreading and coastal subsidence hazards.
- Most of Oregon’s critical and non-critical energy infrastructure has been constructed with seismic design deficiencies, and not initially built to with-stand earthquakes.

Substantial improvements, investments, and a uniform set of design and construction codes are needed to minimize extensive direct earthquake damage, indirect losses, and possible ripple effects.

- A CSZ event will cause the failure of numerous power system components, and over half of the region’s electrical grid may suffer medium to high damage on all grid-levels. Outages and blackouts may occur not only within 100 miles of the coastline, but even in areas that were not directly affected by the earthquake. The destruction on the coastal areas may be severe enough as to render the equipment and structures irreparable. In the I-5 corridor, considerable damage on generation and distribution levels may result in the loss of over half of the system’s capacity.
- Oregon’s liquid fuel supply is extremely vulnerable. Besides the high dependency on Washington State – more than 90% of Oregon’s refined petroleum products come from the Puget Sound area, which is also vulnerable to a CSZ earthquake – the storage facilities along Oregon’s Willamette River lie on liquefiable riverside soils. This significantly affects most sectors of the economy critical to emergency response and economic recovery.
- Estimated restoration time of electrical grid after a CSZ event ranges from 1-3 months (in the Willamette Valley) to 3-6 months (Coastal region), depending on the degree of destruction, available utility personnel, contractors and road conditions.

The PNW, and specifically Oregon, is prone to earthquakes, just like all other regions inside the Pacific Ring of Fire. Even though small steps – conducted studies, funded research, legislative changes — have been taken in the recent years to start and accelerate the needed change in this issue, Oregon’s electrical grid today is still far from resilient to the impacts of a CSZ event.

Geomagnetic Disturbances

GMDs are driven by severe space weather: mainly, large solar flares and associated coronal mass ejections during solar maximums, and co-rotating interaction regions (high-speed solar winds) during solar minimums. Charged and magnetized particles are being blown away from the Sun, which then interact with and perturb the Earth’s magnetic field, bringing about rapid short-term variations in its configuration [50, 51]. The created low-frequency geoelectric fields (0.1 [mHz] – 1 [Hz]) over the surface of the affected region generate geomagnetically induced currents (GICs) at the surface. These quasi-dc currents – which depend on the rate of change of magnetic field experienced at a location, and the deep earth conductivity at that location – appear in the conductive infrastructure and flow into the high-voltage network through the neutrals of transformers [51–54].

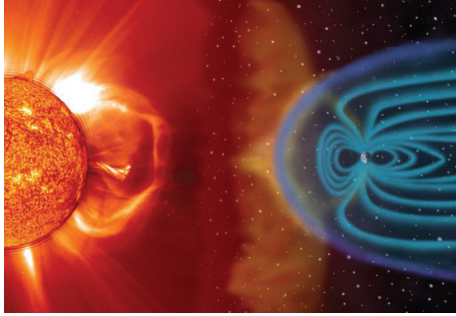


Figure 1.2: The space weather environment [7]

GICs may adversely impact power transmission systems and equipment, as they are superimposed on the ac currents, consequently increasing the maximum currents throughout the entire system. They have the potential to induce harmonics by causing half-cycle saturation in transformers, which may lead to the misoperation of protection devices causing system relay interference and tripping of over-current relays. Premature aging, lasting damage or complete failure of large high-voltage transformers due to overheating and thermal degradation is also a great threat. The increased reactive power consumption caused by the circulating GICs in the network may lead to the loss of reactive power support and to voltage collapses. In the worst case, widespread infrastructure damage and tripping of transmission lines may lead to cascading failures and extended power disruptions [55–59].

Understanding and mitigating the impacts of GMDs on power systems has been a subject of research for many years now. There have been significant improvements in GIC modeling and monitoring both in regulatory level and in the electric power industry [7, 57, 59–62]. Efforts have been made to include GIC related analysis in power system simulation [63–66]; as of today, a handful of commercial software solutions provide modeling and analysis capabilities, such as MATLAB[®] based MATGMD [67], PowerWorld[®]'s GIC add-on [68], and PSS[®]E's GIC module [69]. Regarding mitigation, the current main approach is reducing transformer reactive power consumption with dc-current blocking devices; installation of such devices, however, is very expensive, even if they are selectively and strategically placed by optimization algorithms [56, 57, 70–72]. Another approach would be limiting transformer heating caused by GICs, however, current research is limited in this area [73, 74].

The first comprehensive, in every aspect accessible and open-source software for both analyzing and mitigating the impacts of GMDs is PowerModelsGMD.jl (PMsGMD) [2]. PMsGMD is a Julia [75] package, an extension to the PowerModels.jl framework [76] developed by the Advanced Network Science Initiative (ANSI) at Los Alamos National Laboratory (LANL). It was designed to be an easy-to-handle and customizable toolkit, which evaluates the risks of GICs, and also provides mitigation strategies by treating the transformer overheating problem as an optimal transmission switching formulation.

1.3 Formed Hypotheses

General wisdom that complicated solutions have a tendency to waste money and only create more problems; simple, thoughtful solutions that cut through complexity are the only way to move forward. This dissertation proposes a simple, elegant solution to the problem of determining operational schedules for generating units in restoration processes during and following HILF disasters.

The presented generation prioritization method – starting with available renewable generating units then lowering priority to conventional units – conveniently supports power system restoration processes. As it was specifically designed for real-life power systems – with modern generation and load profiles, and mid- to high-level renewable penetrations – the planned operational schedules are well-balanced and optimal, in which the fulfillment of power demands are maximized at every movement. In the light of all these, the following two hypotheses are formed and proven in this research:

Hypothesis I.

In electric power systems with significant renewable penetration, the proposed Generation Participation Weight index is more adequate, relative to common approaches, to characterize the importance of generating units in any given system state.

Hypotheses II.

In electric power systems with significant renewable penetration, during time-sensitive system restoration, the proposed (GPW index based) Universal Selection Scheme method is a faster, more adequate technique to determine the optimal operational schedule of generating units, than common approaches.

Chapter 2: Case Study Datasets

The power systems research community greatly relies on network models to explore and study a wide range of (current and future) operating conditions, and to compare, evaluate and validate developed tools, algorithms and techniques. Due to the sensitive nature of such data, detailed real-world models are hard to obtain, even under non-disclosure agreements. As a result, researchers are forced to use fictitious test cases that mimic existing infrastructure. These, however, are often designed for a specific purpose and not for general use, sometimes outdated and far-from-realistic representations of power systems, lacking important characteristics and key network parameters.

Over the years there have been efforts to collect frequently used test cases into databases and archives, while at the same time improve them through reconstruction and completion. Datasets are typically available in a variety of different formats: often the IEEE Common Data Format [77] or the MATPOWER case format [78], PowerWorld[®] Simulator format [68], and PSS[®]E format [69]. The transition between different formats usually happens through a Comma-Separated Values (CSV) source file.

Arguably, the most commonly used open format today is the MATPOWER (file extension “.m”) case format; a significant number of networks have been curated in this format, and also many are distributed within the MATPOWER research platform [78]. Several universities have created notable test case archives for purposes of research and education; e.g. the University of Washington [79], the University of Illinois [80], the University of Edinburgh [81], and the University of Cyprus [82]. The NICTA Energy Systems Test Case Archive [83], and its successor, the Institute of Electrical and Electronics Engineers (IEEE) Power & Energy Society (IEEE PES) Power Grid Library (PGLib-OPF) [84, 85] are both comprehensive collections of AC transmission network models that were primarily designed to enable power flow optimization benchmarking studies.

To remedy the shortage of modern AC power system network models and data, the U.S. Department of Energy’s (DOE) Advanced Research Projects Agency - Energy (ARPA-E) has been funding the Generating Realistic Information for the Development of Distribution and Transmission Algorithms (GRID DATA) program [86]. A number of new synthetic test cases has been generated, which are designed to be statistically and functionally similar to real-world electrical grids, while containing no confidential critical energy infrastructure information. Several such cases are available through the Experiment Station of the Texas A&M University [87].

A test case is appropriate for the purposes of this research if it meets the following two criteria. First, it must be representative of modern power systems: realistic system-characteristics with up-to-date parameters and limits; inclusion of both conventional and renewable generating units, using modern fleet and generation mix; openly accessible and version-controlled dataset. Second, its associated dataset must have timeseries data for generations and consumptions, which enables long-run simulation processes. Based on these criteria, the IEEE Reliability Test System of the Grid Modernization Laboratory Consortium (RTS-GMLC) [88] (see Section 2.1) test case, and its extended version that allows GMD studies, the RTS-GMLC-GIC (see Section 2.2) test case, and their associated dataset are used in this research.

2.1 RTS-GMLC

The IEEE Reliability Test System (RTS) has been a key tool for many decades both in academic and industry research. It was developed to provide a standardized platform for studying power system operations strategies and issues. The first version was published in 1979 (RTS-79) [89], and since then it has undergone several modifications, with the most recent update being issued in 1996 (RTS-96) [90]. In order to continue serving as a commonly used model for testing and comparing results, its modernization was necessary; RTS has grown outdated and not representative of modern power systems or the complex challenges posed by their operation [8].

As part of the DOE’s Grid Modernization Initiative (GMI) [91], the Grid Modernization Laboratory Consortium (GMLC) [92], a strategic partnership between the DOE and U.S. national laboratories, has modernized the RTS test system. The dataset of the 2019 RTS, also known as RTS-GMLC, is provided by the National Renewable Energy Laboratory (NREL) and publicly accessible via a GitHub repository [88].

RTS-GMLC meets all expectations desired from a modern 21st century test case. It reflects the changes of the past two decades in power system composition, allows to examine challenges and opportunities of new generation sources, and enable the analysis of various contemporary operational issues. Just as earlier RTS versions, it is not aimed to represent a specific, real-life power system, but rather to be representative of technologies and configurations that could be encountered in any power system. [8, 93]

Numerous critical updates to the RTS-96 were implemented in RTS-GMLC to fix shortcomings and add improvements [8, 93]:

- Created relative node locations based on line distances to enable network geo-location. Assigned the system to an arbitrary geographical location in the southwestern U.S.
- Enabled the simulation of hourly and 5-minute operations for a year: from Jan. 1st to Dec. 31st, 2020. Added temporal variability in the form of 5-minute load, wind

and solar data; each with a corresponding hourly time series representing day-ahead forecasts based on weather patterns experienced in the selected region.

- Revised and improved the transmission system. Introduced a generation mix more representative of modern power systems.
- Modernized the sources of generation by adding natural gas (combustion turbine and combined-cycle), wind, solar (photovoltaic, rooftop photovoltaic, and concentrated solar power), and energy storage to the model. Added new generation profiles, updated heat rates, and introduced production cost models.

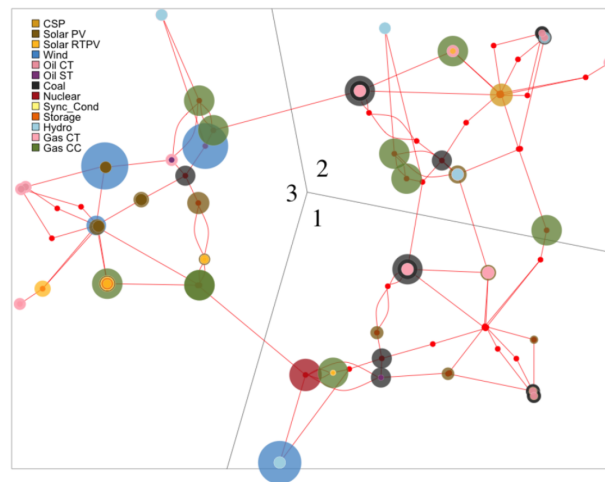


Figure 2.1: Network layout of RTS-GMLC, annotated with the relative size and location of generation capacity [8]

The base RTS-GMLC case represents a peak load flow state, with (by default) disconnected wind and solar generations. The system is built up of:

- 3 interconnected areas, each of which consisting 7 subareas respectively. Area 1 is associated with the California-Arizona border region; Area 2 is associated with the southern Nevada region; and Area 3 is associated with the Los Angeles and its suburban areas region.
- 73 buses equally divided among the areas (24-24-25 in each area respectively).
- 158 generating units: 73 conventional (1 nuclear, 10 CC combined-cycle gas, 27 CT combustion turbine gas, 12 CT combustion turbine oil, 7 ST steam turbine oil, and 16 coal) and 81 renewable units (20 hydro, 4 wind, 1 CSP concentrated solar power, 25 PV utility solar photovoltaic, and 31 RTPV rooftop solar photovoltaic). Additionally, 3 synchronous condensers (1 in each area), and 1 disconnected storage unit (in Area 3). Total active power generation is minimum 3,775 [MW] and maximum 14,549.8 [MW]; total reactive power generation is minimum -1,615 [MVar] and maximum 4,406 [MVar].

- 100 HVAC transmission lines equally divided among the areas (33-33-34 in each area respectively), 5 HVAC transmission lines connecting individual areas (3 between Area 1 and Area 2, 1 between Area 2 and Area 3, and 1 between Area 1 and Area 3), and 1 HVDC transmission line (between Area 1 and Area 3). Additionally, each area contains 5 high-voltage transformers (xfmr) that are connecting the 138 [kV] and 230 [kV] voltage levels of the system.
- 51 loads (consumers) equally divided among the areas (17-17-17 in each area respectively). Total active load is 8,550 [MW] and total reactive load is 1,740 [MVar].

The set case-values of system components are based on the RTS-96 case-values, and do not correspond to any given value of the 2020 year. Forecasted hourly and 5-minute data are available for the active power generations of hydro, wind, and solar units, and for the active power demands of the system. Data are not provided for the reactive power generations and demands, conventional generating units, synchronous condensers, and the storage unit.

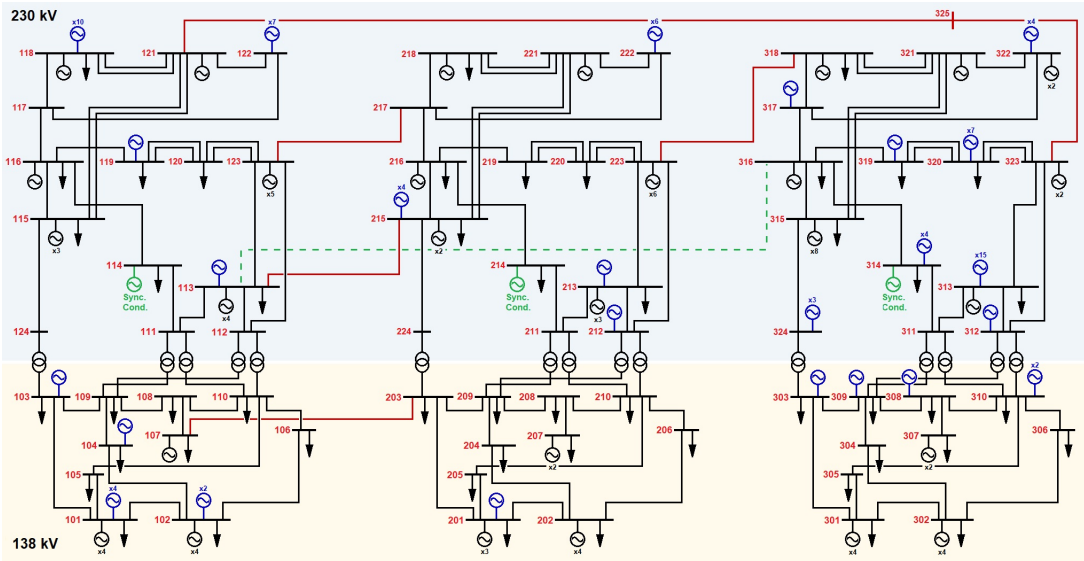


Figure 2.2: One-line diagram of RTS-GMLC

2.2 RTS-GMLC-GIC

Even though RTS-GMLC is a general-purpose test case, by design, it does not allow the performance of GMD studies. To enable the time-domain simulation of the impacts of GICs on the model, the RTS-GMLC-GIC extended test case has been developed. In the following, the details of modeling are discussed, and RTS-GMLC-GIC is introduced.

Modeling Geomagnetic Disturbances

Modeling aims to accurately simulate the impacts of GMDs, consequently determining and analyzing the exact threat from GICs at any location and time in a power system. In this complex process, the level of detail required to model a particular system is more than what is needed in- and provided for a traditional positive-sequence simulation [60].

A GMD is essentially a temporal variation in the magnetic field of the Earth (see Section 1.2); it induces a slow varying potential, known as geoelectric field (GEF), on the Earth's surface [94]. GICs, driven by GEFs, depend on the interplay between a number of factors that all need to be considered in modeling: grid topology and configuration (geographical location of substations, resistance of assets, characteristics of transformers), geomagnetic source fields (amplitude, frequency content, and spatial characteristics), and electrical conductivity structure of the Earth's crust and mantle (modeling method, substation grounding resistance, influence on GEFs).

The foundations of modeling have been laid out over the years [58,95–99]. Early models only comprised transmission lines at the highest voltage level, and single resistances representing the combined paths to ground through each substation. Often a fixed, uniform GEF was used; a uniform field is a useful simplifying assumption in many cases, however, it does not have the same properties as realistic GEFs, it is a mathematical oddity [51].

GIC calculations today involve transmission lines at different voltage levels, the resistances of individual transformers, and detailed characteristics of the geomagnetic fields and the Earth's conductivity structure [51,94]. Importantly, the availability of required type of data has remained a challenge: verifiable information on the threat and detailed description of the system is needed for accurate results, but often are not easy to obtain [95].

To efficiently simulate the induced GICs in large power systems, the modeled network needs to be converted to- and described as a network of admittance [51,94,100,101]. Since the impedances of each phase of the system are identical – i.e., phase conductors (transmission lines and transformer windings in each phase) provide identical parallel paths for GIC flows – the calculation of GICs can be performed for a single phase only, and the same result applies to all phases. This is often done by combining the parallel paths of all three phases to produce an equivalent circuit for calculating the total GIC in all three phases.

Each resistive branch is replaced with its corresponding admittance value and a voltage source in series. Transmission lines with series capacitive compensation are omitted as series capacitors block the flow of GICs. Transformers are modeled with their winding resistances to the substation neutral, and in case of autotransformers, both series and common windings are represented explicitly [9]. In the equivalent dc circuit the line resistances and transformer winding resistances need to be divided by 3, and the substation grounding resistance is the appropriate value to use. Determining the nodal voltages, the currents in the lines, and the

currents flowing to ground from each node may be done by using the Nodal Admittance Matrix (NAM) method or the Lehtinen-Pirjola (LP) method. Both is based on Kirchoff's current law, and they are mathematically equivalent [9, 51, 100].

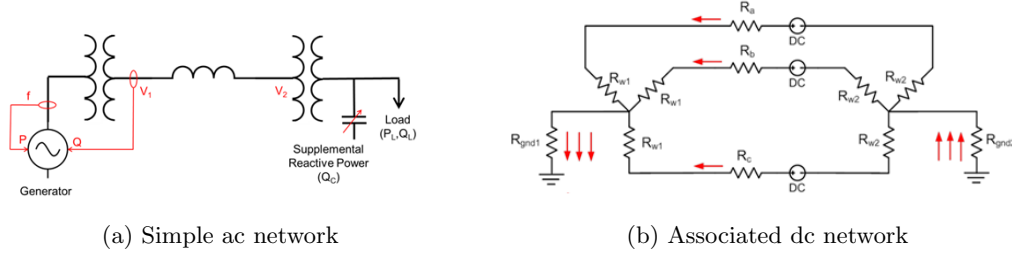


Figure 2.3: Formulation of equivalent dc network [9]

To calculate the voltage potential induced on a transmission line, the GEF is integrated over the length of the line. With the common assumption that the GEF is uniform (i.e., the north and the east components are constant in the geographical area of the line) [60, 71, 100, 102], the induced dc voltage \mathcal{V} is calculated as:

$$\mathcal{V} = \mathcal{E}_N L_N + \mathcal{E}_E L_E = |\mathcal{E}|(\sin(\phi)L_N + \cos(\phi)L_E) \quad (2.1)$$

where L_N and L_E are the north and east components of the displacement of the line, \mathcal{E}_N and \mathcal{E}_E are the strength of the north- and east GEF, and ϕ is the angle of the GEF relative to east (assuming that ϕ is measured in the counter-clockwise direction from the positive x axis). The induced voltages are converted to the dc current injections through Norton Equivalent, and the total current injections are derived from Kirchoff's law [51, 100].

This above described practice assumes a GEF associated with 1-D ground electrical conductivity structure. In reality, GEFs are non-uniform (their directions vary with geographical location) and the Earth has a 3-D conductivity structure (lateral variations in conductivity at any given depth in the Earth's crust and mantle) [103, 104]. Detailed information about its structure is necessary to determine the Earth transfer functions, which enable calculations of the GEFs to be used as inputs in the GIC modeling. When available, conductivity data obtained from magnetotelluric (MT) surveys involving colocated measurements of magnetic and electric fields is used to calculate the transfer function between electric and magnetic fields at the Earth's surface [51].

One-dimensional (1-D) conductivity models consist of a set of horizontal layers with varying thickness and different conductivities chosen to reproduce the conductivity variation with depth within the Earth. These values are determined by using a recursive calculation of the response of the bottom layer that is then used as the terminating impedance for

calculations for the next layer, and so on, to give the transfer function at the surface of the Earth. 1-D models ignore lateral variations in the Earth conductivity structure. However, different 1-D models have been constructed for different regions, so GIC modeling for a particular system would use the 1-D model for the area of that power system [51]. Two-dimensional (2-D) and three-dimensional (3-D) conductivity models are more accurate – may result in large deviations in induced voltages relative to Eq. 2.1 – but also more work to develop. They involve a tensor impedance function and electric fields that are not necessarily orthogonal to the magnetic field variations [51].

It is important to note that substation grounding resistance is often approximated using nonlinear regression based on substation size, maximum kV level, and number of incoming lines as predictor variables.

RTS-GMLC-GIC

To enable GMD simulations, an extended version of the RTS-GMLC test case (see Section 2.1), hereinafter referred to as RTS-GMLC-GIC, has been developed with the assistance of LANL ANSI. By adding GMD-specific data to the system, a wide range of studies – currently the analysis of power system dynamics due to GMDs, load-flow-based solution of GIC impacts, and solution of nonlinear effects such as transformer saturation – became possible [2]. RTS-GMLC-GIC is based on a modified version of the base RTS-GMLC case.

To form the dc network model of RTS-GMLC-GIC, first the (by default) disconnected wind and solar generating units were removed from the system. Next, as Fig. 2.4 illustrates, the location of conventional- and hydro generating units were changed to make the model more realistic: instead of directly connecting to buses or substations, individual generator buses were added to each generating unit, which connect to the original load buses or substations through added generator step-up (GSU) transformers. Altogether 111 new GSU transformers were added to the system.

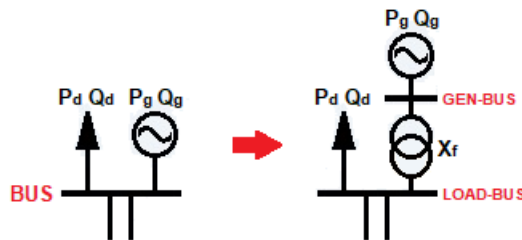
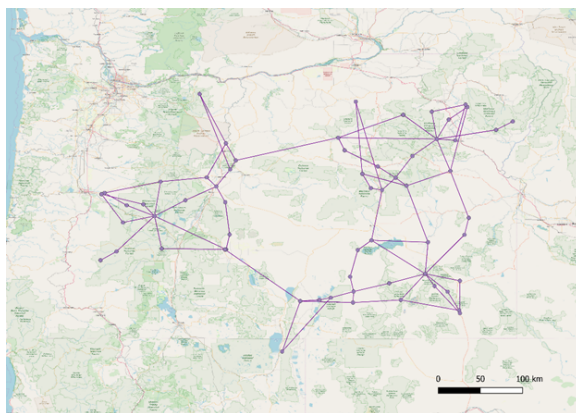


Figure 2.4: Modified location of generating units in RTS-GMLC-GIC

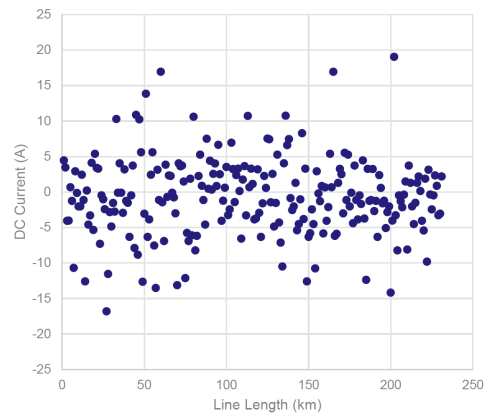
Determining parameters required for GMD analysis – e.g., geographic coordinates- and grounding resistances of substations, transformer configurations – is a critical step.

- Geographical location was modified to enable more realistic simulations (GMDs have greater impacts on higher latitude locations) and also highlight the local relevance and ties of this research. RTS-GMLC-GIC was shifted over the State of Oregon (see Fig. 2.5): while the relative distances of node locations and the lengths of transmission lines were kept unchanged, latitude coordinates were moved by (+9) degrees and longitude coordinates were moved by (-4) degrees throughout the whole system.
- Determining substation grounding grid resistances is difficult. One approach (that PowerWorld[®] Simulator [68] uses) is to use nonlinear regression, and estimate values based on substation sizes (maximum kV voltage level) and number of incoming transmission lines.
- When unknown, transformer winding configurations can be estimated with good accuracy. GSU transformers are typically ‘delta-gwye’ with delta on low side. Load transformers are typically ‘delta-gwye’ with delta on high side. ‘Gwye-gwye-auto’ transformers are typically connect portions of the transformer grid where voltage ratio ≤ 3 . ‘Gwye-gwye’ transformers are typically connect portions of the transformer grid where voltage ratio > 3 .

Fig. 2.5 depicts the characteristics of the RTS-GMLC-GIC test case. Fig. 2.5a depicts the modified geographical location of the system, and Fig. 2.5b scatter plot diagram depicts the DC currents in each lines related to the length of the lines; GIC voltages on lines were caused by an assumed 1 V/km uniform EW direction GEF. A key observation about RTS-GMLC-GIC is that a number of transmission lines are overlapping; this will result in high neutral currents for the transformers at substations at the end of those lines.



(a) Geographical location



(b) Induced GICs in lines

Figure 2.5: Characteristics of the RTS-GMLC-GIC test case [10]

Chapter 3: Dataset Customization

To better fit the intended application environment and requirements, the above introduced dataset is customized and further improved. The following sections present and discuss in detail all implemented changes.

The below used term “*timestep*” refers to a single 5-minute or 1-hour period of time. The RTS-GMLC dataset consists of 105,408 5-minute-sized and 8,784 hour-sized *timesteps*.

3.1 Identification Numbers

Individual identification numbers are assigned to each system asset to easily distinguish, handle and locate them during simulations.

A 3-digit **BusID** number is assigned to each bus based on their respective areas. The first digit distinguishes between different areas, and the second and third digits distinguish between individual buses. As mentioned above, RTS-GMLC has 3 areas (numbered from 1 to 3), each of which consisting 7 subareas respectively (numbered from 1 to 7).

A 4-digit **GenID** number is assigned to each generating unit based on their resource and unit types. The first digit distinguishes between different resource types, the second digit distinguishes between different unit types, and the third and fourth digit distinguish between individual units. RTS-GMLC has Hydro (1), Wind (2), Solar (3), Nuclear (5), Gas (6), Oil (7), and Coal (8) resource types, and Other Assets (9); furthermore, Solar CSP (1) - PV (2) - RTPV (3), Gas CC (1) - CT (2), and Oil CT (1) - ST (2) unit types, and Synchronous Condenser (1) and Storage (2) other assets.

A 4-digit **BranchID** number is assigned to each branch (line and xfmr) based on their respective areas and voltage levels. The first digit distinguishes between different areas, the second digit distinguishes between different voltage levels, and the third and fourth digits distinguish between individual branches. The area of a certain branch is determined based on its “FromBus” area. As mentioned above, RTS-GMLC has two voltage levels, 138 [kV] and 230 [kV], and a handful of connecting xfmr-type branches.

3.2 Asset States

Input Format

The key properties of system assets, discussed later in this section, may be defined through two implemented input channels. Besides listing disconnected- (i.e., offline or non-restored) and special assets in individual arrays, for convenience and to ease definition in large power systems, input CSV tables may be used as well.

Input arrays manually list all disconnected- and special assets using the earlier assigned identification numbers (see Section 3.1). Empty or zero-length array means that there are no such asset in the system in that particular simulation. Input CSV tables – separate template tables are used for each group of assets, i.e., for the buses, generating units, and branches – in their first columns contain the assigned identification numbers of assets, and in the subsequent column(s) define the properties of these assets in the form of binary values. “0” state of these variables mean that the asset does not have that certain property (e.g. not a disconnected asset during the simulation), and “1” state means that it does.

Critical and Dispatchable Loads, and Disconnected Buses

The criticality- and dispatchable state of a certain load are both set through its corresponding bus. Critical buses, and consequently connected critical loads, are defined either by an array that lists these assets, or in the second column of the input CSV bus-table. Dispatchable buses, and consequently connected dispatchable loads, are defined either by an array that lists these assets, or in the third column of the input CSV bus-table. A bus that is defined as critical and/or dispatchable must have a connected load (i.e., given active or reactive power demand in a certain *timestep*), otherwise it is automatically redefined to non-critical and/or non-dispatchable.

The supply of critical loads takes priority when the available generating capability in the system is less than the actual demand; dispatchable loads are able to supply a certain portion of their total demands. Such event often happens during restoration processes when a great number of generating units may be offline. For details, see Section 4.1.

The list of disconnected buses is an important input as it determines system topology. Disconnected buses are defined either by an array that lists these assets, or in the fourth column of the input CSV bus-table. In order to avoid floating-assets in the system, an algorithm checks for such conditions and corrects the state of assets if needed.

Blackstart- and Disconnected Generating Units

Generating units that are capable of blackstart are defined either by an array that lists these assets, or in the second column of the input CSV gen-table. Disconnected generating units are defined either by an array that lists these assets, or in the third column of the input CSV gen-table. In order to avoid floating-assets in the system, an algorithm checks for such conditions and corrects the state of assets if needed.

Critical Paths and Disconnected Branches

A series of branches (both lines and xfmr) may be designated to form a critical path, or paths, between key loads and generating units in the system. It is assumed that assets of such path cannot become disconnected, i.e., are able to withstand any damage caused by any threats. Critical branches, and consequently formed critical path(s), are defined either by an array that lists these assets, or in the second column of the input CSV branch-table.

The list of disconnected branches is an important input as it determines system topology. Disconnected branches are defined either by an array that lists these assets, or in the third column of the input CSV branch-table. In order to avoid unintentional formulation of islands or floating-assets in the system, an algorithm checks for such conditions and corrects the state of assets if needed. If a critical path asset is incorrectly defined as disconnected, automatically redefined to non-disconnected, so as well its buses at both ends.

3.3 Power Demand Profiles

Depending on dataset, active and/or reactive power demand timeseries data may or may not be directly available to be used in simulations. This section discusses how the base loads of buses are modified and updated in the used dataset.

Active Power Demand

In case of RTS-GMLC, active power demand (P_d) timeseries data is provided for each system area individually. To get the updated P_d nodal load (denoted with $newMW$, in units of [MW]) of a specific bus in a specific *timestep*:

$$newMW = oldMW \cdot scaler \tag{3.1}$$

where $oldMW$ is the P_d in the previous *timestep* (or at the beginning of a simulation the base RTS-GMLC value), and *scaler* ratio is calculated as:

$$scaler = \frac{timestep_load}{total_demand} \quad (3.2)$$

where *timestep_load* is the provided regional timeseries demand of the bus' area, and *total_demand* is the determined total power demand of the entire area. It should be noted, evidently, that each area has a *scaler* ratio in each *timestep* of the simulations.

Reactive Power Demand

In case of RTS-GMLC, reactive power demand (Q_d) timeseries data is not provided. When the test case was created, the base Q_d of buses were kept unchanged from the RTS-96 version values (see Section 2.1). Using a fixed, peak load flow state value in simulations, however, is not an accurate characterization of actual reactive load profiles, which varies throughout a day, a week, a month, and even a year. Consequently, the load profiles of buses must be improved and modified.

To get the updated Q_d nodal load (denoted with *newMVar*, in units of [MVar]) of a specific bus in a specific *timestep*:

$$newMVar = oldMVar \cdot scaler \quad (3.3)$$

where *oldMVar* is the Q_d in the previous *timestep*, and *scaler* is the above introduced ratio of the bus' area. Reactive load profiles now resemble active load profiles (i.e., vary depending on the time of the year), thus are more realistic in each *timestep* of the simulations.

3.4 Energy Portfolio

The base energy portfolio of the used dataset is modified for two reasons. On the one hand, to achieve a more realistic testing environment, the provided generation specific data needed to be further improved. It is desired to highlight the local relevance and ties of this research, therefore to change the portfolio to resemble the PNW region's expected portfolio of the year 2020. On the other hand, to ease the execution of validation experiments, creating flexible yet fully controlled testing environments is necessary. It is desired to enable the setting of varying renewable penetration levels: to be able reach a portfolio with solely conventional generation, or a portfolio with continuously high renewable penetration (which characterizes the region).

Generation in the Pacific Northwest

Since the late 1800s, when the first turbines were installed, hydropower has been playing the most important role in the energy portfolio of the PNW. This resource, supplemented by small steam plants (fueled by coal, oil and wood), provided most of the region's electricity up until the 1960s. As demand increased and surpassed available hydro generation, other types of power plants were added: baseload coal and nuclear steam-electric plants, small peaking combustion turbines fueled by natural gas, and later highly efficient natural gas combined-cycle plants. In recent years, large numbers of wind turbines have been constructed to sustainably meet increasing energy needs [105].

In spite of changing trends, today's energy portfolio is still dominated by hydropower: more than half of the generated electricity comes from this source. Most of it is generated along the Columbia River and its tributaries, and there are a number of dams on other major rivers as well; the exact generatable amount greatly varies with weather-, and consequently water conditions. Almost the third of the region's generation capacity is at plants that burn fossil fuels: most natural gas fueled, while less and less coal is being used. More than tenth is coming from wind, which resource represents a continuously increasing share in the region's energy portfolio. The single operating nuclear plant, located in eastern Washington, also accounts for a few percent of the region's generation. Altogether, current installed nameplate capacity (i.e., how much power the plants are designed to produce at full load operation) is about 63 [GW], and generating capability (i.e., how much power the plants are capable of producing over the course of an average year) is about 34 [GW] throughout the region [105, 106].

The Northwest Power and Conservation Council (NPCC) [107] – established and operated by the U.S. States of Washington, Oregon, Idaho, and Montana – serves as a comprehensive planning agency for energy policy in the PNW. This independent organization is responsible for developing resource strategies: forecasting electricity load-growth and assisting in the decisions of which resources should be build and used. Most member-states have enacted renewable portfolio standards (RPS), policies that are aimed to encourage renewable resource development; these have been created to diversify energy mixes, promote domestic energy production, and encourage economic development. Roughly half of the growth in the U.S. renewable energy generation since 2000 can be attributed to enacted state renewable requirements [108]. However, as NPCC identifies in their latest regional analysis, the ongoing renewable expansion in the PNW is largely motivated by the need to satisfy aggressive standards rather than to meet actual demand growth [107].

RPS policies widely vary on several elements: set target-goals (typically a percentage of retail electric sales), involved entities (typically investor-owned utilities, occasionally municipalities and electric cooperatives), eligible resources to meet requirements (typically

wind, solar, biomass, geothermal and some hydroelectric facilities), and cost caps (that limit increases to a certain percentage of ratepayers' bills) [108]. In the PNW:

- Idaho has no enacted RPS policies or state-wide renewable energy goals; nearly three-fourth of the consumed energy comes from out of state, nevertheless, more than three-fourth of the state's generated electricity comes from renewable resources, primarily from hydropower [108, 109].
- Montana, in its *Montana State Renewable Resource Standard* that was enacted in 2005, requires all investor-owned public utilities and competitive electricity suppliers in the state to obtain at least 15% of their retail electricity sales from eligible renewable resources by 2015 and each year thereafter [108–110].
- Washington, in its *Washington State Energy Independence Act* that was enacted in 2006, requires all major utilities in the state (that provide 80% of the electricity sold to retail customers) to obtain at least 15% of their generated power from renewable sources by 2020 and each year thereafter [108, 109, 111]. In 2019 additional requirements were enacted: transitioning the state's electricity supply to one hundred percent carbon neutral by 2030, and achieving entirely carbon free electricity supply by 2045 [112].
- Oregon, in its *Oregon State Renewable Portfolio Standard* that was enacted in 2007 and increased in 2016 [113], requires that 50% of the used electricity in the state must be derived from renewable sources by 2040. All utilities and retail suppliers are subjected to RPS targets depending on their size, which targets increase over time; e.g. large investor-owned utilities (those with 3% or more of the state's load) are subjected to a 20% mandate by 2020 and subsequent calendar years [108, 109, 114].
- British Columbia – even though almost all of its electricity is derived from renewable sources [115] – enacted its *British Columbia Clean Energy Act* in 2010, which requires that 93% of all electricity must come from clean or renewable sources by 2020 [116].

It is anticipated that the already ongoing renewable expansion in the PNW will continue in the next years [107]. Hydropower will remain to be the foundation of the region's power supply. Wind (currently representing about 15% of the total installed generation capacity) and solar (about 500 [MW] capacity installed just over the past five years) resources will likely continue to increase their share in the energy portfolio. With the scheduled retirement of the Centralia 1 (688 [MW]), Boardman (642 [MW]), North Valmy (127 [MW]) and Colstrip (308 [MW]) coal power plants in 2020 and 2021, the region will need to add new generating capacity, which likely will be renewable-based [117, 118].

In this research – based on historical data, current trends and anticipated generation-changes [117–121] – the energy portfolio of the PNW in the year 2020 is predicted to be:

Table 3.1: Predicted 2020 energy portfolio of the PNW

<i>Hydro</i>	<i>Wind</i>	<i>Solar</i>	<i>Other Renew.</i>	<i>Nuclear</i>	<i>Gas</i>	<i>Oil</i>	<i>Coal</i>
47.25%	14.25%	1.0%	1.5%	3.25%	22.0%	0.25%	10.5%

Regarding renewable resources, it is assumed that hydro generation remains the same, while both wind- and solar-based generating capabilities significantly increase compared to past years. Regarding conventional resources, it is assumed that nuclear and gas generation remain approximately the same, while both oil- and coal-based generating capabilities significantly decrease compared to past years.

Renewable Portfolio Options

For the purposes of this research, the renewable portfolio of the used dataset is modified to resemble the PNW region’s portfolio in every *timesteps* of the simulation processes. Target penetrations of different resources are listed above, in Table 3.1. Based on the above discussed legal mandates, it is assumed that the minimum renewable generation requirement in 2020 is 20% of the total generation. Due to the fact that the network structure of the used dataset was not designed to operate with (close to) 100% renewable penetration, it is assumed that the maximum allowed renewable generation is 75% of the total generation; this parameter can be adjusted.

Table 3.2 presents the four renewable portfolio options that are used in the benchmarking and validation experiments.

Table 3.2: Implemented renewable portfolio options

	<i>Hydro</i>	<i>Wind</i>	<i>Solar</i>	<i>Other Renew.</i>	<i>Min. Req.</i>	<i>Max. Allow.</i>
<i>Opt. 1.</i>	0%	0%	0%	0%	0%	0%
<i>Opt. 2.</i>	47.25%	14.25%	1.0%	1.5%	20%	75%
<i>Opt. 3.</i>	47.25%	14.25%	1.0%	1.5%	50%	75%
<i>Opt. 4.</i>	47.25%	14.25%	1.0%	1.5%	64%	75%

- *Option 1.*: a portfolio without any renewable generation
- *Option 2.*: average renewable generation is aimed to be greater than 20% – i.e., minimum renewable generation requirement is set to the assumed PNW 2020 mandate
- *Option 3.*: average renewable generation is aimed to be greater than 50% – i.e., minimum renewable generation requirement is set to the Oregon 2040 mandate
- *Option 4.*: average renewable generation is aimed to be greater than 64% – i.e., minimum renewable generation requirement is set to the predicted PNW 2020 renewable penetration level

Achieving Desired Portfolio

To achieve a desired portfolio, the provided timeseries data of renewable generating units are modified. All renewable units are enabled that are forecasted to have available generation – being the highest priority assets, as discussed in Section 5.2 – however, their scheduled generations are adjusted according to the following:

- In case of RTS-GMLC, the desired 1.5% Other Renewable generation is proportionally distributed between the Wind and Solar categories based on scheduled generations.
- Hydro, wind, and solar change ratios are introduced and used in each *timestep*:
 - total active power demand of the entire system (*load_mw_total*) is calculated (see Section 3.3)
 - total available active power generation of each resource-type (*total_avail_type*, where “*type*” is *hydro*, *wind*, or *solar*) is determined by ignoring disconnected units
 - individual generating units of a specific resource-type are only allowed to generate as much total active power (P_{gmax}) as their *total_avail_type* share of the *load_mw_total* is less (or equal) to the corresponding desired percentage of that “*type*”
 - if a “*type*’s” share is less than the desired portfolio percentage, P_{gmax} maximum generations limits are set to be the forecasted generations; otherwise, forecasted generations are rescaled to achieve the desired percentage, then set as P_{gmax} limits
 - to safely meet the set minimum renewable generation requirement (*Min. Req.*), a +15% buffer is applied
 - in case the *Min. Req.* requirement is not met by this point, and potential is remained in the forecasted maximum generations, the allowed P_{gmax} generations of appropriate units are increased with the remainder generations so as to try to met the *Min. Req.* requirement.
- The minimum active power generation limits (P_{gmin}) are kept unchanged.

3.5 Reactive Power Generation

Transitioning to higher renewable penetration comes with challenges. With greater use of asynchronous generating units (such as wind and solar), supplying sufficient reactive power throughout the entire electrical grid may become harder and harder. Reactive support is a vital ancillary service: it is necessary to ensure the continuity of power flows, the stability and controllability of the system. Consequently, increasing variable renewable generation without accounting for adequate reactive resources adversely impacts grid resilience.

To simply put, reactive power is the form of energy that creates or is stored in the magnetic field surrounding a piece of equipment. It plays an important role in both transmission and distribution networks: provides inertia that maintains a constant voltage level and keeps the system frequency within acceptable ranges. Traditionally it has been generated or absorbed by synchronous generating units; the presence of heavy rotating equipment, such as steam and gas turbines, have served as reliable inertia for years. Even though legacy baseload units are still able to readily supply reactive power – due to their inconsistent and increasingly uneconomical operations, and ongoing retirements – their participation are declining, thus other sources need to be incorporated. A variety of modern technologies (e.g. capacitors banks, static VAR compensators, synchronous condensers) are ready to take over, but only where it is specifically designed, required, and implemented [122–124].

Reactive power does not travel as far as active power is capable of, so it is best generated where it is consumed. This attribute, however, poses a challenge because addressing it locally is not evident when asynchronous generating units are present. Variable generation are often located in remote locations with weak transmission connections. Wind farms are not directly connected to the grid, and the frequency-converters between the turbines and the grid prevent their rotating mass from providing inertia. Solar plants, while directly connected to the grid, are without any existing rotating mass. As a results, in systems with high renewable penetration, power electronics must assist in supplying reactive power and correcting the power factor when needed [123, 125, 126].

The renewable generating units of the used dataset are not – or in the case of hydro units, only little – contributing towards the supply of reactive power (see Chapter 2). With the introduced high renewable penetration portfolios (see Section 3.4) and preferred use of renewable units (see Section 5.2), this leads to cases with insufficient reactive support and substantial generation imbalances across the system. For this reason, the dataset must be updated and improved with the addition of power electronics.

Synchronous Condensers

A synchronous condenser (sync-cond) is essentially a large synchronous motor with a freely rotating shaft and a DC exciter system. It is a dynamic source, which stores energy in the form of inertia, and can continuously adjust and quickly change its output as necessary to supply or absorb reactive power [124, 127, 128].

In case of RTS-GMLC, the base case contains 3 sync-cond devices: at the approximate center of each area, at Bus 114, Bus 214, and Bus 314 (see Section 2.1). These devices are updated to better serve the modified energy portfolios: their minimum reactive power generation limits (Q_{gmin}) are adjusted to -150 [MVar], maximum reactive power generation limits (Q_{gmax}) are adjusted to 150 [MVar], and voltage magnitude setpoint adjusted to

1 [per unit] Furthermore, since hydro generating units are capable of operating in *condense* mode, i.e., as a sync-cond, the 20 hydro units of the base case – 6 units at Bus 122, 1 unit at Bus 201, 3 units at Bus 215, 6 units at Bus 222, and 4 units at Bus 322 – are updated. After considering typical sync-cond ratings in electrical grids, the reactive power generation limits of these units are adjusted to -25 [MVar] Q_{gmin} and 25 [MVar] Q_{gmax} .

Variable Generation

As the number of asynchronous generating units, and consequently the share of variable renewable generation, have grown beyond insignificant in power systems, it is desired to require these units to participate in providing reactive power support. The initial approach – treating variable generation like negative demand, and placing the burden on conventional (synchronous) generating units to respond properly when active and reactive power generation output changes – has evolved to using power electronics to aid the compliance with applicable reactive support requirements and standards [126, 129].

For the most part, wind turbines use doubly-fed asynchronous generators or full-conversion machines with self-commutated electronic interfaces, which have considerable dynamic reactive and voltage capability. Solar PV inverters have a similar technological design to full-converter wind generators, and can be equipped with reactive power capability when needed. Both wind and solar plants can be further enhanced with the addition of SVC, STATCOMS or other reactive support equipment at the plant level [126, 129, 130].

In case of RTS-GMLC, wind and solar generating units do not have reactive power generation capability. To compensate for the lack of reactive support and reduce the system-level generation imbalance, fictional power electronics are added to them to provide this capability. Since the technology and exact design of individual units are unknown, the following is assumed. The 4 wind units of the base case – each equivalent to a single wind farm at Bus 122, Bus 303, Bus 309, and Bus 317 – are updated. In each *timestep* of the simulation, the Q_{gmin} minimum and Q_{gmax} maximum generation limits of these units are adjusted to $-/+ 25\%$ [MVar] of the unit's earlier determined (see Section 3.4), current active power generation (P_g), respectively. The 57 solar units of the base case – 1 CSP solar: 1 unit at Bus 212; 25 PV solar: 4 unit at Bus 101, 2 units at Bus 102, 1 unit at Bus 103, 1 unit at Bus 104, 1 unit at Bus 113, 1 unit at Bus 119, 1 unit at Bus 215, 2 unit at Bus 310, 1 unit at Bus 312, 2 units at Bus 313, 4 units at Bus 314, 1 unit at Bus 319, 1 unit at Bus 320, and 3 units at Bus 324; 31 RTPV solar: 10 units at Bus 118, 1 unit at Bus 213, 1 unit at Bus 308, 13 units at Bus 313, and 6 units at Bus 320 – are similarly updated as well. In each *timestep*, their Q_{gmin} and Q_{gmax} limits are adjusted to $-/+ 15\%$ [MVar] of the unit's earlier determined P_g generation, respectively.

3.6 System Topology

Slack Bus

A *slack* (also known as swing or reference) bus is a mathematical necessity in power system simulation. It allows that the solution of the non-linear set of equations, which describe the system and the flow of power, to be feasible; removes all uncertainty that arise from the lack of knowledge of the system-state. The arbitrarily selected slack has no physical relationship to any actual buses. On the one hand, it serves as an ideal generating unit that regulates the existing supply-dem unbalances: absorbs or emits active and/or reactive power to and from the power system until a system-wide balance is achieved. On the other hand, it serves as a virtual reference for all other buses: its voltage magnitude is assumed to be 1 [per unit], and voltage phase angle is set to 0° [122].

Traditional power flow studies rely on a defined single slack bus. In case of high-voltage transmission networks, this usually is the generator bus with the largest generating unit (i.e., unit with the greatest active power generating capability) that has a large number of transmission lines connected to it [131]. In case of terrestrial distribution networks, where the voltage level is between 4 [kV] and 69 [kV], this generally is a bus that represents a substation [132]. Numerous authors have suggested methods, e.g. [133–135], that provide solution for load-flow formulations without reliance on a slack.

With increasing number of renewable energy sources in power systems, distributed generation has been rapidly growing. Primarily in distribution networks, the concept of *distributed slack* has emerged: multiple generator buses serve as slacks based on defined scalar participation factors. This remedy the inadequacy of a single slack bus, and is a more realistic representation of real world dynamics [132, 136–138]. Another path is selecting the slack bus during load flow studies; [132] presents a method which selects the best slack bus, or buses, in such a way that the system power imbalance is minimized.

For the purposes of this research, since transmission networks are simulated and analyzed, a single slack bus is selected according to the following:

- [139] argues that instead of typical empirical rules, which have no validity in regard to the optimum choice of slack, using the impedance matrix of the system leads to finding the optimum: the smallest diagonal element of any impedance matrix of a system coincides in almost all cases with the optimum reference-slack bus location.
- Consequently, the default slack (Bus 113 in RTS-GMLC) is deselected, and a new slack is determined from the list of non-disconnected buses for the simulation.
- The new default slack is updated in each *timestep* after the operational status and setpoint of each renewable and conventional generating unit is decided.

To select a new slack, first the impedance matrix of the system is created: MATPOWER's [78] *makeYbus* function builds the bus admittance matrix, which then is converted to the impedance matrix by using MATLAB's [140] *y2z* function. Next, the smallest diagonal element corresponding to a generator bus is located (a slack must have an enabled generating unit connected to it); this leads to finding the optimal slack for the current system state. Finally, the voltage magnitude and angle of the new slack is set to 1 [per unit] and 0° , respectively.

Topology Adjustment

The following adjustments are made to prepare the used dataset for simulation, and to enhance it to be a better representation of real-life power systems:

- Each simulation is set to start with a flat start; the voltage magnitudes and angles of buses are set to 1 [per unit] and 0° , respectively.
- Voltage limits of buses, according to industry practice, are updated to 0.95 [per unit] minimum and 1.05 [per unit] maximum limits.
- The branch angle difference limits – namely the allowed minimum and maximum angle differences of individual branches – are updated to -180° minimum and 180° maximum values.
- The different MVA rating of individual branches – namely A long-term, B short-term, and C emergency ratings – are kept unchanged from the base dataset values.

Additional topology adjustments are made to simplify the used dataset. The storage unit(s) is kept disconnected throughout the simulation. The DC transmission line(s) is set to be out-of-service. The area assignment of system assets is clarified and improved as needed to facilitate proper simulation.

3.7 Operational Details

Key operational details of generating units are modified to better fit the application circumstances. This includes the proper setting of total operational costs, the addition of modern heat rate values, and the modification of operation related properties of units.

In the used MATPOWER format dataset, the total cost model of each generating unit is provided as a piecewise linear cost function [78]; two end- and two break-points are defined by coordinates, which are formed by parameters given in units of [\$/hr] and [MW]. For the purposes of this research, piecewise linear functions are interpreted in two ways. To quicken the algorithm, for each generating unit, units of [\$/hr/MW] values are calculated for every point of a function, which then are averaged into a single value that is set to characterize the individual unit. To use more accurate cost data, for each generating unit,

the provided conditionally defined function is accurately modeled using MATLAB's [140] *piecewise* function; it is assumed that the points are connected by straight linear lines, which gives exact unit of [\$/hr/MW] values that characterize individual units.

Heat rate is a measure that quantify how effectively a generating unit converts its fuel into heat and into electricity. It is commonly expressed in units of [Btu/kWh] – i.e., British thermal units per net generated kilowatt-hour – and represents the amount of energy used by a generating unit to generate and supply one [kWh] of electricity to the power system. The operating heat rates of different energy sources are updated according to the latest available U.S. Energy Information Administration (EIA) data [141]; for convenience, in this research units of [MMBtu/MWh] – i.e., million British thermal units per net generated megawatt-hour – values are used. Renewable generating units (hydro, wind and solar resources) are set to 9.118 [MMBtu/MWh] average heat rate values; using EIA's captured energy approach [142], it is assumed that their efficiency is 37.4%. Conventional generating units are set to the following average heat rate values: Nuclear to 10.455 [MMBtu/MWh] (32.6% efficiency), Gas CC to 7.627 [MMBtu/MWh] (44.7% efficiency), Gas CT to 9.009 [MMBtu/MWh] (37.9% efficiency), Oil CT to 10.326 [MMBtu/MWh] (33.0% efficiency), Oil ST to 10.270 [MMBtu/MWh] (33.2% efficiency), and Coal to 10.015 [MMBtu/MWh] (34.1% efficiency).

A number of operation related properties are modified as well:

- Ramp rates (ramp-up and ramp-down limits) restrict the generation-changing ability of generating units between consecutive hours. Values are changed from the given units of [MW/min] to [MW/hr]; values of disconnected units are set to 0 [MW/hr].
- Minimum up- and minimum down-times are the number of hours a generating unit must be online, or must be offline before it can be brought online again. Values are provided in units of [h], and are rounded up to the nearest integer using MATLAB's [140] *ceil* function.
- Start-up cost represents the cost of starting-up a generating unit, and shut-down cost represents the cost of shutting-down a unit. Values are provided in units of [\$/switch]; when a unit was online (enabled) in the previous *timestep*, its start-up cost is changed to 0 [\$/switch], as it is already operating.
- Fuel cost represents the cost of resources that are needed to power a generating unit. Values are provided in units of [\$/MMBTU].

Chapter 4: Prioritization of System Assets

The main objective during system restoration is to maximize the total available generating capability and minimize the unserved power demand at all times. In HILF events, the number of affected consumers and generating units varies (see Section 1.2): there may be significantly more demand than available generation, or perhaps the opposite, i.e., substantial generation that greatly exceeds demand. To best achieve the objective, successfully balance the power system, and ultimately quickly conclude the restoration process, the system assets must be prioritized and adequately scheduled in advance.

4.1 Demand Prioritization

When available generation is insufficient to meet all consumer demand – e.g., due to sudden increase in system loads, or unexpected outage of generating units or other assets – intervention is needed to restore and/or preserve the normal operating state of the system. The protection action consisting in intentionally disconnecting demand in part of a transmission or distribution network, with the goal of avoiding the cascading failure of the entire grid, is called load shedding [143, 144].

Load shedding, alongside with other types of load curtailment or demand management that electric utilities use when necessary, has an extensive background and application history in distribution networks [143–151]. The concept of critical loads describe key consumers which are given high priority during system operation and restoration; these assets take precedence over non-critical loads to be restored and fully supplied [144, 145]. The concept of dispatchable loads describe controllable consumers whose demands may be adjusted (i.e., partially fulfilled) based on available generation [145, 146].

In transmission networks, these concepts and procedures are interpreted in a slightly different way, given the demand aggregation abstraction as one steps up in voltage levels, and thus related protection and restoration literature is scarce. A load represents a substation (i.e., a large group of consumers) rather than a single local demand, consequently its *size* is only adjustable to a limited extent. Individual consumers belonging to a particular substation are often not known, knowledge about them and their characteristics are not available, consequently they are treated as one, and criticality means giving high priority to all of them. In light of all these, since transmission networks are simulated and analyzed in this research, consumers (loads) are prioritized and scheduled as follows.

By using the earlier introduced criticality- and dispatchable states of loads – which both are set though their corresponding buses (see Section 3.2) – demands in a certain *timestep* are rated and fulfilled according to these priorities:

1. higher priority is given to critical loads over non-critical loads,
2. higher priority is given to dispatchable loads over non-dispatchable loads, and
3. loads are ordered based on their reactive power demands (P_d), from the largest value to the smallest.

In case the available generation is less than the scheduled active power demand (a 15% buffer is added for safety), load shedding is performed in each system area separately: starting from the lowest priority load in the area, demands are adjusted to 0, one after another, until balance between generation and demand is reached. If a load is dispatchable, load curtailment is performed: its demand may be adjusted in 25% increments, i.e. can be reduced to 75% - 50% - 25% - 0% of its total value when necessary.

4.2 Generation Prioritization

In power system operation, the process of prioritizing and scheduling generating units (i.e., deciding when to start certain ones up and with what generation set-points, and then when to shut them down) is called Unit Commitment (UC) [122, 152]. UC, in other words, indicates the advanced selection of an optimal set of units to be placed in operation over a certain time span, and the best allocation of loads and reserves among these online (i.e., synchronized with the rest of the system) units [153, 154].

Determining the optimal schedule for a system is a complex mathematical optimization problem that is subjected to numerous operational constraints. These constraints usually are: the forecasted power demand and interchange within the system, the reserve requirements, the availability of generating units, the physical limitations of units (such as starting limitations and capability limits: minimum up- and minimum down-times, ramp-up and ramp-down limits, maximum generation capability), and the costs of operation (such as start-up-, operating-, and fuel costs) (see Section 3.7). In most cases (traditional UC problem), the economic aspects of generation-scheduling define how *optimal* is interpreted: the target objective of optimization is to minimize the operational costs throughout the system over the commitment period, while also satisfying all other constraints [153–155].

Countless UC solution approaches have been explored, developed and tested over the years; methods and techniques for regulated and deregulated markets, for systems with renewable energy resources and energy storage units, for distributed generation systems, and many more [154–160]. They have in common that they all combine mathematical programming approaches with certain approximations and assumptions to make the UC problem tractable and the solution optimal.

The approaches of Exhaustive Enumeration (EE), Priority List (PL) (see Section 4.3), and Dynamic Programming (DP) are among the earliest and less complex solution techniques. EE solves the UC problem by enumerating all possible generating unit status-combinations, then identifying the solution that yields to the combination with the lowest cost. PL arranges the generating units into a ranked list based on specific guidelines (combination of decided criteria and given unit-characteristics), and then uses this list to commit units to meet the power demand. Although its a fast and straightforward approach, the found solutions are often not optimal or feasible. DP builds and evaluates the entire solution-space – which consists of the commitment statuses of all generating units throughout the whole time horizon – in order to find the optimal solution, either searched in a forward or backward direction on the decision tree. DP methods tend to be overly complex for large power systems, consequently most of them are utilizing PL techniques to reduce the size of the solution-space and quicken the search.

In the utility industry, traditionally the Lagrangian Relaxation (LR) approach was used to solve UC problems; it remains a powerful solution technique even today. LR is based on dual optimization: the UC problem is decomposed into a master problem and several (more manageable) sub-problems, which are linked together by calculated LaGrange multipliers. Each sub-problem iteratively determines a near-optimal solution (commitment) for a single generating unit, and then the LaGrange multipliers are passed and updated between the two level until an overall solution converges. LR methods are able to handle a large number of units, however, convergence or feasible solutions are not guaranteed.

With the widespread proliferation of efficient commercial solvers (such as CPLEX [161], GUROBI [162], and MATLAB [140] optimization toolboxes), nowadays the common and most efficient way to solve UC problems is through Mixed-Integer Programming (MIP). MIP methods consist of an objective function as a function of parameters, a number of variables (e.g., commitment status of units), and constraints for the variables (e.g., constraining a variable to be a binary value). Integer and mixed-integer programming approaches divide the original generation-scheduling problem into two subsets: a nonlinear economic dispatch-, and a pure-integer nonlinear UC problem. MIP techniques solve the UC problem by ignoring infeasible solutions. In case of Mixed-Integer Linear Programming (MILP) (see Section 4.4) methods, linear problems or sub-problems are continuously solved until the linear program results in an integer solution.

Beyond all these deterministic approaches, more complex techniques also exist that are aimed to optimally solve UC problems. Without going into details, there are advanced meta-heuristic- (such as Expert Systems (ES), Fuzzy Logic (FL), Artificial Neural Networks (ANN), Genetic Algorithm (GA), Evolutionary Programming (EP), Particle Swarm Optimization (PSO))(such as Expert Systems (ES), Fuzzy Logic (FL), Artificial Neural Networks (ANN), Genetic Algorithm (GA), Evolutionary Programming (EP), Particle Swarm

Optimization (PSO)), hybrid-, and multi-agent system approaches available today. Since these are not used in utility-level decision making, they are out of the scope of this research.

4.3 Priority List Unit Commitment

Table 4.1: Attributes of PL approaches

<i>Modeling</i>	<i>Optimization</i>	<i>Scaling</i>	<i>Computation</i>
straightforward structure	approximation with advanced heuristics	able to handle large optimization problems	generally fast; linearly increasing comp. speed

PL approaches select the generating units to be placed in operation by using predetermined ranked lists. On these lists, typically, the most preferable units are at the top and committed first, and the rest are listed in descending preference orders and committed only when needed. The actual order of units greatly depends on individual unit-characteristics and the chosen optimization criteria; ranking is commonly done based on total operational costs and generation capabilities, while UC decisions are made based on unit generation limits and the power demand that needs to be met.

The introduced methods of [163–167] all use maximum active power generation limit (P_{gmax}) and/or heat rate values to form ranked lists. The Extended Priority List of [163] is a reverse list: units with greater P_{gmax} are at the bottom and have higher priority; in case generation capacities are equal, units are started up in ascending order of their heat rate values. The Methodological Priority List of [164] is similar to [163], however, the most preferable units are at the top of the list. The Improved Priority List (IPL) of [165] is based on the *Cost per MW* values of units, which can be obtained from the maximum power generation rate cost function; units are primarily ranked by their P_{gmax} values (greater capacity results in higher rank on the list), and when those are equal, lower *Cost per MW* values have higher priority. In [166], units with greater power rating have higher priority on the list, and then a meta-heuristic (EP) method is used to determine the UC statuses. In [167], *per MW cost at maximum power output* values are calculated, and then less costly units are committed first by utilizing a meta-heuristic (PSO) method.

Each method in [168–173] uses operation related costs to rank units. [168] presents two deterministic (LR and PL), and [169] presents a deterministic (PL) and two meta-heuristic (GA and FL) methods to solve thermal UC problems; to form lists, *full load average costs* are calculated, and then higher priority is given to those units that have lower costs. [170] presents a hybrid (PL-PSO) method in which thermal generating units are integrated with other renewable resources; *full load average production costs* are calculated, and then lists are formed based on *incremental cost* values (lower cost is preferred for commitment, while higher cost is preferred for decommitment). [171] presents a deterministic (PL) and a

meta-heuristic (PSO) method to solve ramp rate constrained UC problems; the introduced Improved Priority List is based on *priority index of average production cost* values (lower value have higher priority on the formed list). [172] presents a hybrid (PL based GA) method; the PL uses *average production cost* values: units with lower costs are committed first. [173] presents a hybrid (PL based MILP) method; the introduced Modified Priority List (MPL) uses aggregated operation-related costs to form a list (units are ordered from the least to the most costly ones), which then is used in a MILP method to determine the statuses of units.

Recent work, [174], proposes a New Priority List (NPL), which considers three factors to determine the position of a unit on the formed list: fuel costs, starting costs, and P_{gmax} values. Based on fuel cost, less costly units have greater priority as they reduce the total system costs of operation. Based on starting cost, units with higher costs have greater priority as it is desired to keep these units continuously operational. Based on P_{gmax} , units with greater values have higher priority as they satisfy the spinning reserve constraints and minimize the needed commitment status-changes due to power demand variations. The three factors are expressed in dimensionless values, and are summed to get the actual ranked list.

PL methods are simple (implementational advantage), generally fast (computational advantage), and well suited for both small- and large-scale UC problems (broad applicability advantage). However, regardless of their complexity and level of detail, their provided solutions remain rather poor: PLs cannot guarantee neither an optimal (total operating costs are often high), nor an always feasible schedule for generating units.

Implemented Priority List Methods

To demonstrate the effectiveness and advantageousness of the proposed GPW index (see Section 5.1) in ranking generating units, three relevant PL methods (briefly described above) are implemented and compared qualitatively and quantitatively with it. These, in chronological order of their publication dates, are introduced in [173], [165], and [174].

MPL [173] is introduced as a key tool in a two-step hybrid UC method, which aims to improve generic MILP UC approaches. During normal operation, in a system with stable power demand patterns, the commitment statuses of many generating units remain the same for an extended period of time. These always online and always offline units can be identified and removed from the MILP problem formulation to reduce its dimensionality, consequently shortening computational time-frames. MPL is proposed and used to identify these removable subsets of units.

In the MPL, units are ranked based on their aggregated operation-related costs (denoted with C in units of [\$/MWh]), which are calculated as:

$$C = F \cdot H + O \quad (4.1)$$

where F is the fuel cost in units of [\$/MMBtu], H is the average heat rate in units of [MMBtu/MWh], and O is the operating & maintenance costs in units of [\$/MWh]. The unit with the lowest C has the highest priority on the formed list, and the rest are listed in increasing order by their C values.

First step decisions are made by using P_{gmax} values of units and scale factors that adjust the amounts of committed and uncommitted generation (thereby adjusting the trade-off between computational time and achieved optimality). Once the always online and always offline units are removed, in the second step, the commitment statuses of remaining units are determined with a chosen MILP solution approach and tool.

In spite of its advantages, the applicability of the hybrid, MPL based MILP method is very limited. In power systems with significant renewable penetration, due to the high variability of renewable resources, the long-term commitment status of units greatly varies and is unpredictable; in these cases this method cannot be fully used. Also, during restoration, when the available units and the power demand throughout the system is often unforeseeable and may change unexpectedly, this method cannot be used.

IPL [165] is introduced as an advanced list that is used in solving UC problems in the presence of renewable, specifically wind and solar generations.

In the IPL, generating units are ranked based on their P_{gmax} and *Cost per MW* values (denoted with $CpMW$ in units of [\$/MWh]), which are calculated as:

$$CpMW = HR \cdot FC \quad (4.2)$$

where HR is the heat rate in units of [MMBtu/MWh], and FC is the fuel cost in units of [\$/MMBtu]. The unit with the largest P_{gmax} value has the highest priority on the formed list, and the rest of the units are listed in decreasing order by their P_{gmax} values. When multiple units have the same P_{gmax} value, the one with lower $CpMW$ value has higher priority.

Commitment decisions are made by using the ranked IPL list: units are committed one after another, from higher priority to lower, until the power demand and required spinning reserves of the system are satisfied. Minimum up- and minimum down-time constraints are used to improve solution, to commit additional units if needed or turn off units to reduce operating costs while still satisfying all other constraints.

This IPL based PL method considerably reduces total operational costs of UC solutions by incorporating renewable generating units into the commitment-problems; the solutions are near-optimal and provided relatively fast. However, the description of the proposed list and solution method is vague and deficient, also lacks of sufficient verification tests and explanations, which makes the actual implementation and its use challenging.

NPL [174] is introduced with the purpose to solve large-scale UC problems quick and efficiently through an NPL based PL method.

In the NPL, generating units are ranked based on *Priority Criteria* values (denoted with f), which are calculated as:

$$f = \frac{F}{\max(F)} + 1/\frac{S}{\max(S)} + 1/\frac{P_{gmax}}{\max(P_{gmax})} \quad (4.3)$$

where F is the fuel cost in units of [\$/MMBtu], S starting cost in units of [\$/switch], and P_{gmax} is the maximum active power generation limit in units of [MW]. The values of $\max(F)$, $\max(S)$ and $\max(P_{gmax})$ represent the system-wide maximum values of each factor considering all generating units. The three factors are individually expressed in dimensionless values, and then summed into a single value, to f .

The unit with the lowest F value comes first on the formed list as it reduces the total operational costs the most. The unit the highest S value comes first on the formed list as operating the most expensive units continuously (avoiding frequently commitment status change) is desired. The unit with the highest P_{gmax} value comes first on the formed list as it satisfies the required spinning reserve constraints and avoids frequent commitment status change due to power demand fluctuations. Consequently, the ranking of generating units goes as follows: the unit with the lowest f value has the highest priority, and the rest of the units are listed in increasing order by their f values.

Commitment decisions are divided into three sub-problems. First, the initial status of each unit is determined based on the ranked NPL, and that status is used as an operational constraint. Second and third, the status of certain units are adjusted when the active power demand (load and reserve constraints) change in the system, while generation limits (P_{gmin} and P_{gmax}) and minimum up- and minimum down-time constraints of units are also taken into consideration.

Even though this NPL based PL method was compared to 23 different UC solution techniques, which tests verify the fast execution time and provided low total cost solutions, the verification experiments were performed on a small, artificial and non-lifelike power system model. This raises questions about the reliability of conclusions, especially that the description of the method is confusing and not detailed enough to be reproducible.

4.4 Mixed-Integer Linear Programming Unit Commitment

Table 4.2: Attributes of MILP UC approaches

<i>Modeling</i>	<i>Optimization</i>	<i>Scaling</i>	<i>Computation</i>
clearly written and easily adaptable equations	optimization with commercial solvers	limited scalability; better at small optimization problems	exponentially increasing comp. speed

MILP algorithms adopt linear programming to solve and check for an integer solution [160],[175]. It is required that the objective function and constraints be a linear function of the decision variables. Their greatest advantage over other approaches is global optimality; they guarantee a solution that is globally optimal or one with an acceptable tolerance [175] –[176]. On the other hand, they scale poorly and fail when the number of units increases, or when additional modeling detail is integrated. Their efficiency also suffer from computational delay and the need for large memory [160],[175].

Implemented Mixed-Integer Linear Programming Method

To demonstrate the effectiveness and advantageousness of the proposed USS method (see Section 5.2) in determining optimal operational schedules for generating units, a MILP UC method is implemented and compared qualitatively and quantitatively with it. The method is based upon an openly-accessible UC script by *MathWorks*: [177]; the MILP computation is solved using the INTLINPROG solver of MATLAB’s Optimization Toolbox.

MathWorks’ UC script is customized for the case studies in the following manner:

- It is implemented for each system area separately to account for the unique properties of the areas, and executed in each *timestep* separately.
- After renewable generating units are enabled and dispatched by default, conventional generating units are to be optimized; data of other system asset is ignored.
- Input data of datasets is changed to fit the application circumstances:
 - Forecasted power demand (missing active power generation of the area) is increased by 5% to serve as spinning reserve for the generators of the area and to compensate for potential variabilities and modelling inaccuracies.
 - The objective function is the sum of three variables: cost of turning the generator on (Status x Start-up cost), cost of running the generator if it is on (P_g x Operating cost), and cost of generating power (P_g x Fuel cost).
 - Integrated modeling details are kept low to increase computational speed.

Chapter 5: Proposed Generation Prioritization Method

A key step in any restoration process – as discussed in Section 1.1 – is the determination of an operational schedule for all available generating units. Common UC approaches are not completely adequate in the restorative stage of system operation: widely used methods may take an extended amount of time to find realistic and/or optimal schedules, and are not necessarily suitable for modern power systems with significant renewable penetrations. It is clear that a novel solution is needed to tackle prevailing challenges; a method that is able to:

- broadly leverage renewable resources, regardless of the available amount;
- support quick and reliable decisions based on extremely limited data;
- be used in a wide range of scenarios and network sizes;
- and applicable in both online and offline system operation support.

The proposed **Universal Selection Scheme method** (see Section 5.2), which relies on the proposed **Generation Participation Weight index** based ranking of generating units (see Section 5.1), fully meets these needs. This efficient toolset ensures the achievement of optimal operational schedules (Section 6.2), consequently greatly shortening system recovery times and improving grid resilience. The following sections introduce and discuss in detail this proposed generation prioritization method.

Table 5.1: Attributes of the GPW index based USS method

<i>Modeling</i>	<i>Optimization</i>	<i>Scaling</i>	<i>Computation</i>
straightforward algorithm	advanced heuristics guarantee optimality	able to handle any problem sizes	extremely fast; linearly increasing comp. speed

5.1 Generation Participation Weight

To characterize the importance of generating units in any given system state, the Generation Participation Weight (GPW) index is proposed. GPW is comprised of four relevant, easy-to-calculate factors: Previous State (PS), Area Participation Factor (APF), Q/P ratio, and Maximum Power (MP). GPW is used to rank available units in a certain *timestep*: create a prioritized list that distinguishes between significant and less significant ones from the perspective of optimal system operation. An optional fifth factor, the Simplified Operating Cost (SOC) is also introduced; it is a secondary ranking value whose relevance and usage is discussed later in this section.

The formed GPW index based lists resemble priority lists presented in Section 4.3. Some mentioned drawbacks of those lists are alleviated by simplifying problem formulations and reducing required computational times. Furthermore, due to the conscious selection and designed nature of component-factors, GPW based lists are more adequate to be used in modern power systems than those others.

The GPW of a certain generating unit is dimensionless, and calculated as:

$$\text{GPW} = \text{PS} + \text{APF} + \text{Q/P} + \text{MP} \quad (5.1)$$

PS: Previous State

Refers to the operational status of the unit in the previous *timestep*.

Keeping the operation of renewable and conventional units continuous is desired. Frequent changes between online and offline statuses of a unit is non-realistic (due to starting limitations, such as slow ramp rates, or required minimum up- and down-times), economically not beneficial (due to costs associated with starting up and shutting down the unit), and not advised (continuity is better from the operational point of view, and also preferred by the operating personnel; inevitable wear and tear) regardless of provided generation capacity. Consequently, previously operating units should have greater probability to continue operating in the current *timestep* (i.e., higher position on the GPW index ranked list).

PS is a dimensionless, binary index. Units that were committed to operate in the previous *timestep* receive a value of 1, and all other units receive 0.

APF: Area Participation Factor

Refers to the contribution of the unit towards the supply of active and reactive power demands within its own system area in the current *timestep*.

The concept of participation factors was developed to quantify the individual responsibilities of units to serve the loads, losses, and scheduled interchanges within their area; the unit with the largest factor contributes the most, while the unit with the lowest one contributes the least. Participation factors are usually set based on the maximum active power generation capacities or the available reserve powers of the units; alternatively, a hard-coded uniform value may be used. They are especially useful when good economic information is unavailable to describe the units [178–180].

APF is comprised of two sub-factors, *APF-P* and *APF-Q*, and calculated as:

$$\text{APF} = \text{APF-P} + \text{APF-Q} \quad (5.2)$$

where *APF-P* is based on the P_g active power generation-, and *APF-Q* is based on the Q_g reactive power generation of the unit.

The idea of these sub-factors comes primarily from [181] – specifically from [181, 182] in the case of $APF-P$, and from [181, 183] in the case of $APF-Q$ – which work was rethought and modified. To obtain their values, first the P_{gmin} generation limits of all units are set to 0 [MW], and then an optimal power flow study (see Section 6.2) is conducted in the system; by doing so, the ideal contribution of the unit is determined. Next, using the results, in each area separately: 1) total P_{g-area} and Q_{g-area} are calculated (after increasing results with absolute-valued lowest generation values); 2) the individual contribution of the unit is calculated, consequently getting $APF-P$ and $APF-Q$ dimensionless values.

In a certain area, a unit's $APF-P$ and $APF-Q$ factors both add up to 1-1, respectively. Therefore, the APF factor of a unit is dimensionless, and takes a value between 0 and 2; higher APF corresponds to a more important unit.

Q/P ratio

Refers to the ratio of the unit's two generation limits: the Q_{gmax} maximum reactive power generation limit is divided by the P_{gmin} minimum active power generation limit.

As the number of renewable units increases in a power system, the unbalance between reactive power demand and generation grows due to the lack of renewables' ability to contribute. In order to restore this balance, conventional units with appropriate reactive generation capacity need to be used and enabled: units that reduce the systemwide reactive power generation imbalance more, than they contribute towards active power generation. These units have high Q_{gmax}/P_{gmin} ratios.

After determining the Q/P ratio of each unit, individual values are mapped into relative values compared to the maximum of the current *timestep*. Therefore, Q/P is a dimensionless factor, and takes a value between 0 and 1.

MP: Maximum Power

Refers to the maximum output of the unit compared to the largest renewable or conventional unit of the power system.

MP is comprised of two sub-factors, $MP-P$ and $MP-Q$, and calculated as:

$$MP = MP-P + MP-Q \quad (5.3)$$

where $MP-P$ is based on the P_{gmax} maximum active power generation limit-, and $MP-Q$ is based on the Q_{gmax} maximum reactive power generation limit of the unit. Renewable and conventional units are treated separately, i.e., the type of the unit is taken into account.

The largest unit(s) greatly contribute towards the supply of active and/or reactive power demands. It is both impractical and infeasible to frequently change between their online and offline statuses. To keep them generally enabled, and their operation continuous when possible, $MP-P$ and $MP-Q$ sub-factors are introduced.

To obtain their values, first the relative P_{gmax} and Q_{gmax} of the unit is determined after identifying the largest units of the system. Next, $MP-P$ and $MP-Q$ values are decided based on relative sizes (as percentages of the largest units), using the following table:

Table 5.2: Determination of $MP-P$ and $MP-Q$ values

$< 80\%$	$80\% - 95\%$	$95\% \leq$
MP-P = 0	MP-P = 0.25	MP-P = 0.5
MP-Q = 0	MP-Q = 0.25	MP-Q = 0.5

The MP factor of a unit is dimensionless, and takes a value between 0 and 1; only the largest units in the system receive values in the current *timestep*.

SOC: Simplified Operating Cost

This optional, secondary factor refers to the minimal operating cost of the unit.

In the development of the GPW index based USS method the primary target was to minimize required computational times while at the same time maximizing the optimality of determined schedules. Even though cost related data is not being used in the GPW index, it may be beneficial to take the financial aspect into account as well when distinguishing and prioritizing the units of the system. For this reason, the SOC factor is introduced to further describe individual units, and later used to form advanced ranked lists.

The SOC is calculated as:

$$\text{SOC} = \text{FC} \cdot \text{HR} \cdot \text{MG} \quad (5.4)$$

where FC is the fuel cost in units of [\$/MMBtu], HR is the heat rate in units of [MMBtu/MWh], and MG is the P_{gmin} minimum active power generation limit in units of [MW]. Consequently, it is expressed in units of [\$/h], and reflects the operating cost of the already online unit.

To actually use SOC for prioritization, relative values are determined for every units in the current *timestep*. Therefore, the SOC factor of a unit is dimensionless, and takes a value between 0 and 1; higher SOC corresponds to a more costly unit to operate.

Ranking Generating Units

The GPW indexes of generating units are calculated according to Eq. 5.2; values of disconnected units are set to (-1).

A larger GPW corresponds to higher rank (greater importance) on the form list of units. When the GPW indexes of multiple units are equal, lower SOC value (calculated according to Eq. 5.4) is preferred and prioritized; SOC serves as a secondary ranking value.

5.2 Universal Selection Scheme

To determine the optimal operational schedule of generating units during an ongoing restoration process, the Universal Selection Scheme (USS) method is proposed. This GPW index (see Section 5.1) based algorithm identifies the ideal subset of units to be placed in operation, while – by fully leveraging available renewable generation – supporting an accelerated system recovery. Fig. 5.1 depicts the general structure of this method.

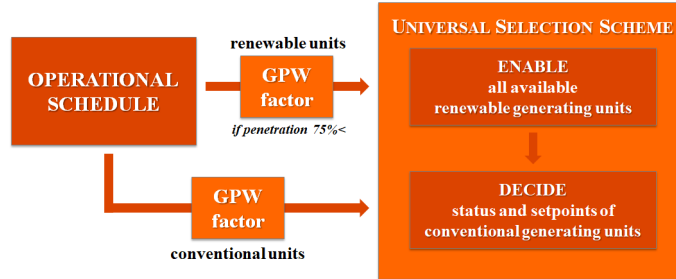


Figure 5.1: Block diagram of the two-level USS method

First, renewable generating units throughout the system are designated as *quasi black-start* units. They all are enabled by default and allowed to generate their full potentials, subjected to the assumptions that their forecasted generations are 100% accurate and will not vary during a *timestep*. When the total renewable generation exceeds the set 75% maximum allowed system-wide penetration (see Section 3.4), the GPW index is used to prioritize units and select important ones to operate; excess generation is disabled, consequently the set upper limit is enforced at all times.

To decide which conventional units (and with what generation setpoints) ought to be enabled alongside the renewable ones, the following information is needed:

- hour of the day for the current *timestep*;
- renewable share of total active power demand (i.e., planned renewable penetration);
- and unassigned active and reactive power demands (i.e., missing generations); power transmission losses are considered- and a 10% spinning reserve is added.

Second, by using the GPW index ranked list of conventional units, commitment decisions are made in each system area in each *timestep*. Conventional units are enabled as long as there is missing generation in their respective areas, following the below process:

1. take the (first or) next generating unit from the GPW-ranked list;
2. identify the area and asset setting (i.e., connected or disconnected) of the unit;
3. decide – based on Step I. through Step III. – the commitment status of the unit;
4. update the unassigned active and/or reactive power demands of the respective area after a unit is enabled (i.e., quantify the effect of the unit);

As Fig. 5.2 depicts, the USS method selects the conventional units to be placed in operation by relying on a 3-step approach. Each step further specifies 3) and 4) of the above introduced general decision-making process, and enables a desired amount of units. An optimal power flow study (see Section 6.2) is conducted after each step to verify the optimality of the system-setup (based on: operationally feasible schedule, required computational time, number of dispatched units, and total costs of operation), and to decide if proceeding to the next step is necessary.

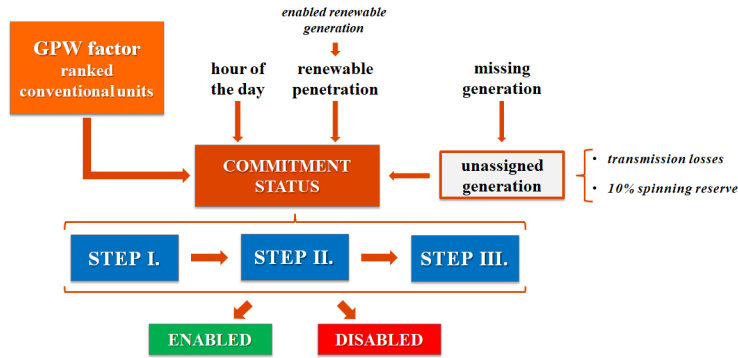


Figure 5.2: USS method decision making – conventional generating units

In the first step (see Fig. 5.3), as few conventional units are enabled as possible. The decision making process is concluded once either the unassigned active or reactive power demand goes below 0, or once the entire GPW-ranked list of units is reviewed. In case the optimal operational schedule was not found, the USS method proceeds to *Step II.*

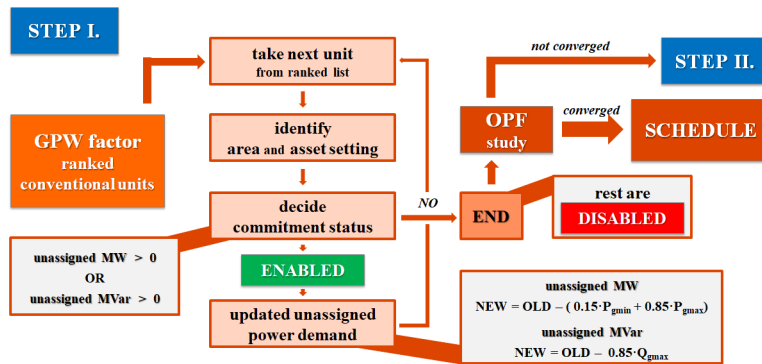


Figure 5.3: Second level of the USS method – *Step I.*

In the second step (see Fig. 5.4), a realistic number of units are enabled based on the active power generation capacities of conventional units. The unassigned active power demand is updated depending on the planned renewable penetration of the system. When renewable generation is low, individual *timesteps* require more conventional units (with

setpoints closer to their P_{gmax} maximum active power generation limits) for system balance; when generation is high, individual *timesteps* require less conventional units (with setpoints closer to their P_{gmin} minimum active power generation limits). As in *Step I.*, in case the optimal operational schedule was not found, the USS method proceeds to *Step III.*

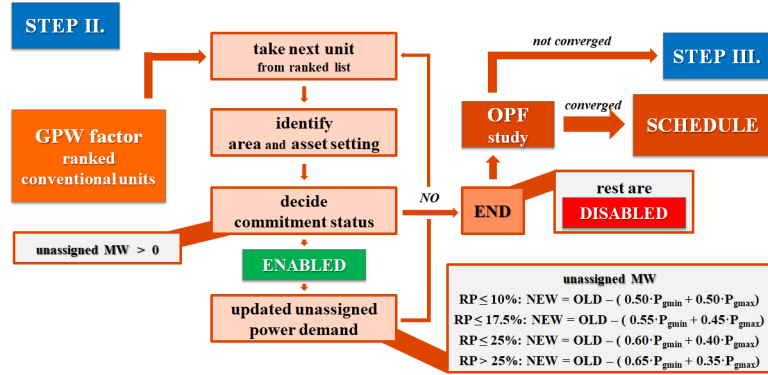


Figure 5.4: Second level of the USS method – *Step II.*

In the last step (see Fig. 5.5), a realistic number of units are enabled based on the reactive power generation capacities of conventional units. The unassigned reactive power demand is updated depending on the time of the day. During the night, when power demand is low, individual *timesteps* require less conventional units for system balance; during the day, when power demand is higher, individual *timesteps* require more conventional units.

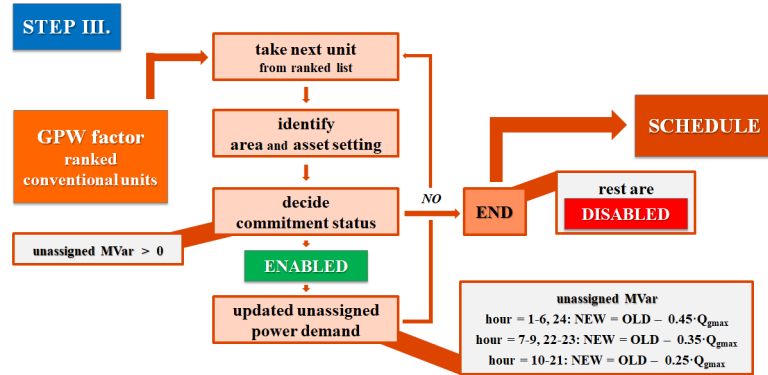


Figure 5.5: Second level of the USS method – *Step III.*

As the performed benchmarking and validation experiments demonstrate (see Chapter 7), once the USS method is concluded – after either Step I., Step II., or Step III. – the optimal operational schedule (see Section 6.2) of generating units is determined. The exact setpoints of enabled units may be determined by performing a power flow- or optimal power flow study (see Section 6.2), in which convergence is guaranteed.

Chapter 6: Properties of Case Studies

The performed benchmarking experiments are aimed to validate the proposed USS method (see Chapter 5), i.e., prove that its performance is better and the required computational times are lower than what common generation prioritization approaches (see Section 4.2) are capable of. This chapter discusses the background and key characteristics of these case studies.

6.1 Simulation Process Structure

The general structure of simulation and evaluation processes is presented below. In each *timestep*, one after another, old (previous) snapshots of the used dataset get updated with forecasted new timeseries data of generations and demands. During this update, new snapshots are customized and improved according to Chapter 3, by using custom-made main functions (*SystemUpdate.m*, *SystemConvState.m*, and *SystemFinal.m*) and sub-functions; these all are included in Appendix A.

1st step: New Dataset Initialization

Each simulation process begins with necessary preparatory steps:

- Individual identification numbers are assigned to each system asset according to Section 3.1, by using the *addID.m* sub-function.
- The state of assets – critical and dispatchable loads, and disconnected buses; blackstart and disconnected generating units; critical paths and disconnected branches – are defined according to Section 3.2, by using the *updateAssetState.m* sub-function.
- Simulation details – simulation interval; first *timestep* and last *timestep*; desired renewable portfolio – are specified.
- The type of each bus – PQ load bus; PV generator bus – is updated based on the state of generating units and branches, by using the *updateBusType.m* sub-function. A new Slack (reference bus) is selected by using the *updateSlack.m* sub-function. System topology is adjusted according to Section 3.6.
- Operational details are set according to Section 3.7, by using the *setCosts.m* sub-function.

As the simulation process is continuously going on, in each *timestep*, the old snapshot of the dataset gets duplicated to start creating the new snapshot. Once this is done, the update and customization of the *timestep*-snapshot begins as follows.

2nd step: Power Demand Update

Active and reactive power demands of buses are updated according to Section 3.3. The prioritization of loads – in case available active power generation is less than the power demand – is done according to Section 4.1; scheduled loads are adjusted when needed and finalized for the *timestep*. Lastly, total demands of each area- and of the entire system are calculated.

The following figures illustrate how the load profiles of the RTS-GMLC dataset are modified and updated. The day of May 5th is simulated in 5-minute intervals (i.e., total 288 *timesteps*), assuming normal system state (i.e., no outage of system assets).

Fig. 6.1 depicts improved active (6.1a) and reactive (6.1b) power demands. Instead of constant 8,550 [MW] and 1,740 [MVar] system-wide demands (dashed lines on figures) – which belongs to the base case (see Section 2.1) – total demands now are changing throughout the days; this is a more realistic load profile that is a better fit for extended simulations.

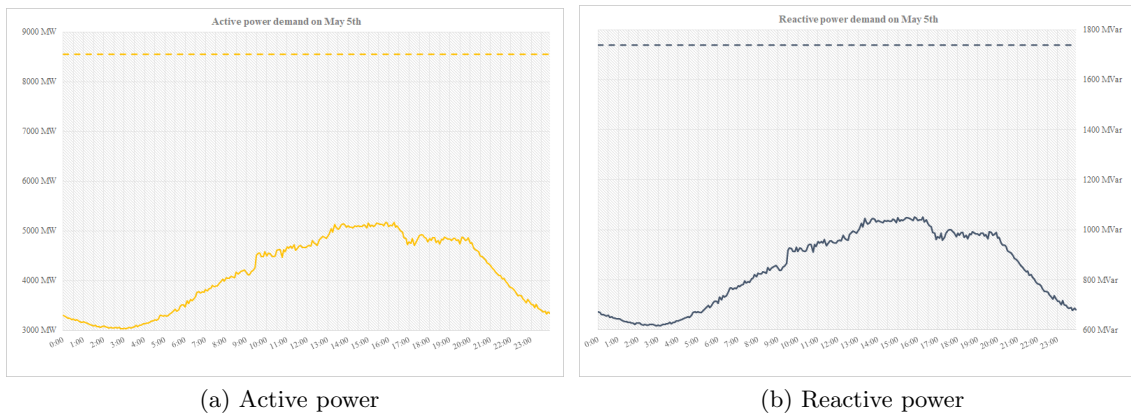


Figure 6.1: Improved power demand profiles of RTS-GMLC on May 5th

Fig. 6.2 (on page 47) depicts the total reactive power demands of each system area, highlighting the unique characteristics of the network and its individual parts.

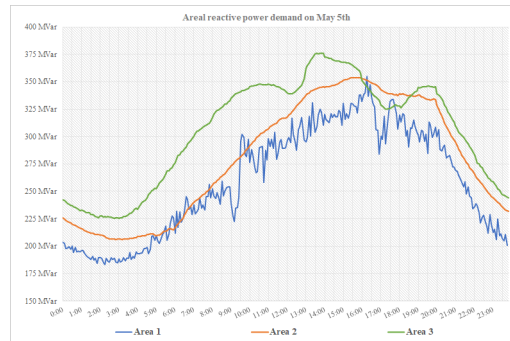


Figure 6.2: Improved reactive power demand of each system area on May 5th

3rd step: Renewable Portfolio Modification

The renewable portfolio of the RTS-GMLC dataset is based on the southwestern U.S., a region dominated by wind and solar resources (see Section 2.1). This portfolio is modified according to Section 3.4 to resemble the PNW region’s portfolio in each *timestep* of the simulation processes. Reactive power supply throughout the system is modified according to Section 3.5: the sync-conds and hydro generating units are updated, and the variable generating units (wind and solar) are improved with added reactive generation capability.

The following figures illustrate how the energy portfolio of RTS-GMLC is modified and updated. The week of May 3rd (Sunday) to May 10th (Sunday) is simulated in 1-hour intervals (i.e., total 168 *timesteps*), assuming normal system state. When necessary, the operational statuses of renewable and conventional generating units are determined by using the proposed USS generation prioritization method (see Chapter 5).

Fig. 6.3 depicts the base- (Fig. 6.3a) and the desired (Fig. 6.3b) energy portfolios of RTS-GMLC, in percentages of different resource types.

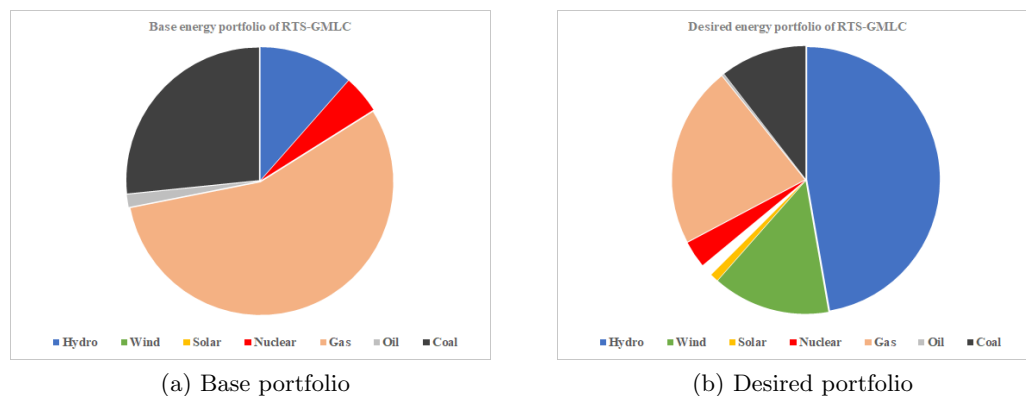


Figure 6.3: Energy portfolio of RTS-GMLC

Fig. 6.4 depicts the achieved renewable portfolios of RTS-GMLC in the *timestep* of May 8th, 12pm. Different renewable portfolio options are analyzed (see Section 3.4), which yield to different minimum renewable generation requirements. As observable, available hydro generation is entirely exploited, forecasted wind generation is almost unavailable, and more and more solar generation is used to achieve the set requirements.

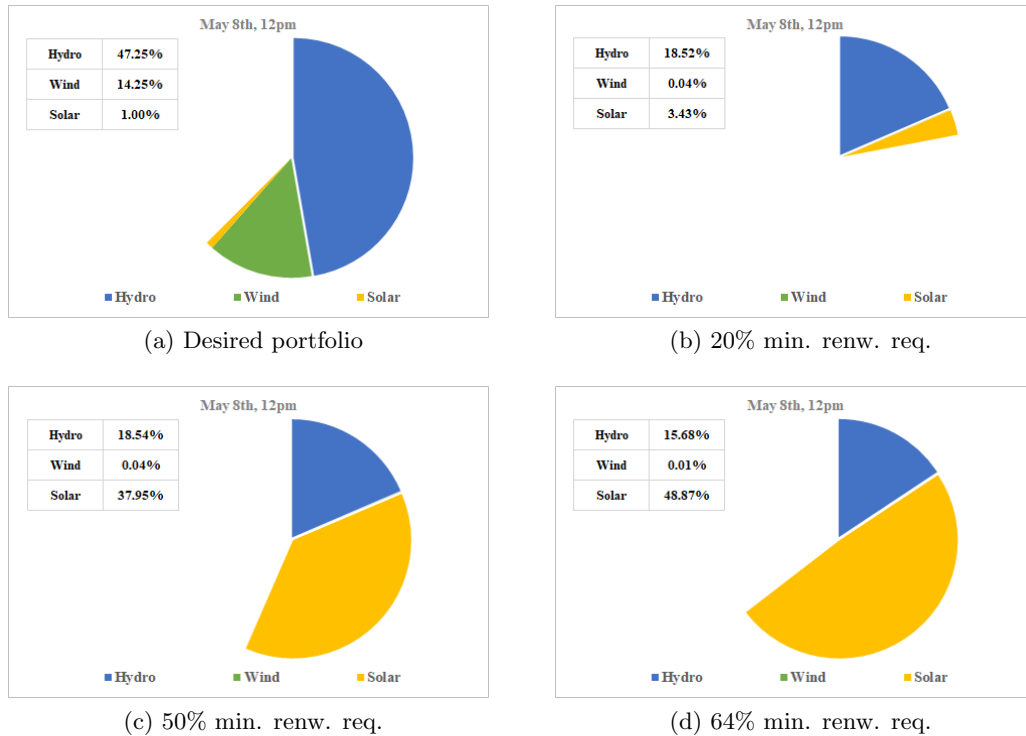
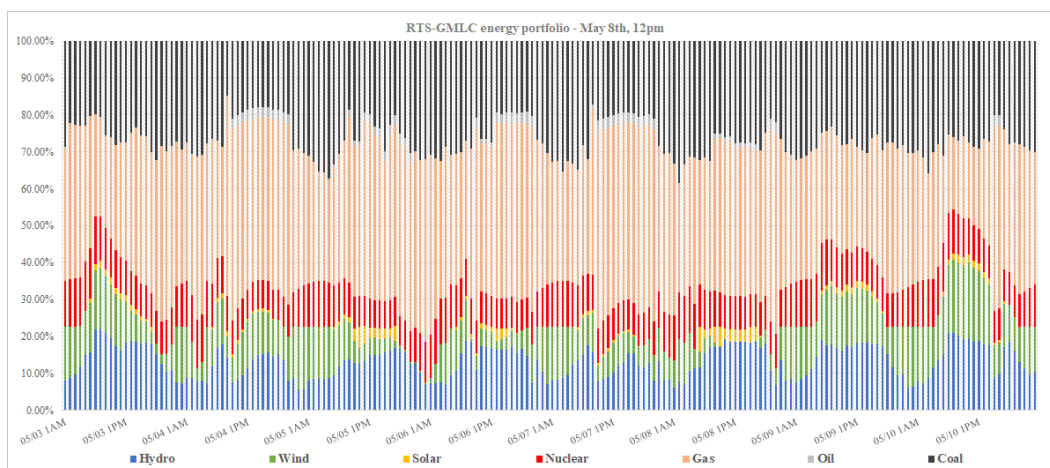
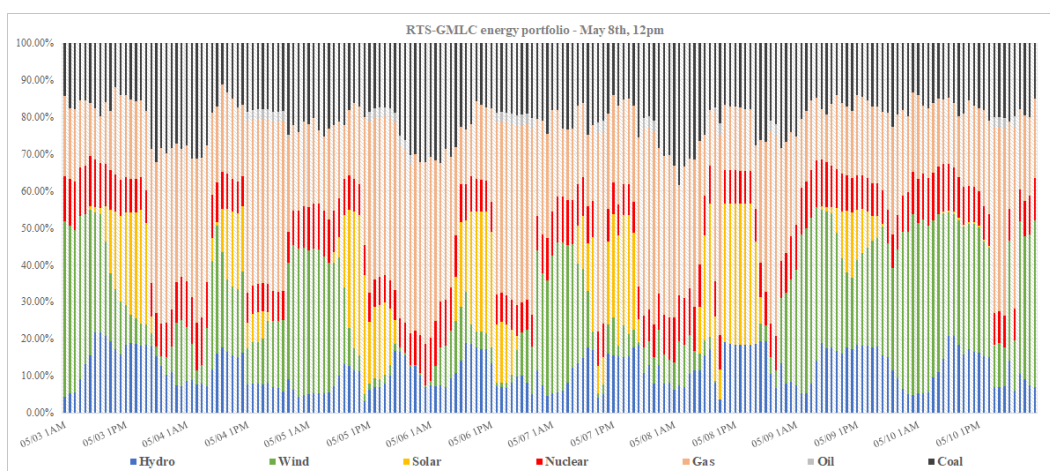


Figure 6.4: Energy portfolio of RTS-GMLC on May 8th, 12pm

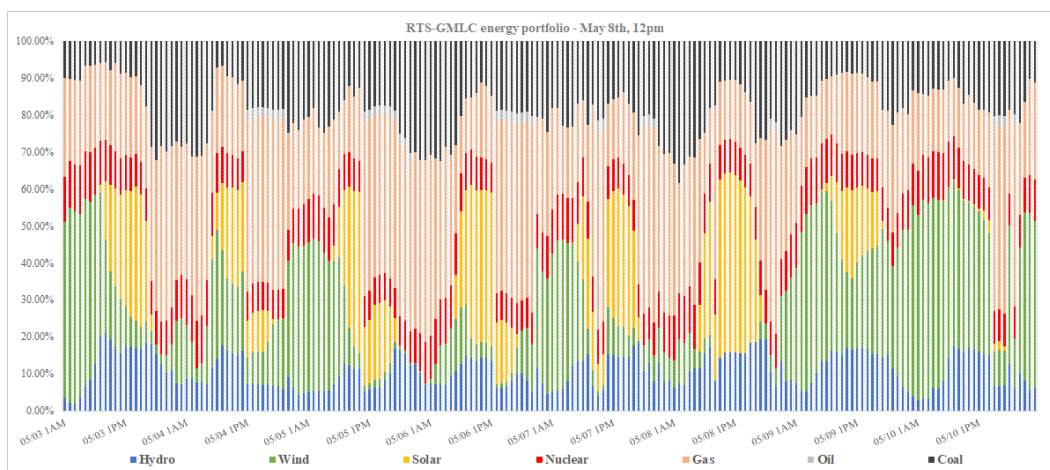
Fig. 6.5 (on page 49) depicts the modified energy portfolios of RTS-GMLC when different renewable portfolio options are selected. As expected, renewable generations fluctuate throughout the days and the week. Since hydro generation is insufficient, solar generation is used to try to fulfill the set minimum generation requirements. While it is achieved in case of Fig. 6.5a (average 23.70% renewable penetration), not in case of Fig. 6.5b (average 39.18% renewable penetration) and Fig. 6.5c (average 41.45% renewable penetration); this is caused by the insufficient amount of forecasted generations in the majority of *timesteps*. Nevertheless, as clearly observable, the modified portfolios broadly resemble the PNW's predicted 2020 portfolio.



(a) *Option 2.* renewable portfolio – 20% min. renw. req.



(b) *Option 3.* renewable portfolio – 50% min. renw. req.



(c) *Option 4.* renewable portfolio – 64% min. renw. req.

Figure 6.5: Modified energy portfolio of RTS-GMLC

4th step: Generating Unit Commitment

First, available renewable generating units get scheduled. As Section 5.2 discussed, these units are set to operate as *quasi blackstart* units: they all are enabled by default and allowed to generate their full potentials at all times (subjected to previously performed renewable portfolio modification), while it is assumed that their forecasted generation-predictions are 100% accurate and will not vary during a *timestep*.

Second, available conventional generating units are selected to be placed in operation alongside the already committed renewable ones. Units are prioritized according to Section 4.2 or Section 5.1. Unassigned power demands (i.e., missing generations) of each area- and of the entire system are calculated; transmission losses are considered- and a 10% spinning reserve is added by increasing these values by 15%. Key units are identified and scheduled to supply the unassigned demand according to Section 4.2 or Section 5.2.

6.2 Testing Environment

Hardware and Software Setup

The testing of the proposed generation prioritization method is done on a machine with Intel[®] Core[™]i7-7500 2.70GHz/2.90GHz CPUs and 12GB of memory. The operating system is a 64-bit Microsoft Windows 10 Pro.

In the benchmarking and validation experiments, the MATPOWER v7.0 [78] evaluations are conducted using 64-bit MATLAB R2019b [140] and default solvers provided for power flow and optimal power flow problems. GMD event related simulations are done with PMSGMD v0.1 [2] using Julia v1.1.1 [75]. Further processing and visualization of results is done using Microsoft Office 365 ProPlus.

Reported runtimes focus on the solver runtime (i.e., actual required computational times of different methods) and do not include the times of test case loading, model building, or dataset modification and update.

Objective

In order to be able to define an objective for the benchmarking case studies, first the following terms need to be introduced:

Power Flow (PF) is a basic tool to study the steady-state operation of a power system; to plan ahead and prepare for various hypothetical situations, and assist in the future expansion of the network. PF enables the numerical analysis of the flow of power in an interconnected area, and characterizes the system's capability to adequately supply all connected loads. It determines the voltage magnitude and angle at each bus, the active and

reactive power flows at all assets connecting the buses, and the losses throughout the system. However, it only finds mathematical solutions, not necessarily physically feasible or optimal ones; PF equations, describing the system, do not take account of generating unit or transmission line limitations [122, 184, 185].

Optimal Power Flow (OPF) is an advanced tool to optimize the steady-state operation of a power system; a combination of power flow and economic dispatch, the short-term determination of the optimal outputs of generating units to meet all system loads. OPF, in its most realistic form, is a non-linear, non-convex problem, which includes both binary and continuous variables. Its goal is to minimize an objective function while respecting all physical, operational and technical constraints: Ohm and Kirchhoff laws, operational limits of generating units, loading limits of transmission lines, voltage levels, and many others. A realistic OPF implementation includes thousands of variables and constraints, and is the most accurate representation of the flow of powers. The solution of the non-convex problem is not guaranteed, however, relaxation enables that formulations can be solved [122, 186–188].

In this research, the objective in the performed benchmarking case studies (see Section 6.4) is to determine optimal operational schedules for the generating units at all times. Due to the time-sensitive nature of restoration processes (see Section 1.2), the term *optimal* is defined as: the quick prioritization and ideal scheduling of generating units, while integrating and utilizing available renewable generation to the most possible extent. Ideality is measured by conducted PF and OPF studies: a determined schedule is feasible when the PF study of the resulting system converges, and it is optimal when the OPF study converges; in any other cases, the schedule is either non-optimal and/or non-feasible. In general – contrary to traditional UC approaches (see Section 4.2) – the target objective of optimization here is to minimize required computational time and maximize optimality, while also satisfying all constraints of the system.

6.3 Priority List Comparison

To verify the applicability of the proposed GPW index to rank generating units (see Section 5.1), and partially prove Hypothesis I. (see Section 1.3), comparison experiments are performed. A GPW index based PL method is compared to alternative PL methods (see Section 4.3) to examine its performance. Results and findings are presented in Section 7.1.

The week of May 3rd (Sunday) to May 10th (Sunday) is simulated in 1-hour intervals (i.e., total 168 *timesteps*), assuming normal system state. Two renewable portfolios are analyzed: *Option 1.* and *Option 2.* (see Section 3.4).

In these validation experiments, PLs are compared in three different application scenarios. Generating units are selected to be placed in operation using one of the following:

- *Scenario I*: unassigned demand is fulfilled based on P_{gmax} limits
- *Scenario II*: half of unassigned demand is fulfilled based on P_{gmax} limits, and the rest is by using the *Enable and Try* approach
- *Scenario III*: *Enable and Try*, i.e., generating units enabled one-by-one, until the OPF study of the resulting system converges

In *Scenario I*, generating units are enabled – in each area separately – based on their maximum active power generation limits (P_{gmax}), until the complete unassigned demand is supplied in the system.

In *Scenario II*, generating units are enabled – in each area separately – based on their P_{gmax} limits, until half of the unassigned demand is supplied in the system. Then, the *Enable and Try* approach is used to determine the rest of the units to be enabled.

In *Scenario III*, generating units are enabled by using the *Enable and Try* approach: enable units one-by-one, following the priority list (from the top to the bottom), until the resulting system’s OPF study converges.

6.4 Benchmarking Case Studies

To verify the applicability of the proposed USS method (see Section 5.2), and subsequently prove Hypothesis I. and II. (see Section 1.3), benchmarking experiments are performed. The USS method is compared to implemented common generation prioritization approaches – an NPL based *Scenario II* PL UC method (see Section 4.3), and a MILP UC method (Section 4.4) – to examine its performance and highlight its advantageousness.

Normal Operation

First, validation experiments are performed during normal system operation: all assets are continuously operational and connected to the grid, without the occurrence of a HILF threat. Assets are treated equally, i.e., critical and dispatchable loads, and critical paths are not defined. Results and findings are presented in Section 7.2.

In the first group of case studies, five months of data is simulated in 1-hour intervals (i.e., depending on the month 720 or 744 *timesteps*, which is total 3696 *timesteps*): the months with the lowest (March, June, and October), and the months with the highest (July and August) areal- and total system loads. One renewable portfolio is analyzed: *Option 2*. (see Section 3.4). All three generation prioritization approaches are compared to each other.

In the second group of case studies, the month of May is simulated in 1-hour intervals (i.e., total 744 *timesteps*). All four renewable portfolios are analyzed: *Option 1.*, *Option 2.*, *Option 3.*, and *Option 4.* (see Section 3.4). The USS method is directly compared to the MILP UC method.

Cascadia Subduction Zone Event

Second, validation experiments are performed during an ongoing system operation process that is disturbed by a hypothetical CSZ earthquake event. The event triggers the necessary execution of a restoration process; based on historical data and expected consequences (see Section 1.2), a fictional operation and restoration timeline is created. As before, critical and dispatchable loads, and critical paths are not defined. Results and findings are presented in Section 7.3.

In this simulation process, worst case restoration scenario under the most probable load and generation conditions is presumed. Certain parts of the system are out of operation for a defined amount of time, consequently some assets are disconnected. As new data is received about the changing state of the system, the updated status of its assets, and of forecasted generations and demands, the goal is to determine the optimal operational schedule for the available generating units.

To establish a direct connection between RTS-GMLC and the PNW, it was assumed that Area 1 corresponds to the coastal region of the PNW, Area 2 to the region between the Coast- and the Cascade Ranges, and Area 3 to the region east of the Cascades. Two weeks of data, from January 26th (Sunday) to February 9th (Sunday), is simulated in 5-minute intervals (i.e., total 4032 *timesteps*), following the below detailed operational timeline. Fig. 6.6 (on page 54) depicts the one-line diagram of RTS-GMLC during this restoration process. Two renewable portfolios are analyzed: *Option 2.* and *Option 4.* (see Section 3.4).

Hypothetical CSZ earthquake event operational timeline:

1. Normal operation: January 26th, 12am to January 26th, 9pm
 - all assets are continuously operational and connected to the grid
2. CSZ earthquake event: January 26th, 9pm to January 29th, 9am
 - at 9pm local time a megathrust earthquake struck the entire region
 - Area 1 and Area 2 enter into a complete blackout and disconnect, while Area 3 remains intact and continues to operate
3. Phase I. restoration: January 29th, 9am to February 3rd, 6pm
 - about three days after the CSZ event the 230 [kV] voltage level of Area 2 is restored, including all loads and generating units (orange dashed lines in Fig. 6.6)
 - restored sub-region is connected to Area 3 and continues to operate together

4. Phase II. restoration: February 3rd, 6pm to February 9th, 12am

- about a week after the CSZ event the 138 [kV] voltage level of Area 2 is also restored, including all loads and generating units (red dashed lines in Fig. 6.6)
- Area 2 and Area 3 are interconnected and operates together, while Area 1 remains non-operational (gray lines in Fig. 6.6)

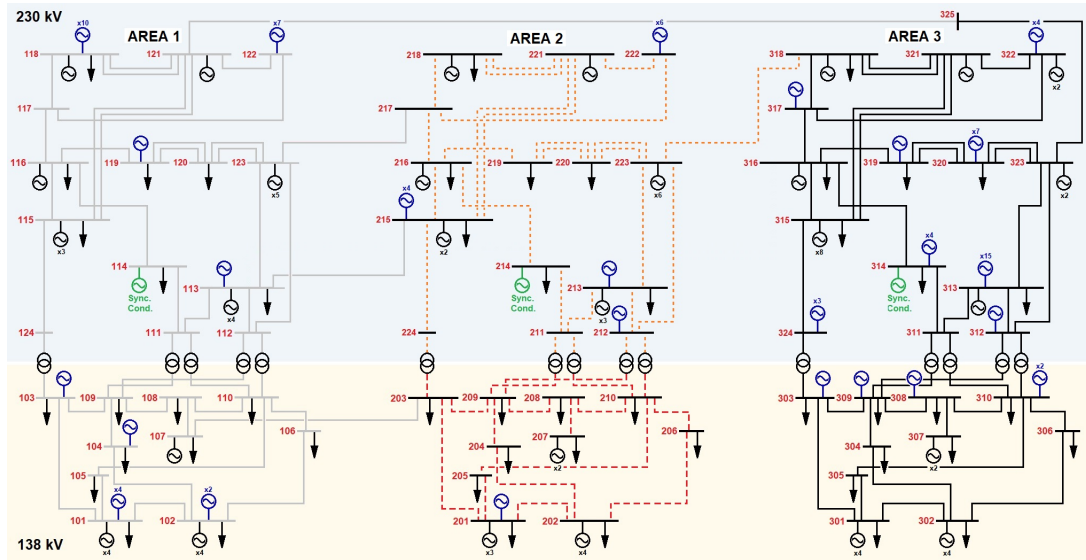


Figure 6.6: One-line diagram of RTS-GMLC – CSZ event restoration timeline

Geomagnetic Disturbance Event

Third, validation experiments are performed during an ongoing system operation process that is disturbed by a major GMD event. The event is the *Halloween storms of 2003* – hereinafter referred to as *Halloween storm* – at the peak of solar activity between October 29th and 31st. Simulations and GIC calculations are done as discussed below, in accordance with Section 2.2; related Julia algorithms are included in Appendix B.

A critical path, and consequently a group of critical loads, is defined: both on Fig. 6.7 (on page 56) and Fig. 6.8 (on page 57), the thick green lines represent the designated critical path(s), between the nuclear generating unit (connected to Bus 121) and the 138 kV side of Area 1. It is assumed (see Section 3.2) that the assets of this path(s) – due to their increased resilience – cannot become damaged or disconnected, i.e., are able to withstand the GMD event without experiencing any disruption. Dispatchable loads are not defined. Results and findings are presented in Section 7.4.

The Halloween storm is the largest ever recorded GMD event: a series of coronal mass ejections and solar flares – specifically 17 major flares, among which the largest measuring over 13 times the size of the Earth – that occurred from mid-October to early November in 2003. It peaked between October 29–31 (which explains its nickname), by exhibiting a series of two extreme disturbances, one closely following the other [103, 189]. Recorded GEFs of this solar storm serve as realistic inputs to the RTS-GMLC-GIC test case (see Section 2.2). A 3-D geophysical modeling technique, introduced in [104], is used to model the electrical conductivity structure of the Earth, and calculate the dc voltages induced by the GEFs on the transmission lines; results are voltage-increases or -decreases along the lines, in units of [V]. Actual calculations were done by colleagues in the College of Earth, Ocean, and Atmospheric Sciences (CEOAS) at Oregon State University (OSU); thereafter PMSGMD was used to simulate and analyze the effects of the event.

In PMSGMD [2], the dc network couples into the ac network by means of reactive power loss in transformers. The calculated dc voltages serve as input parameters to an ac OPF study (i.e., are added to the transmission lines), which determines the exact state of the power system and its assets; the increase in transformer reactive power consumption is calculated as well. Results of the OPF study are evaluated at every *timestep*. When the voltage level of a bus exceeds its set limits – decreases below 0.85 [p.u.] or increases above 1.15 [p.u.] – the bus itself, and consequently its connected generating units and branches (transmission lines and transformers), become disconnected. When the hot-spot temperature of a transformer increases above the set 150°C temperature limit, the transformer itself, and its connected generating unit become disconnected.

In the first group of case studies, the most intense hour of the Halloween storm (October 30th, 7:30pm to 8:30pm) is simulated in 5-minute intervals (i.e., total 12 *timesteps*). One renewable portfolio is analyzed: *Option 2*. (see Section 3.4). All three generation prioritization approaches are compared to each other.

Fig. 6.7 (on page 56) depicts the assessment of the performed PMSGMD OPF studies. Voltage limits are violated at Bus 213, Bus 301, Bus 302, and Bus 315. In each of these location, the violations occur on the generating unit side of the GSU transformers that are directly connected to these buses. Since there are only generator bus voltage violations throughout the system, it is assumed that the generating unit or the transformer will take care of them. The hot-spot temperatures of transformers never increase above the temperature limit. Consequently, even though this is the most intense hour of the Halloween storm, there are no outages of system assets (i.e., no disconnected buses, generating units, or branches) during the simulation process.

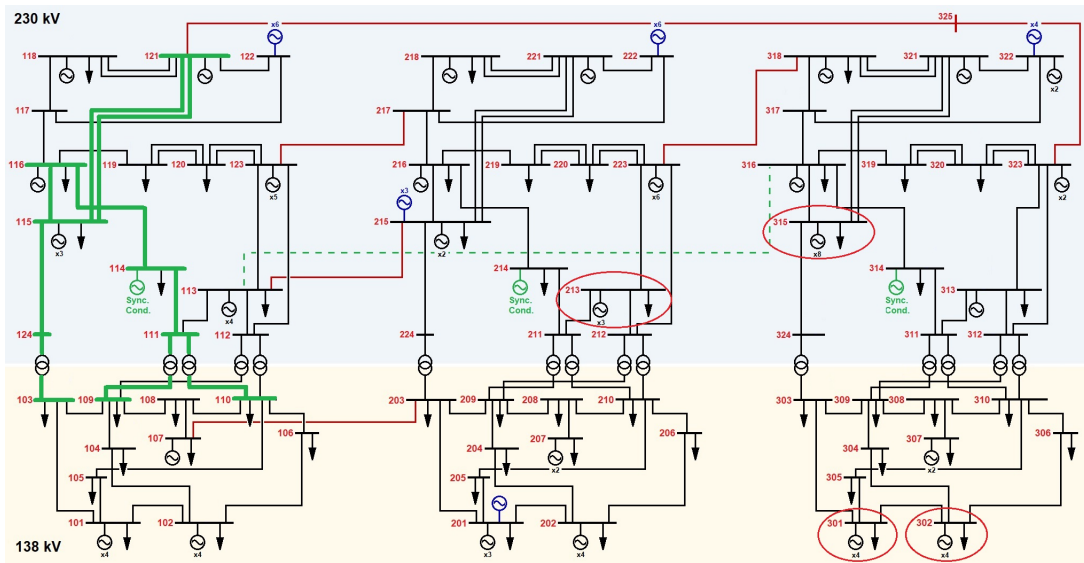


Figure 6.7: One-line diagram of RTS-GMLC-GIC – Most intense hour of the Halloween storm GMD event

In the second group of case studies, the evening of October 30th (from 6pm to 10pm) is simulated in 5-minute intervals (i.e., total 48 *timesteps*), however, the Halloween storm is assumed to be 10 times more powerful. One renewable portfolio is analyzed: *Option 2*. (see Section 3.4). All three generation prioritization approaches are compared to each other.

Fig. 6.8 (on page 57) depicts the assessment of the performed PMsGMD OPF studies. Voltage limits are violated at Bus 213, Bus 301, Bus 302, Bus 314, Bus 315, Bus 318, Bus 321, and Bus 322. Just as earlier, in each of these location, the violations occur on the generating unit side of the GSU transformers that are directly connected to these buses. None of these violations are extreme enough to justify the disconnection of a bus; it is assumed that the generating unit or the transformer will take care of them. The hot-spot temperatures of transformers exceed the 150°C temperature limit in numerous locations; GSU transformers at Bus 223, Bus 315, Bus 322, and Bus 323 are overheating during the simulation process, and the transformer at Bus 310 also overheats in certain *timesteps*.

After evaluating the results of the PMsGMD simulation, it is concluded that Bus 223, Bus 310, Bus 315, Bus 322, and Bus 323 all become disconnected due to the intensified Halloween storm. Consequently, many branches and generating units also become disconnected, which eventually results in the complete blackout of Area 3 during the entire simulation. It is important to note that the majority of transformers do not experience high neutral currents and are at risk for half-cycle saturation, so their temperatures stays below the temperature limits; the transformers at risk tend to be those towards the edge of a network or those near natural geographic boundaries.

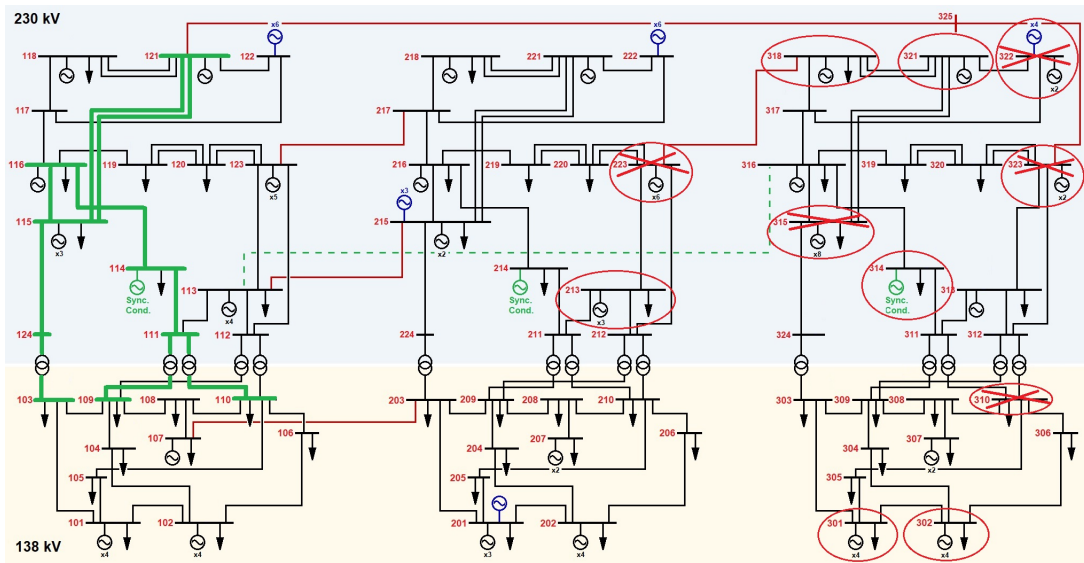


Figure 6.8: One-line diagram of RTS-GMLC-GIC – Intensified evening of the Halloween storm GMD event

Chapter 7: Method Validation Experiments

The following sections present the results of benchmarking and validation experiments. Simulation processes are as described above (see Chapter 6), and the goal is to make qualitative and quantitative comparisons towards obtained solution and required computational time, so as to showcase the advantageousness of the proposed USS method.

7.1 Ranking Generating Units

First, the *timestep* of May 8th, 12pm is simulated and examined separately. Fig. 7.1 depicts the ranked lists of conventional generating units based on different prioritization methods. The top of these lists (i.e., top 15 units in descending priority) are compared in table format; resource types, GenID identification numbers, and system areas are displayed.





























































<u>MPL</u>			<u>IPL</u>			<u>NPL</u>			<u>GPW</u>		
	<i>GenID</i>	<i>Area</i>		<i>GenID</i>	<i>Area</i>		<i>GenID</i>	<i>Area</i>		<i>GenID</i>	<i>Area</i>
	5001	1		5001	1		5001	1		5001	1
	8013	2		6101	1		8008	1		6225	3
	8014	2		6102	1		8015	2		8015	2
	8012	2		6103	2		6101	1		6106	3
	8015	2		6104	2		6102	1		6108	3
	8003	1		6105	2		6103	2		6104	2
	8004	1		6106	3		6104	2		8008	1
	8007	1		6107	3		6105	2		6102	1
	8005	1		6108	3		6106	3		6101	1
	8001	1		6109	3		6107	3		8016	3
	8002	1		6110	3		6108	3		6105	2
	8008	1		8008	1		6109	3		8012	2
	8010	2		8015	2		6110	3		6109	3
	8011	2		8005	1		8005	1		6110	3
	8016	3		8006	1		8006	1		8013	2

Figure 7.1: Ranked lists of conventional generating units

As observable, each list has a strong preference towards the approx. same group of units: the nuclear unit is always at the top (highest priority to commit), but exact unit-orders after that vary. By design, MPL prefers coal units, while IPL and NPL both prefer gas ones. In case of GPW, unit-characteristics are carefully evaluated before key units are rewarded with higher priority in a certain *timestep*; this results in constantly changing lists that always best fit to prevailing system conditions.

Fig. 7.2 and Fig. 7.3 (on page 60) depict the detailed results of different PL methods, organized by the selected renewable portfolios and the investigated scenarios. As mentioned in Section 6.3, one week of data is simulated in 1-hour intervals (i.e., total 168 *timesteps*).

	<u>Modified Priority List</u>					<u>Improved Priority List</u>				
Scenario I.	Converged:	98	70	0	58.33% OPF	Converged:	96	72	0	57.14% OPF
	168 / 168	OPF	PF	NOT		168 / 168	OPF	PF	NOT	
	100%					100%				
	Total Comp. Time: 0.07 min					Total Comp. Time: 0.07 min				
	Avg. Conv. num.: 23.79		Avg. Renw.: 0%			Avg. Conv. num.: 15.64		Avg. Renw.: 0%		
	Avg. Total Op. Cost: \$ 81,860 /OPF/					Avg. Total Op. Cost: \$ 90,786 /OPF/				
Scenario II.	Converged:	168	0	0	100% OPF	Converged:	168	0	0	100% OPF
	168 / 168	OPF	PF	NOT		168 / 168	OPF	PF	NOT	
	100%					100%				
	Total Comp. Time: 6.23 min					Total Comp. Time: 8.17 min				
	Avg. Conv. num.: 30.01		Avg. Renw.: 0%			Avg. Conv. num.: 26.11		Avg. Renw.: 0%		
	Avg. Total Op. Cost: \$ 98,624 /OPF/					Avg. Total Op. Cost: \$ 108,617 /OPF/				
Scenario III.	Converged:	168	0	0	100% OPF	Converged:	168	0	0	100% OPF
	168 / 168	OPF	PF	NOT		168 / 168	OPF	PF	NOT	
	100%					100%				
	Total Comp. Time: 8.12 min					Total Comp. Time: 9.11 min				
	Avg. Conv. num.: 30.83		Avg. Renw.: 0%			Avg. Conv. num.: 26.11		Avg. Renw.: 0%		
	Avg. Total Op. Cost: \$ 98,680 /OPF/					Avg. Total Op. Cost: \$ 108,617 /OPF/				
AVERAGE	Avg. Converged:		Avg. Total Comp. Time: 4.80 min/wk			Avg. Converged:		Avg. Total Comp. Time: 5.78 min/wk		
	100% (86.11% OPF)					100% (85.71% OPF)				
	Avg. Conv. num.: 28.21		Avg. Renw.: 0%			Avg. Conv. num.: 22.62		Avg. Renw.: 0%		
	Avg. Total Op. Cost: \$ 93,055 /OPF/					Avg. Total Op. Cost: \$ 102,674 /OPF/				

(a)

	<u>New Priority List</u>					<u>GPW Factor</u>				
Scenario I.	Converged:	96	72	0	57.14% OPF	Converged:	99	69	0	58.93% OPF
	168 / 168	OPF	PF	NOT		168 / 168	OPF	PF	NOT	
	100%					100%				
	Total Comp. Time: 0.06 min					Total Comp. Time: 0.67 min				
	Avg. Conv. num.: 15.64		Avg. Renw.: 0%			Avg. Conv. num.: 17.57		Avg. Renw.: 0%		
	Avg. Total Op. Cost: \$ 90,694 /OPF/					Avg. Total Op. Cost: \$ 89,192 /OPF/				
Scenario II.	Converged:	168	0	0	100% OPF	Converged:	168	0	0	100% OPF
	168 / 168	OPF	PF	NOT		168 / 168	OPF	PF	NOT	
	100%					100%				
	Total Comp. Time: 6.93 min					Total Comp. Time: 7.54 min				
	Avg. Conv. num.: 26.11		Avg. Renw.: 0%			Avg. Conv. num.: 27.65		Avg. Renw.: 0%		
	Avg. Total Op. Cost: \$ 107,006 /OPF/					Avg. Total Op. Cost: \$ 108,283 /OPF/				
Scenario III.	Converged:	168	0	0	100% OPF	Converged:	168	0	0	100% OPF
	168 / 168	OPF	PF	NOT		168 / 168	OPF	PF	NOT	
	100%					100%				
	Total Comp. Time: 8.08 min					Total Comp. Time: 8.66 min				
	Avg. Conv. num.: 26.15		Avg. Renw.: 0%			Avg. Conv. num.: 27.65		Avg. Renw.: 0%		
	Avg. Total Op. Cost: \$ 106,962 /OPF/					Avg. Total Op. Cost: \$ 108,283 /OPF/				
AVERAGE	Avg. Converged:		Avg. Total Comp. Time: 5.02 min/wk			Avg. Converged:		Avg. Total Comp. Time: 5.62 min/wk		
	100% (85.71% OPF)					100% (86.31% OPF)				
	Avg. Conv. num.: 22.63		Avg. Renw.: 0%			Avg. Conv. num.: 24.29		Avg. Renw.: 0%		
	Avg. Total Op. Cost: \$ 101,554 /OPF/					Avg. Total Op. Cost: \$ 101,919 /OPF/				

(b)

Figure 7.2: Comparison of PL methods – *Option 1*. renewable portfolio

On the figures: “*Converged*” displays the number of *timesteps* in which PF or OPF studies ended in converged system state (i.e, the determined operational schedules were functional); the percentage of successful OPF-*timesteps* are also indicated. “*Avg. Conv. num*” displays the average number of committed conventional units. “*Avg. Renw.*” displays the average renewable penetration. “*Avg. Total Op. Cost*” displays the average total operational costs of *timesteps* throughout the simulation process.

	<u>Modified Priority List</u>				<u>Improved Priority List</u>					
Scenario I.	Converged: 168 / 168 100%	105 OPF	63 PF	0 NOT	62.50% OPF	Converged: 168 / 168 100%	105 OPF	63 PF	0 NOT	62.50% OPF
	Total Comp. Time: 0.06 min				Total Comp. Time: 0.05 min					
	Avg. Conv. num.: 19.51		Avg. Renew.: 17.24%		Avg. Conv. num.: 11.16		Avg. Renew.: 17.41%			
	Avg. Total Op. Cost: \$ 59,850 /OPF/				Avg. Total Op. Cost: \$ 69,711 /OPF/					
Scenario II.	Converged: 168 / 168 100%	168 OPF	0 PF	0 NOT	100% OPF	Converged: 168 / 168 100%	168 OPF	0 PF	0 NOT	100% OPF
	Total Comp. Time: 7.18 min				Total Comp. Time: 8.74 min					
	Avg. Conv. num.: 26.30		Avg. Renew.: 23.42%		Avg. Conv. num.: 22.99		Avg. Renew.: 22.96%			
	Avg. Total Op. Cost: \$ 75,173 /OPF/				Avg. Total Op. Cost: \$ 85,435 /OPF/					
Scenario III.	Converged: 168 / 168 100%	168 OPF	0 PF	0 NOT	100% OPF	Converged: 168 / 168 100%	168 OPF	0 PF	0 NOT	100% OPF
	Total Comp. Time: 10.72 min				Total Comp. Time: 9.73 min					
	Avg. Conv. num.: 27.79		Avg. Renew.: 23.26%		Avg. Conv. num.: 23.02		Avg. Renew.: 22.94%			
	Avg. Total Op. Cost: \$ 75,062 /OPF/				Avg. Total Op. Cost: \$ 85,392 /OPF/					
AVERAGE	Avg. Converged: 100% (87.50% OPF)		Avg. Total Comp. Time: 5.98 min/wk		Avg. Converged: 100% (87.50% OPF)		Avg. Total Comp. Time: 6.18 min/wk			
	Avg. Conv. num.: 24.53		Avg. Renew.: 21.30%		Avg. Conv. num.: 19.06		Avg. Renew.: 21.10%			
	Avg. Total Op. Cost: \$ 70,028 /OPF/				Avg. Total Op. Cost: \$ 80,179 /OPF/					

(a)

	<u>New Priority List</u>				<u>GPW Factor</u>					
Scenario I.	Converged: 168 / 168 100%	104 OPF	64 PF	0 NOT	61.90% OPF	Converged: 168 / 168 100%	105 OPF	63 PF	0 NOT	62.50% OPF
	Total Comp. Time: 0.05 min				Total Comp. Time: 0.82 min					
	Avg. Conv. num.: 11.20		Avg. Renew.: 17.34%		Avg. Conv. num.: 13.69		Avg. Renew.: 17.79%			
	Avg. Total Op. Cost: \$ 67,996 /OPF/				Avg. Total Op. Cost: \$ 65,987 /OPF/					
Scenario II.	Converged: 168 / 168 100%	168 OPF	0 PF	0 NOT	100% OPF	Converged: 168 / 168 100%	168 OPF	0 PF	0 NOT	100% OPF
	Total Comp. Time: 8.23 min				Total Comp. Time: 9.33 min					
	Avg. Conv. num.: 23.00		Avg. Renew.: 22.98%		Avg. Conv. num.: 24.76		Avg. Renew.: 23.73%			
	Avg. Total Op. Cost: \$ 82,564 /OPF/				Avg. Total Op. Cost: \$ 82,216 /OPF/					
Scenario III.	Converged: 168 / 168 100%	168 OPF	0 PF	0 NOT	100% OPF	Converged: 168 / 168 100%	168 OPF	0 PF	0 NOT	100% OPF
	Total Comp. Time: 9.03 min				Total Comp. Time: 9.98 min					
	Avg. Conv. num.: 23.23		Avg. Renew.: 22.87%		Avg. Conv. num.: 24.74		Avg. Renew.: 23.72%			
	Avg. Total Op. Cost: \$ 83,235 /OPF/				Avg. Total Op. Cost: \$ 82,263 /OPF/					
AVERAGE	Avg. Converged: 100% (87.30% OPF)		Avg. Total Comp. Time: 5.77 min/wk		Avg. Converged: 100% (87.50% OPF)		Avg. Total Comp. Time: 6.71 min/wk			
	Avg. Conv. num.: 19.14		Avg. Renew.: 21.06%		Avg. Conv. num.: 21.06		Avg. Renew.: 21.75%			
	Avg. Total Op. Cost: \$ 77,932 /OPF/				Avg. Total Op. Cost: \$ 76,822 /OPF/					

(b)

Figure 7.3: Comparison of PL methods – *Option 2.* renewable portfolio

When *Option 1.* renewable portfolio is selected (Fig. 7.2), considering all investigated scenarios, NPL and GPW perform the best. While NPL dispatches less conventional units, GPW is more successful in determining optimal operational schedules that also cost less to operate. Based on required computational time, NPL slightly outperforms GPW, especially in *Scenario I.* Regarding other methods: IPL performs quite similar to NPL, but it is slower than GPW; MPL, while both fast and quite successful at determining operational schedules, it dispatches significantly more units than other methods.

When *Option 2* renewable portfolio is selected (Fig. 7.3), considering all investigated scenarios, IPL and NPL perform the best. Both methods dispatch approx. same amount of conventional units, achieve around 21% renewable penetration, and similarly successful in determining optimal schedules. In some aspects, however, GPW outperforms them: even though it dispatches more conventional units to operate alongside the renewable ones, total operational costs are lower and achieved renewable penetrations are higher; however, required computational time is the greatest among all the methods.

The results of performed comparison experiments prove that the proposed GPW index is a consistently adequate – in some aspects a better – alternative to common PL approaches to characterize the importance of generating units. Even though the required computational time of GPW is slightly greater, obtained solutions are more optimal, especially in power systems with notable renewable penetration.

In the following benchmarking experiments, based on the above discussed performance of different methods and scenarios, an NPL based *Scenario II* PL UC method is used. Although PL UC methods are typically solved through *Scenario I* due to its computational advantageousness, as experienced, *Scenario II* is a more preferable choice as it is a good compromise between required computational time and determined schedule-optimality.

7.2 Normal System Operation

Fig. 7.4 (on page 62) and Fig. 7.5 (on page 63) depict the detailed results of different generation prioritization approaches, organized by the individual simulation processes and the selected renewable portfolios. As mentioned in Section 6.4, altogether six months of data is simulated in 1-hour intervals (i.e., total 4440 *timesteps*).

In the first group of case studies (Fig. 7.4), when *Option 2* renewable portfolio is selected, the USS method outperforms common generation prioritization approaches.

Even though both the NPL UC method and the USS method are capable of successfully determining optimal operational schedules in every *timesteps*, the former one is substantially slower. The MILP UC method, on the other hand, provides schedules that are neither feasible in many *timesteps* nor optimal in about 60% of the time; notice, however, that performance is significantly better when areal- and total system load is low. The set 20% minimum renewable generation requirement is not fulfilled by either methods in most of the months; the USS method gets the closest, with average 19.7% penetration in the five-month interval. The MILP UC method dispatches the least amount of conventional units, which results in the lowest average total operational costs at all times; the USS method dispatches about twice as many units, but at the same time achieves greater renewable penetration and schedule-optimality.

		<u>New Priority List</u>				<u>Mixed Integer Linear Programming</u>				<u>Universal Selection Scheme</u>						
LOW - LOAD	March	Converged: 744 / 744 100%	744 OPF	0 PF	0 NOT	100% OPF	Converged: 744 / 744 100%	447 OPF	297 PF	0 NOT	60.08% OPF	Converged: 744 / 744 100%	744 OPF	0 PF	0 NOT	100% OPF
			Total Comp. Time: 37.55 min				Total Comp. Time: 9.24 min				Total Comp. Time: 5.90 min					
			Avg. Conv. num.: 23.51		Avg. Renw.: 18.74%		Avg. Conv. num.: 16.69		Avg. Renw.: 18.76%		Avg. Conv. num.: 28.33		Avg. Renw.: 19.42%			
			Avg. Total Op. Cost: \$ 79,904 /OPF/				Avg. Total Op. Cost: \$ 58,672 /OPF/				Avg. Total Op. Cost: \$ 80,628 /OPF/					
	June	Converged: 720 / 720 100%	720 OPF	0 PF	0 NOT	100% OPF	Converged: 720 / 720 100%	283 OPF	437 PF	0 NOT	39.31% OPF	Converged: 720 / 720 100%	720 OPF	0 PF	0 NOT	100% OPF
			Total Comp. Time: 42.09 min				Total Comp. Time: 9.18 min				Total Comp. Time: 5.85 min					
		Avg. Conv. num.: 30.68		Avg. Renw.: 21.03%		Avg. Conv. num.: 22.45		Avg. Renw.: 15.65%		Avg. Conv. num.: 43.92		Avg. Renw.: 21.11%				
		Avg. Total Op. Cost: \$ 103,306 /OPF/				Avg. Total Op. Cost: \$ 67,048 /OPF/				Avg. Total Op. Cost: \$ 111,172 /OPF/						
October	Converged: 744 / 744 100%	744 OPF	0 PF	0 NOT	100% OPF	Converged: 744 / 744 100.00%	424 OPF	320 PF	0 NOT	56.99% OPF	Converged: 744 / 744 100%	744 OPF	0 PF	0 NOT	100% OPF	
		Total Comp. Time: 39.46 min				Total Comp. Time: 9.45 min				Total Comp. Time: 5.38 min						
		Avg. Conv. num.: 24.84		Avg. Renw.: 19.36%		Avg. Conv. num.: 18.53		Avg. Renw.: 16.37%		Avg. Conv. num.: 29.60		Avg. Renw.: 19.33%				
		Avg. Total Op. Cost: \$ 86,542 /OPF/				Avg. Total Op. Cost: \$ 63,493 /OPF/				Avg. Total Op. Cost: \$ 87,875 /OPF/						
HIGH - LOAD	July	Converged: 744 / 744 100%	744 OPF	0 PF	0 NOT	100% OPF	Converged: 740 / 744 99.46%	137 OPF	603 PF	4 NOT	18.41% OPF	Converged: 744 / 744 100%	743 OPF	1 PF	0 NOT	99.87% OPF
			Total Comp. Time: 55.05 min				Total Comp. Time: 13.67 min				Total Comp. Time: 6.80 min					
			Avg. Conv. num.: 37.89		Avg. Renw.: 19.96%		Avg. Conv. num.: 26.79		Avg. Renw.: 12.46%		Avg. Conv. num.: 52.33		Avg. Renw.: 20.09%			
			Avg. Total Op. Cost: \$ 120,643 /OPF/				Avg. Total Op. Cost: \$ 75,745 /OPF/				Avg. Total Op. Cost: \$ 131,182 /OPF/					
August	Converged: 744 / 744 100%	744 OPF	0 PF	0 NOT	100% OPF	Converged: 738 / 744 99.19%	207 OPF	531 PF	6 NOT	27.82% OPF	Converged: 744 / 744 100%	744 OPF	0 PF	0 NOT	100% OPF	
		Total Comp. Time: 48.73 min				Total Comp. Time: 20.87 min				Total Comp. Time: 6.82 min						
		Avg. Conv. num.: 35.40		Avg. Renw.: 18.56%		Avg. Conv. num.: 26.31		Avg. Renw.: 11.86%		Avg. Conv. num.: 50.13		Avg. Renw.: 18.62%				
		Avg. Total Op. Cost: \$ 118,988 /OPF/				Avg. Total Op. Cost: \$ 81,659 /OPF/				Avg. Total Op. Cost: \$ 128,445 /OPF/						
YEARLY APPROX.	Avg. Converged: 100% (100% OPF)	Avg. Total Comp. Time: 44.6 min/mo				Avg. Converged: 99.73% (40.53% OPF)	Avg. Total Comp. Time: 12.5 min/mo				Avg. Converged: 100% (99.97% OPF)	Avg. Total Comp. Time: 6.2 min/mo				
		Compared to USS: $\times 7.23$				Compared to USS: $\times 1.99$										
		Avg. Conv. num.: 30.46		Avg. Renw.: 19.53%		Avg. Conv. num.: 22.16		Avg. Renw.: 15.02%		Avg. Conv. num.: 40.86		Avg. Renw.: 19.71%				
		Avg. Total Op. Cost: \$ 101,877 /OPF/				Avg. Total Op. Cost: \$ 69,323 /OPF/				Avg. Total Op. Cost: \$ 107,860 /OPF/						

Figure 7.4: Comparison of generation prioritization methods – normal operation, *Option 2*, renewable portfolio

In the second group of case studies (Fig. 7.5), the USS method is directly compared to the MILP UC method while different renewable portfolio options are selected. As observable, the USS method outperforms the MILP UC method in almost every aspects.

Even though the MILP UC method dispatches significantly less conventional units at all times (average half as many as the USS method), which results in notably lower operational costs, the determined schedules are not optimal in more than 40% of the time. The MILP UC method takes more than twice as much time to make decisions than the USS method; considering the small size of RTS-GMLC, this is a significant difference in computational capability. Sufficient renewable generation is not available throughout the simulated month to fulfill the set minimum renewable generation requirements; both methods, however, are using as much renewable generation as possible.

		Mixed-Integer Linear Programming					Universal Selection Scheme				
MAY	Option 1.	Converged: 399 / 744 99.46%	399 OPF	341 PF	4 NOT	53.63% OPF	Converged: 744 / 744 100%	744 OPF	0 PF	0 NOT	100% OPF
	Total Comp. Time: 10.75 min					Total Comp. Time: 4.84 min					
	Avg. Conv. num.: 25.09		Avg. Renew.: 0%			Avg. Conv. num.: 37.08		Avg. Renew.: 0%			
	Avg. Total Op. Cost: \$ 87,114 /OPF/					Avg. Total Op. Cost: \$ 117,537 /OPF/					
MAY	Option 2.	Converged: 744 / 744 100%	399 OPF	345 PF	0 NOT	53.63% OPF	Converged: 744 / 744 100%	744 OPF	0 PF	0 NOT	100% OPF
	Total Comp. Time: 10.46 min					Total Comp. Time: 6.12 min					
	Avg. Conv. num.: 19.43		Avg. Renew.: 18.53%			Avg. Conv. num.: 34.53		Avg. Renew.: 22.26%			
	Avg. Total Op. Cost: \$ 62,737 /OPF/					Avg. Total Op. Cost: \$ 93,458 /OPF/					
MAY	Option 3.	Converged: 744 / 744 100%	483 OPF	261 PF	0 NOT	64.92% OPF	Converged: 744 / 744 100%	744 OPF	0 PF	0 NOT	100% OPF
	Total Comp. Time: 15.89 min					Total Comp. Time: 5.95 min					
	Avg. Conv. num.: 16.05		Avg. Renew.: 36.77%			Avg. Conv. num.: 31.25		Avg. Renew.: 35.36%			
	Avg. Total Op. Cost: \$ 48,694 /OPF/					Avg. Total Op. Cost: \$ 78,944 /OPF/					
MAY	Option 4.	Converged: 744 / 744 100%	472 OPF	272 PF	0 NOT	63.44% OPF	Converged: 744 / 744 100%	744 OPF	0 PF	0 NOT	100% OPF
	Total Comp. Time: 10.73 min					Total Comp. Time: 6.03 min					
	Avg. Conv. num.: 15.47		Avg. Renew.: 39.07%			Avg. Conv. num.: 31.01		Avg. Renew.: 36.82%			
	Avg. Total Op. Cost: \$ 46,289 /OPF/					Avg. Total Op. Cost: \$ 77,661 /OPF/					
YEARLY APPROX.	Avg. Converged: 99.87% (58.90% OPF)					Avg. Converged: 100% (100% OPF)					
Avg. Total Comp. Time: 12.0 min/mo					Avg. Total Comp. Time: 5.7 min/mo						
Avg. Conv. num.: 19.01					Avg. Conv. num.: 33.47						
Avg. Renew.: 23.59%					Avg. Renew.: 23.61%						
Avg. Total Op. Cost: \$ 61,208 /OPF/					Avg. Total Op. Cost: \$ 91,900 /OPF/						

Figure 7.5: Comparison of MILP UC and USS methods – normal operation, variable renewable portfolio

7.3 Cascadia Subduction Zone Event

Fig. 7.6 (on page 64) and Fig. 7.7 (on page 65) depict the detailed results of different generation prioritization approaches, organized by the phases of the ongoing restoration process and the selected renewable portfolios. As discussed in Chapter 5 and Section 6.1, available renewable generating units are enabled to generate their full potential by default, and conventional units are selected to be placed in operation alongside them using one of the implemented methods. As mentioned in Section 6.4, two weeks of data is simulated in 5-minute intervals (i.e., total 4032 *timesteps*).

In the first group of case studies (Fig. 7.6), when *Option 2.* renewable portfolio is selected, the USS method similarly outperforms common generation prioritization approaches as it did during normal system operation (see Section 7.2).

Even though the NPL UC method is equally successful at determining optimal operational schedules in every *timesteps* as the USS method, it is almost 2.5 times slower; also, although less conventional units are dispatched, yet the average total operational costs are approximately the same or slightly higher. The MILP UC method, on the other hand, is not able to provide optimal operational schedules in about 40% of the time; also, while it dispatches the least amount of units, which results in the lowest average total operational costs at all times, it is 1.4 times slower than the USS method. As expected, prioritization approaches become faster as the size of the system (and number of dispatchable units) is

reduced; this is especially true to the MILP UC method. The set 20% minimum renewable generation requirement is mostly fulfilled by all methods: average renewable penetration during the simulation process is around 22%.

	<u>New Priority List</u>	<u>Mixed Integer Linear Programming</u>	<u>Universal Selection Scheme</u>
Normal operation	Converged: 252 0 0 100% OPF 252 / 252 100% Total Comp. Time: 2.41 min Avg. Conv. num.: 9.06 Avg. Renew.: 24.47% Avg. Total Op. Cost: \$ 64,237 /OPF/	Converged: 241 11 0 95.63% OPF 252 / 252 100% Total Comp. Time: 3.41 min Avg. Conv. num.: 15.96 Avg. Renew.: 24.37% Avg. Total Op. Cost: \$ 57,264 /OPF/	Converged: 252 0 0 100% OPF 252 / 252 100% Total Comp. Time: 1.73 min Avg. Conv. num.: 14.21 Avg. Renew.: 24.40% Avg. Total Op. Cost: \$ 64,333 /OPF/
CSZ earthquake event	Converged: 720 0 0 100% OPF 720 / 720 100% Total Comp. Time: 5.08 min Avg. Conv. num.: 6.32 Avg. Renew.: 29.60% Avg. Total Op. Cost: \$ 30,029 /OPF/	Converged: 418 302 0 58.06% OPF 720 / 720 100% Total Comp. Time: 3.34 min Avg. Conv. num.: 4.24 Avg. Renew.: 27.01% Avg. Total Op. Cost: \$ 25,218 /OPF/	Converged: 720 0 0 100% OPF 720 / 720 100% Total Comp. Time: 4.02 min Avg. Conv. num.: 12.08 Avg. Renew.: 27.98% Avg. Total Op. Cost: \$ 33,886 /OPF/
Phase I. restoration	Converged: 1548 0 0 100% OPF 1548 / 1548 100% Total Comp. Time: 27.98 min Avg. Conv. num.: 12.47 Avg. Renew.: 21.57% Avg. Total Op. Cost: \$ 49,954 /OPF/	Converged: 932 616 0 60.21% OPF 1548 / 1548 100% Total Comp. Time: 11.52 min Avg. Conv. num.: 7.35 Avg. Renew.: 25.41% Avg. Total Op. Cost: \$ 34,665 /OPF/	Converged: 1548 0 0 100% OPF 1548 / 1548 100% Total Comp. Time: 9.38 min Avg. Conv. num.: 14.70 Avg. Renew.: 24.12% Avg. Total Op. Cost: \$ 48,219 /OPF/
Phase II. restoration	Converged: 1512 0 0 100% OPF 1512 / 1512 100% Total Comp. Time: 36.19 min Avg. Conv. num.: 16.75 Avg. Renew.: 18.24% Avg. Total Op. Cost: \$ 65,372 /OPF/	Converged: 826 686 0 54.63% OPF 1512 / 1512 100% Total Comp. Time: 13.55 min Avg. Conv. num.: 12.45 Avg. Renew.: 16.28% Avg. Total Op. Cost: \$ 49,502 /OPF/	Converged: 1512 0 0 100% OPF 1512 / 1512 100% Total Comp. Time: 8.67 min Avg. Conv. num.: 19.76 Avg. Renew.: 18.10% Avg. Total Op. Cost: \$ 64,493 /OPF/
TOTAL	Total Converged: Total Comp. Time: 71.66 min 100% (100% OPF) Compared to USS: $\times 2.45$ Avg. Conv. num.: 12.76 Avg. Renew.: 21.94% Avg. Total Op. Cost: \$ 53,070.68 /OPF/	Total Converged: Total Comp. Time: 31.82 min 100% (59.95% OPF) Compared to USS: $\times 1.40$ Avg. Conv. num.: 9.24 Avg. Renew.: 22.21% Avg. Total Op. Cost: \$ 39,954.55 /OPF/	Total Converged: Total Comp. Time: 23.80 min 100% (100% OPF) Avg. Conv. num.: 16.10 Avg. Renew.: 22.57% Avg. Total Op. Cost: \$ 52,769.63 /OPF/

Figure 7.6: Comparison of generation prioritization methods – CSZ event, *Option 2*. renewable portfolio

In the second group of case studies (Fig. 7.7), the USS method is directly compared to the MILP UC method while *Option 4*. renewable portfolio is selected. As observable, in this high renewable penetration environment, the USS method one again outperforms the MILP UC.

The MILP UC method, as it did during normal system operation (see Section 7.2), dispatches significantly less conventional units (by average half as much as the USS method) that results in notably lower operational costs. On the other hand, determined schedules are non-feasible in some *timesteps* and not optimal in more than 40% of the time. The USS method is about 1.5 times faster during the simulation process, and is able to provided optimal operational schedules at all times. Neither method is able to achieve the set minimum renewable generation requirement (average renewable penetration is aimed to be greater than 64%) as enough renewable generation is not available due to the reduced size of the system.

	Mixed Integer Linear Programming					Universal Selection Scheme				
Normal operation	Converged:	224	28	0	88.89% OPF	Converged:	252	0	0	100% OPF
	252 / 252	OPF	PF	NOT		252 / 252	OPF	PF	NOT	
	100%					100%				
	Total Comp. Time: 3.20 min					Total Comp. Time: 1.77 min				
	Avg. Conv. num.: 10.90		Avg. Renw.: 51.68%			Avg. Conv. num.: 12.30		Avg. Renw.: 49.03%		
	Avg. Total Op. Cost: \$ 32,484 /OPF/					Avg. Total Op. Cost: \$ 44,949 /OPF/				
CSZ earthquake event	Converged:	328	392	0	45.56% OPF	Converged:	720	0	0	100% OPF
	720 / 720	OPF	PF	NOT		720 / 720	OPF	PF	NOT	
	100%					100%				
	Total Comp. Time: 3.56 min					Total Comp. Time: 3.54 min				
	Avg. Conv. num.: 2.17		Avg. Renw.: 70.72%			Avg. Conv. num.: 12.46		Avg. Renw.: 51.20%		
	Avg. Total Op. Cost: \$ 9,547 /OPF/					Avg. Total Op. Cost: \$ 26,436 /OPF/				
Phase I. restoration	Converged:	916	630	2	59.17% OPF	Converged:	1548	0	0	100% OPF
	1546 / 1548	OPF	PF	NOT		1548 / 1548	OPF	PF	NOT	
	99.87%					100%				
	Total Comp. Time: 11.30 min					Total Comp. Time: 7.71 min				
	Avg. Conv. num.: 5.45		Avg. Renw.: 52.84%			Avg. Conv. num.: 13.20		Avg. Renw.: 42.53%		
	Avg. Total Op. Cost: \$ 23,122 /OPF/					Avg. Total Op. Cost: \$ 38,337 /OPF/				
Phase II. restoration	Converged:	925	587	0	61.18% OPF	Converged:	1512	0	0	100% OPF
	1512 / 1512	OPF	PF	NOT		1512 / 1512	OPF	PF	NOT	
	100%					100%				
	Total Comp. Time: 12.72 min					Total Comp. Time: 8.92 min				
	Avg. Conv. num.: 10.47		Avg. Renw.: 33.80%			Avg. Conv. num.: 16.31		Avg. Renw.: 30.75%		
	Avg. Total Op. Cost: \$ 40,507 /OPF/					Avg. Total Op. Cost: \$ 54,462 /OPF/				
TOTAL	Total Converged:		Total Comp. Time: 30.78 min			Total Converged:		Total Comp. Time: 21.94 min		
	99.95% (59.35% OPF)		Compared to USS: $\times 1.43$			100% (100% OPF)				
	Avg. Conv. num.: 7.09		Avg. Renw.: 48.82%			Avg. Conv. num.: 14.18		Avg. Renw.: 40.07%		
	Avg. Total Op. Cost: \$ 27,802.38 /OPF/					Avg. Total Op. Cost: \$ 42,671.86 /OPF/				

Figure 7.7: Comparison of MILP UC and USS methods – CSZ event, *Option 4.* renewable portfolio

7.4 Geomagnetic Disturbance Event

Fig. 7.8 (on page 66) and Fig. 7.9 (on page 66) depict the detailed results of different generation prioritization approaches, organized by the individual simulation processes. As mentioned in Section 6.4, altogether five hours of data is simulated in 5-minute intervals (i.e., total 60 *timesteps*).

In the first group of case studies (Fig. 7.8), when the most intense hour of the Halloween storm (October 30th, 7:30pm to 8:30pm) is simulated, and *Option 2.* renewable portfolio is selected, the USS method similarly outperforms common generation prioritization approaches as it did during normal system operation (see Section 7.2) and the hypothetical Cascadia Subduction Zone event (see Section 7.3).

Even though the NPL UC method is equally successful at determining optimal operational schedules in every *timesteps* as the USS method, it is more than 4 times slower. The MILP UC method, on the other hand, is not able to provide optimal operational schedules in about 40% of the time; furthermore, it is twice as slow than the USS method. All three methods dispatch the approximately same amount of conventional units, so the average total operational costs are approximately the same.

		<u>New Priority List</u>					<u>Mixed Integer Linear Programming</u>					<u>Universal Selection Scheme</u>					
GMD event	Converged:	12	0	0	100% OPF	Converged:	7	5	0	58.33% OPF	Converged:	12	0	0	100% OPF		
	12 / 12	OPF	PF	NOT		12 / 12	OPF	PF	NOT		12 / 12	OPF	PF	NOT			
	100%					100%					100%						
			Total Comp. Time:			0.43 min			Total Comp. Time:			0.20 min			Total Comp. Time:		
		Avg. Conv. num.: 20.17			Avg. Renw.: 10.97%			Avg. Conv. num.: 18.33			Avg. Renw.: 8.03%			Avg. Conv. num.: 19.17			Avg. Renw.: 12.31%
		Avg. Total Op. Cost: \$ 92,011 /OPF/					Avg. Total Op. Cost: \$ 78,653 /OPF/					Avg. Total Op. Cost: \$ 85,618 /OPF/					

Figure 7.8: Comparison of generation prioritization methods – Most intense hour of the Halloween storm GMD event, *Option 2*. renewable portfolio

In the second group of case studies (Fig. 7.9), when the 10 times intensified evening of October 30th (from 6pm to 10pm) is simulated, and *Option 2*. renewable portfolio is selected, the performance of the three methods are quite similar.

All generation prioritization method are capable of successfully determining optimal operational schedules in every *timesteps*. Furthermore, both the NPL UC method and the USS method are equally fast, about twice as the MILP UC method. Based on average total operational costs, the MILP UC method performs the best, regardless of the fact that it dispatches twice as much units as the otherwise outstanding NPL UC method.

		<u>New Priority List</u>					<u>Mixed Integer Linear Programming</u>					<u>Universal Selection Scheme</u>					
GMD event	Converged:	48	0	0	100% OPF	Converged:	48	0	0	100% OPF	Converged:	48	0	0	100% OPF		
	48 / 48	OPF	PF	NOT		48 / 48	OPF	PF	NOT		48 / 48	OPF	PF	NOT			
	100%					100%					100%						
			Total Comp. Time:			0.21 min			Total Comp. Time:			0.40 min			Total Comp. Time:		
		Avg. Conv. num.: 6.21			Avg. Renw.: 12.38%			Avg. Conv. num.: 12.04			Avg. Renw.: 12.48%			Avg. Conv. num.: 13.15			Avg. Renw.: 12.48%
		Avg. Total Op. Cost: \$ 51,371 /OPF/					Avg. Total Op. Cost: \$ 47,673 /OPF/					Avg. Total Op. Cost: \$ 52,516 /OPF/					

Figure 7.9: Comparison of generation prioritization methods – Intensified evening of the Halloween storm GMD event, *Option 2*. renewable portfolio

Chapter 8: Conclusion

8.1 Evaluation of Results

Performed benchmarking and validation experiments provide sufficient evidence to prove and support the formed hypotheses (see Section 1.3). Hypothesis I. stated that the proposed GPW index is more adequate, relative to common approaches, to characterize the importance of generating units in any given system state; this has been verified, and experiments (see Section 7.1) have also shown it to be a better alternative in certain aspects. Hypothesis II. stated that the proposed USS method, in power systems with significant renewable penetration, during time-sensitive system restoration, is a faster, more adequate technique to determine the optimal operational schedule of generating units, than common approaches; this has been verified, and experiments (see Sections 7.2, 7.3, and 7.4) have demonstrated its convenient, efficient, and diverse usability under various circumstances.

It can be concluded, that the proposed USS method proved to be a fast, efficient and convenient tool under various circumstances. It is advised to be utilized during time-sensitive restoration to rapidly plan the operational schedule of generating units in a power system.

8.2 Performance Scalability

An important characteristic of the proposed USS method is its low computational costs. To further prove its advantageousness over common approaches, its performance and scalability must be analyzed in more detail. Based on performed and presented method validation experiments (see Section 7), Fig. 8.1 (on page 68) and Fig. 8.2 (on page 68) scatter plot diagrams can be prepared. The day of May 5th is simulated in 5-minute intervals (i.e., total 288 *timesteps*), and *Option 4*. renewable portfolio is selected (see Section 3.4).

Fig. 8.1 depicts the required total computational times of the 288 *timesteps*, depending on the total number of generating units that need to be prioritized and dispatched by the USS method. The blue dots represent the cases when the USS method is able to determine the optimal operational schedules for all generating units in every single *timesteps*. The orange dots represent the cases when the USS method is not able to plan feasible operational schedules; this happens either due to the small size of the power system, or due to the lack of generating units in certain cases.

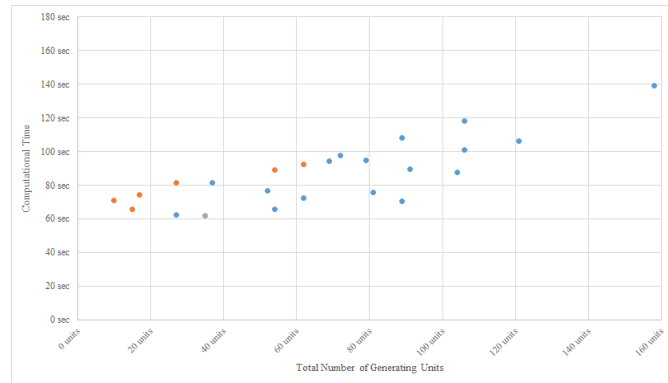


Figure 8.1: Performance of the USS method depending on the number of generating units

Fig. 8.2 is a slightly modified version of Fig. 8.1; solely the cases with 100% optimal operational schedules are depicted, and the x axis is changed to logarithmic scale. A curve was fitted in order to be able to make judgements regarding the scalability of the USS method's performance. Based on the shape of the curve, the computational costs are polynomial; the increase in solution time is somewhere between linear and exponential. It can be concluded, that the USS method would perform well and quite fast in large power system, where the number of variables (i.e., generating units) are significantly greater.

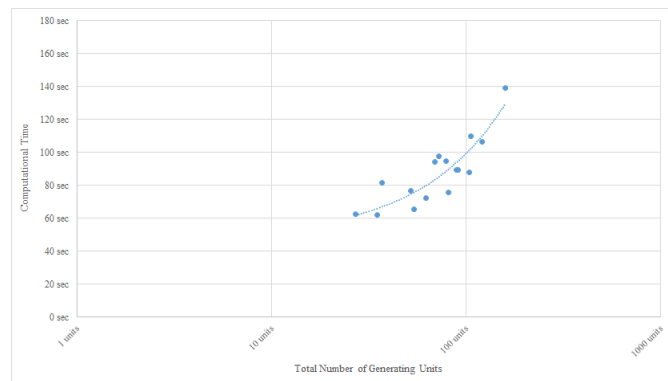


Figure 8.2: Performance scalability of the USS method

Bibliography

- [1] A. Mate, T. Hagan, E. Cotilla-Sanchez, T. K. A. Brekken, and A. von Joanne. Impacts of Earthquakes on Electrical Grid Resilience. In *Proceedings of the 2021 IEEE/IAS 57th Industrial and Commercial Power Systems Technical Conference*, Apr. 2021. <https://arxiv.org/abs/2101.07928>.
- [2] A. Mate, A. K. Barnes, R. W. Bent, and E. Cotilla-Sanchez. Analyzing and Mitigating the Impacts of GMD and EMP Events on the Electrical Grid with PowerModels-GMD.jl, Jan. 2021. <https://arxiv.org/abs/2101.05042>. LA-UR-19-29623.
- [3] P. Cicilio, D. Glennon, A. Mate, A. Barnes, V. Chalishazar, E. Cotilla-Sanchez, B. Vaagensmith, J. Gentle, C. Rieger, R. Wies, and M. H. Kapourchali. Resilience in an Evolving Electrical Grid. *Multidisciplinary Digital Publishing Institute – Energies – Special Issue: Advances in Methods and Metrics for Power Systems, from Reliability to Resilience*, 14(3):1–25, Jan. 2021. LA-UR-20-29808.
- [4] A. Schultz, S. Murphy, E. Cotilla-Sanchez, N. Imamura, A. Mate, and A. Barnes. Fusing Magnetotelluric, Magnetic Observatory and Power Grid Sensor Data with Real-Time Power Flow Analysis: Providing Actionable Information to Mitigate Risk to the Power Grid from Geomagnetic Disturbances/EMP. In *Technical Presentation at the American Geophysical Union 2019 Fall Meeting*, Dec. 2019.
- [5] A. Mate and E. Cotilla-Sanchez. Rapid Method for Generation Prioritization during System Restoration with Renewable Resources. In *Proceedings of the 2019 IEEE/IAS 55th Industrial and Commercial Power Systems Technical Conference*, Jun. 2019. <https://arxiv.org/abs/2101.06355>.
- [6] Cascadia Region Earthquake Workgroup. Cascadia Subduction Zone Earthquakes: A Magnitude 9.0 Earthquake Scenario. <https://www.dnr.wa.gov>, Sep. 2013. [Accessed: Jun. 5, 2021].
- [7] P. Cannon et al. Extreme Space Weather: Impacts on Engineered Systems and Infrastructure. Technical report, Royal Academy of Engineering, Feb. 2013. [Accessed: Jun. 5, 2021].
- [8] C. Barrows, A. Bloom, A. Ehlen, J. Ikaheimo, J. Jorgenson, D. Krishnamurthy, J. Lau, B. McBennett, M. O’Connell, E. Preston, A. Staid, G. Stephen, and J-P. Watson. The IEEE Reliability Test System: A Proposed 2019 Update. *IEEE Transactions on Power Systems*, 35(1):119–127, Jan. 2020.
- [9] R. Horton. Magnetohydrodynamic Electromagnetic Pulse Assessment of the Continental U.S. Electric Grid: Geomagnetically Induced Current and Transformer Thermal Analysis. Technical report, Electric Power Research Institute, Feb. 2017.

- [10] A. K. Barnes. PowerModelsGMD: An Open-Source Framework for Analyzing the Impact of Geomagnetic Disturbances and High-Altitude Electromagnetic Pulse E3 Impact on Bulk Transmission Systems Based on PowerModels.jl. In *Proceedings of the 2019 87th Military Operations Research Society Symposium*, Jun. 2019.
- [11] NERC. High-Impact, Low-Frequency Event Risk to the North American Bulk Power System. Technical report, North American Electric Reliability Corporation, Jun. 2010. [Accessed: Jun. 5, 2021].
- [12] U.S. Congress. Critical Infrastructures Protection Act of 2001. <https://www.congress.gov>, Sep. 2001. [Accessed: Jun. 5, 2021].
- [13] U.S. Department of Homeland Security. Homeland Security Presidential Directive 7: Critical Infrastructure Identification, Prioritization, and Protection. <https://www.cisa.gov>, Sep. 2015. [Accessed: Jun. 5, 2021].
- [14] DOE. Framework for Modeling High-Impact, Low-Frequency Power Grid Events to Support Risk-Informed Decisions. Technical report, Pacific Northwest National Laboratory and U.S. Department of Energy, Dec. 2015. [Accessed: Jun. 5, 2021].
- [15] J. Torres. An Overview of Threats to the Power Grid. Technical report, Sandia National Laboratories, May 2015. [Accessed: Jun. 5, 2021].
- [16] OSSPAC. The Oregon Resilience Plan: Reducing Risk and Improving Recovery for the Next Cascadia Earthquake and Tsunami. Technical report, Oregon Seismic Safety Policy Advisory Commission, Feb. 2013. [Accessed: Jun. 5, 2021].
- [17] J. Kappenman. Geomagnetic Storms and Their Impacts on the U.S. Power Grid. Technical report, Metatech Corporation, Jan. 2010. [Accessed: Jun. 5, 2021].
- [18] DOE. Economic Benefits of Increasing Electric Grid Resilience to Weather Outages. Technical report, U.S. White House and the U.S. Department of Energy, Aug. 2013. [Accessed: Jun. 5, 2021].
- [19] P. H. Larsen, K. H. LaCommare, J. H. Eto, and J. L. Sweeney. Assessing Changes in the Reliability of the U.S. Electric Power System. Technical report, Lawrence Berkeley National Laboratory and Stanford University, Aug. 2015. [Accessed: Jun. 5, 2021].
- [20] M. M. Adibi, L. H. Fink, C. J. Andrews, F. Arsanjani, M. W. Lanier, J. M. Miller, T. A. Volkman, and J. Wrubel. Special Considerations in Power System Restoration. *IEEE Transactions on Power Systems*, 7(4):1419–1427, Nov. 1992.
- [21] M. M. Adibi and L. H. Fink. Power System Restoration Planning. *IEEE Transactions on Power Systems*, 9(1):22–28, Feb. 1994.
- [22] M. M. Adibi and N. Martins. Power System Restoration Dynamics Issues. In *Proceedings of the 2008 IEEE Power and Energy Society General Meeting*, Jul. 2008.
- [23] Y. Liu, R. Fan, and V. Terzija. Power System Restoration: A Literature Review from 2006 to 2016. *Journal of Modern Power Systems and Clean Energy*, 4(0):332–341, Jul. 2019.

- [24] J.D. Willson. System Restoration Guidelines: How to Set-Up, Conduct, and Evaluate a Drill. *IEEE Transactions on Power Systems*, 11(3):1619–1629, Aug. 1996.
- [25] Y. Hou, C.-C. Liu, P. Zhang, and K. Sun. Constructing Power System Restoration Strategies. In *Proceedings of the 2009 IEEE International Conference on Electrical and Electronics Engineering*, Nov. 2009.
- [26] T. Kostic, R. Cherkaoui, A. Germond, and P. Pruvot. Decision Aid Function for Restoration of Transmission Power Systems: Conceptual Design and Real Time Considerations. *IEEE Transactions on Power Systems*, 13(3):923–929, Aug. 1998.
- [27] F. Qiu and P. Li. An Integrated Approach for Power System Restoration Planning. *Proceedings of the IEEE*, 105(7):1234–1252, Jul. 2017.
- [28] A. Golshani, W. Sun, Q. Zhou, Q. P. Zheng, and J. Tong. Two-Stage Adaptive Restoration Decision Support System for a Self-Healing Power Grid. *IEEE Transactions on Industrial Informatics*, 13(6):2802–2812, Dec. 2017.
- [29] A. Golshani, W. Sun, and K. Sun. Advanced Power System Partitioning Method for Fast and Reliable Restoration: Toward a Self-Healing Power Grid. *IET Generation Transmission & Distribution*, 12(1):42–52, Jan. 2018.
- [30] Peak Reliability. Reliability Coordinator Area Restoration Plan. <https://www.nerc.com>, Jun. 2016. [Accessed: Jun. 5, 2021].
- [31] PJM System Operations Division. System Restoration. <https://www.pjm.com>, Jun. 2016. [Accessed: Jun. 5, 2021].
- [32] Midcontinent Independent System Operator. Power System Restoration Plan. <https://www.misoenergy.org>, Mar. 2017. [Accessed: Jun. 5, 2021].
- [33] California Independent System Operator. Reliability Coordinator Area Restoration Plan. <http://www.caiso.com>, May 2021. [Accessed: Jun. 5, 2021].
- [34] ACE. Lifeline Report No. 1: Systems at Risk from Earthquakes, Hydroelectric Power Plant Facilities. Technical report, U.S. Army Corps of Engineers, Sep. 1994. [Accessed: Jun. 5, 2021].
- [35] J. J. Ancona. A Framework for Power System Restoration Following a Major Power Failure. *IEEE Transactions on Power Systems*, 10(3):1480–1485, Aug. 1995.
- [36] S. Abbasi, M. Barati, and G. Lim. Robust Optimization on Power System Restoration Following a Hurricane. In *Proceedings of the 2018 Institute of Industrial Systems Engineers Annual Conference*, May 2018.
- [37] U.S. Energy Information Administration. Renewable Energy Explained. <https://www.eia.gov>, 2018. [Accessed: Jun. 5, 2021].
- [38] ACRE. The Role of Renewable Energy in National Security. Technical report, American Council on Renewable Energy, Oct. 2018. [Accessed: Jun. 5, 2021].

- [39] H. Zhu and Y. Liu. Aspects of Power System Restoration Considering Wind Farms. In *Proceedings of the 2012 IEEE International Conference on Sustainable Power Generation and Supply*, Sep. 2012.
- [40] L. Seca, H. Costa, C. L. Moreira, and J. A. P. Lopes. An Innovative Strategy for Power System Restoration using Utility Scale Wind Parks. In *Proceedings of the 2013 IEEE IREP Symposium-Bulk Power System Dynamics and Control*, Aug. 2013.
- [41] J. Sprooten, T. Gunst, C. Mestdag, and O. Bronckart. Power System Restoration with High Penetration Level of Renewable Generation. In *Proceedings of the 2014 IEEE Saudi Arabia Smart Grid Conference*, Dec. 2014.
- [42] A. M. El-Zonkoly. Renewable Energy Sources for Complete Optimal Power System Black-Start Restoration. *IET Generation Transmission & Distribution*, 9(6):531–539, Apr. 2015.
- [43] H. Becker, A. Naranovich, T. Hennig, A. Akbulut, D. Mende, S. Stock, and L. Hofmann. System Restoration using VSC-HVDC Connected Offshore Wind Power Plant as Black-Start Unit. In *Proceedings of the 2017 IEEE European Conference on Power Electronics and Applications*, Sep. 2017.
- [44] A. Golshani, W. Sun, Q. Zhou, Q. P. Zheng, J. Wang, and F. Qiu. Coordination of Wind Farm and Pumped-Storage Hydro for a Self-Healing Power Grid. *IEEE Transactions on Sustainable Energy*, 9(4):1910–1920, Oct. 2018.
- [45] A. Golshani, W. Sun, Q. Zhou, Q. P. Zheng, and Y. Hou. Incorporating Wind Energy in Power System Restoration Planning. *IEEE Transactions on Smart Grid*, 10(1):16–28, Jan. 2019.
- [46] P. Scruggs and B. F. Gibbon. The Oregon Talent Plan: A Needs Assessment for Professional and Technical Occupations. <https://www.oregon.gov>, Nov. 2015. [Accessed: Jun. 5, 2021].
- [47] Washington and Oregon Whole Community Exercise Design Committee. Cascadia Subduction Zone Catastrophic Earthquake and Tsunami. <https://www.oregon.gov>, Jan. 2015. [Accessed: Jun. 5, 2021].
- [48] C. Goldfinger, C. H. Nelson, A. E. Morey, J. E. Johnson, J. R. Patton, E. Karabanov, J. Gutiérrez-Pastor, A. T. Eriksson, E. Gràcia, G. Dunhill, R. J. Enkin, A. Dallimore, and T. Vallier. Turbidite Event History – Methods and Implications for Holocene Paleoseismicity of the Cascadia Subduction Zone. *U.S. Geological Survey Professional Paper*, 1661(F):1–184, 2012.
- [49] State of Oregon Building Codes Division. Earthquake Design History – A Summary of Requirements in the State of Oregon. <https://www.oregon.gov>, Feb. 2012. [Accessed: Jun. 5, 2021].
- [50] V. D. Albertson, J. M. Thorson Jr., R. E. Clayton, and S. C. Tripathy. Solar-Induced-Currents in Power Systems. *IEEE Transactions on Power Apparatus and Systems*, PAS-92(2):471–477, Mar. 1973.

- [51] D. H. Boteler, , and R. J. Pirjola. Modeling Geomagnetically Induced Currents. *Space Weather*, 15(1):258–276, Jan. 2017.
- [52] R. Pirjola. Geomagnetically Induced Currents During Magnetic Storms. *IEEE Transactions on Plasma Science*, 28(6):1867–1873, Dec. 2000.
- [53] V. D. Abertson, J. M. Thorson Jr., and S. Miske. The Effects of Geomagnetic Storms on Electrical Power Systems. *IEEE Transactions on Power Apparatus and Systems*, 93(4):1031–1044, Jul. 1974.
- [54] K. S. Shetve, A. B. Birchfield, R. H. Lee, T. J. Overbye, and J. L. Gannon. Impact of 1D vs 3D Earth Conductivity Based Electric Fields on Geomagnetically Induced Currents. In *Proceedings of the 2018 IEEE PES Innovative Smart Grid Technologies Conference Europe*, Oct. 2018.
- [55] T. R. Hutchins and T. J. Overbye. The Effect of Geomagnetic Disturbances on the Electric Grid and Appropriate Mitigation Strategies. In *Proceedings of the 2011 North American Power Symposium*, Aug. 2011.
- [56] J. Berge, L. Marti, and R. K. Varma. Modeling and Mitigation of Geomagnetically Induced Currents on a Realistic Power System Network. In *Proceedings of the 2011 Electrical Power and Energy Conference*, Oct. 2011.
- [57] T. J. Overbye, K. S. Shetye, T. R. Hutchins, Q. Qiu, and J. D. Weber. Power Grid Sensitivity Analysis of Geomagnetically Induced Currents. *IEEE Transactions on Power Systems*, 28(4):4821–4828, 2013.
- [58] NERC. Effects of Geomagnetic Disturbances on the Bulk Power System System. Technical report, North American Electric Reliability Corporation, Feb. 2012. [Accessed: Jun. 5, 2021].
- [59] K. S. Shetye and T. J. Overbye. Modeling and Analysis of GMD Effects on Power Systems: An Overview of the Impact on Large-Scale Power Systems. *IEEE Electrification Magazine*, 3(4):13–21, Dec. 2015.
- [60] NERC. Computing Geomagnetically-Induced Current in the Bulk-Power System. Technical report, North American Electric Reliability Corporation, Dec. 2013. [Accessed: Jun. 5, 2021].
- [61] I. A. Erinmez, J. G. Kappenman, and W. A. Radasky. Management of the Geomagnetically Induced Current Risks on the National Grid Company’s Electric Power Transmission System. *Journal of Atmospheric and Solar-Terrestrial Physics*, 64(5):743–756, Apr. 2002.
- [62] Q. Qiu, J. A. Fleeman, and D. R. Ball. Geomagnetic Disturbance: A Comprehensive Approach by American Electric Power to Address the Impacts. *IEEE Electrification Magazine*, 3(4):22–33, Dec. 2015.
- [63] T. R. Hutchins and T. J. Overbye. Power Flow Studies in the Presence of Geomagnetically Induced Currents. In *Proceedings of the 2012 IEEE Power and Energy Conference at Illinois*, Feb. 2012.

- [64] T. J. Overbye, T. R. Hutchins, K. Shetye, J. Weber, and S. Dahman. Integration of Geomagnetic Disturbance Modeling Into the Power Flow. In *Proceedings of the 2012 North American Power Symposium*, Sep. 2012.
- [65] M. Kazerooni, H. Zhu, T. J. Overbye, and D. A. Wojtczak. Transmission System Geomagnetically Induced Current Model Validation. *IEEE Transactions on Power Systems*, 32(3):2183–2192, May. 2017.
- [66] C. Klauber, G. P. Juvekar, K. Davis, T. Overbye, and K. Shetye. Potential for a GIC-inclusive State Estimator. In *Proceedings of the 2018 North American Power Symposium*, Sep. 2018.
- [67] G. P. Juvekar and K. Davis. MATGMD: A Tool for Enabling GMD Studies in MATLAB. In *Proceedings of the 2019 IEEE Texas Power and Energy Conference*, Feb. 2019.
- [68] PowerWorld Corp. PowerWorld[®]. <https://www.powerworld.com>, 2019. [Accessed: Jun. 5, 2021].
- [69] Siemens. PSS[®]E. <https://new.siemens.com>, 2019. [Accessed: Jun. 5, 2021].
- [70] L. Bolduc, M. Granger, G. Pare, J. Saintonge, and L. Brophy. Development of a DC Current-Blocking Device for Transformer Neutrals. *IEEE Transactions on Power Delivery*, 20(1):163–168, Jan. 2005.
- [71] H. Zhu and T. J. Overbye. Blocking Device Placement for Mitigating the Effects of Geomagnetically Induced Currents. *IEEE Transactions on Power Systems*, 30(4):2081–2089, Jul. 2015.
- [72] B. Kovan and F de Leon. Mitigation of Geomagnetically Induced Currents by Neutral Switching. *IEEE Transactions on Power Delivery*, 30(4):1999–2006, Aug. 2015.
- [73] R. Girgis, K. Vedante, and G. Burden. A Process for Evaluating the Degree of Susceptibility of a Fleet of Power Transformers to Effects of GIC. In *Proceedings of the 2014 IEEE PES T&D Conference and Exposition*, Jul. 2014.
- [74] L. Marti, A. Rezaei-Zare, and A. Narang. Simulation of Transformer Hotspot Heating due to Geomagnetically Induced Currents. *IEEE Transactions on Power Delivery*, 28(1):320–327, Jan. 2013.
- [75] J. Bezanson, S. Karpinski, V. B. Shah, and A. Edelman. Julia: A Fast Dynamic Language for Technical Computing. <https://julialang.org>, 2012.
- [76] C. Coffrin, R. Bent, K. Sundar, Y. Ng, and M. Lubin. PowerModels.jl: An Open-Source Framework for Exploring Power Flow Formulations. In *Proceedings of the 2018 Power Systems Computation Conference*, Jun. 2018.
- [77] Institute of Electrical and Electronics Engineers Working Group. Common Format For Exchange of Solved Load Flow Data. *IEEE Transactions on Power Apparatus and Systems*, 92(6):1916–1925, Nov. 1973.

- [78] R. D. Zimmerman, C. E. Murillo-Sánchez, and R. J. Thomas. MATPOWER: Steady-State Operations, Planning and Analysis Tools for Power Systems Research and Education. *IEEE Transactions on Power Systems*, 26(1):12–19, Feb. 2011.
- [79] University of Washington. Power Systems Test Case Archive. <http://labs.ece.uw.edu>. [Accessed: Jun. 5, 2021].
- [80] University of Illinois – Information Trust Institute – Center for a Smarter Electric Grid. Power Cases. <https://icseg.iti.illinois.edu>. [Accessed: Jun. 5, 2021].
- [81] University of Edinburgh. Power Systems Test Case Archive. <https://www.maths.ed.ac.uk>. [Accessed: Jun. 5, 2021].
- [82] University of Cyprus – Center for Intelligent Systems & Networks. Dynamic IEEE Test Systems. <http://www.kios.ucy.ac.cy/testsystems>. [Accessed: Jun. 5, 2021].
- [83] C. Coffrin, D. Gordon, and P. Scott. NESTA, The NICTA Energy System Test Case Archive, Nov. 2014. [Accessed: Jun. 5, 2021].
- [84] S. Babaeinejadsarookolae, A. Birchfield, R. D. Christie, C. Coffrin, C. DeMarco, R. Diao, M. Ferris, S. Fliscounakis, S. Greene, R. Huang, C. Jozs, R. Korab, B. Lesieutre, J. Maeght, D. K. Molzahn, T. J. Overbye, P. Panciatici, B. Park, J. Snodgrass, and R. Zimmerman. The Power Grid Library for Benchmarking AC Optimal Power Flow Algorithms, Aug. 2019. [Accessed: Jun. 5, 2021].
- [85] The IEEE PES Task Force on Benchmarks for Validation of Emerging Power System Algorithm. PGLib Optimal Power Flow Benchmarks. <https://github.com>. [Accessed: Jun. 5, 2021].
- [86] T. Heidel, K. Hedman, and P. McGrath. DGenerating Realistic Information for the Development of Distribution and Transmission Algorithms. <https://arpa.e.energy.gov>. [Accessed: Jun. 5, 2021].
- [87] Texas A&M University – Experiment Station. Electric Grid Test Cases. <https://electricgrids.engr.tamu.edu>. [Accessed: Jun. 5, 2021].
- [88] National Renewable Energy Laboratory. Reliability Test System of the Grid Modernization Lab Consortium (RTS-GMLC). <https://github.com>. [Accessed: Jun. 5, 2021].
- [89] Probability Methods Subcommittee of the Power System Engineering Committee. IEEE Reliability Test System. *IEEE Transactions on Power Apparatus and Systems*, 98(6):2047–2054, Nov. 1979.
- [90] C. Grigg, P. Wong, P. Albrecht, R. Allan, M. Bhavaraju, R. Billinton, Q. Chen, C. Fong, S. Haddad, S. Kuruganty, W. Li, R. Mukerji, D. Patton, N. Rau, D. Reppen, A. Schneider, M. Shahidepour, and C. Singh. The IEEE Reliability Test System-1996. A report prepared by the Reliability Test System Task Force of the Application of Probability Methods Subcommittee. *IEEE Transactions on Power Systems*, 14(3):1010–1020, Aug. 1999.

- [91] U.S. Department of Energy. Grid Modernization Initiative. <https://www.energy.gov>. [Accessed: Jun. 5, 2021].
- [92] U.S. Department of Energy. Grid Modernization Lab Consortium. <https://www.energy.gov>. [Accessed: Jun. 5, 2021].
- [93] E. Preston and C. Barrows. Evaluation Of Year 2020 IEEE RTS Generation Reliability Indices. In *Proceedings of the IEEE International Conference on Probabilistic Methods Applied to Power Systems*, Jun. 2018.
- [94] A. Haddadi, A. Rezaei-Zare, L. Gérin-Lajoie, R. Hassani, and J. Mahseredjian. A Modified IEEE 118-Bus Test Case for Geomagnetic Disturbance Studies – Part I: Model Data. *IEEE Transactions on Electromagnetic Compatibility*, 62(3):955–965, Jun. 2020.
- [95] EPRI. Geomagnetic Disturbance Vulnerability Assessment and Planning Guide. Technical report, Electric Power Research Institute, Dec. 2015.
- [96] J. L. Gilbert. Simplified Techniques for Treating the Ocean–Land Interface for Geomagnetically Induced Electric Fields. *IEEE Transactions on Electromagnetic Compatibility*, 57(4):688–692, Aug. 2015.
- [97] H. Karami, K. Sheshyekani, A. Rezaei-Zare, and J. Mahseredjian. Effect of Mixed Propagation Path on Electromagnetic Fields at Ground Surface Produced by Electrojet. *IEEE Transactions on Electromagnetic Compatibility*, 60(6):2019–2024, Dec. 2018.
- [98] R. J. Pirjola. Effects of Inaccuracies in Power Network Data on Calculations of Geomagnetically Induced Currents. In *Proceedings of the 2009 International Symposium on Electromagnetic Compatibility and Electromagnetic Ecology*, Jun. 2009.
- [99] J. L. Gilbert, W. A. Radasky, and E. B. Savage. A Technique for Calculating the Currents Induced by Geomagnetic Storms on Large High Voltage Power Grids. In *Proceedings of the 2012 IEEE International Symposium on Electromagnetic Compatibility*, Aug. 2012.
- [100] M. Kazerooni and T. J. Overbye. Incorporating the Geomagnetic Disturbance Models into the Existing Power System Test Cases. In *Proceedings of the 2017 IEEE Power and Energy Conference at Illinois*, Feb. 2017.
- [101] A. Haddadi, A. Rezaei-Zare, L. Gérin-Lajoie, R. Hassani, and J. Mahseredjian. A Modified IEEE 118-Bus Test Case for Geomagnetic Disturbance Studies – Part II: Simulation Results. *IEEE Transactions on Electromagnetic Compatibility*, 62(3):966–975, Jun. 2020.
- [102] R. Horton, D. Boteler, T. J. Overbye, R. Pirjola, and R. C. Dugan. A Test Case for the Calculation of Geomagnetically Induced Currents. *IEEE Transactions on Power Delivery*, 27(4):2368–2373, Oct. 2012.

- [103] A. Kelbert, C. C. Balch, A. Pulkkinen, G. D. Egbert, J. J. Love, E. J. Rigler, and I. Fujii. Methodology for Time-Domain Estimation of Storm Time Geoelectric Fields Using the 3-D Magnetotelluric Response Tensors. *Space Weather*, 15(7):1—21, Jun. 2017.
- [104] L. R. Bonner IV and A. Schultz. Rapid Prediction of Electric Fields Associated with Geomagnetically Induced Currents in the Presence of Three-Dimensional Ground Structure. *Space Weather*, 15(1):1—24, Jan. 2017.
- [105] NPCC. Electricity Generation for the Pacific Northwest. Technical report, Northwest Power and Conservation Council, Mar. 2011.
- [106] Northwest Power and Conservation Council. Wind Power. <https://www.nwcouncil.org>. [Accessed: Jun. 5, 2021].
- [107] NPCC. The State of the Columbia River Basin, Fiscal Year 2018. Technical report, Northwest Power and Conservation Council, Sep. 2018.
- [108] National Conference of State Legislature. State Renewable Portfolio Standards and Goals. <https://www.ncsl.org>, Dec. 2019. [Accessed: Jun. 5, 2021].
- [109] The U.S. Energy Information Administration. U.S. Overview. <https://www.eia.gov>. [Accessed: Jun. 5, 2021].
- [110] Montana Code Annotated 2019, Title 69, Chapter 3, Part 20. Montana Renewable Power Production and Rural Economic Development Act. <https://leg.mt.gov>. [Accessed: Jun. 5, 2021].
- [111] Washington State Department of Commerce. Energy Independence Act. <https://www.commerce.wa.gov>. [Accessed: Jun. 5, 2021].
- [112] Washington State Legislature. Senate Bill 5116 – 2019 Regular Session. <http://leg.wa.gov>. [Accessed: Jun. 5, 2021].
- [113] Oregon State Legislature. Senate Bill 1547 – 2016 Regular Session. <https://olis.leg.state.or.u>. [Accessed: Jun. 5, 2021].
- [114] Oregon State Department of Energy. Renewable Portfolio Standard. <https://www.oregon.gov>. [Accessed: Jun. 5, 2021].
- [115] Canada Energy Regulator. Canada’s Renewable Power Landscape 2017. <https://www.cer-rec.gc.ca>. [Accessed: Jun. 5, 2021].
- [116] Province of British Columbia. Clean Energy Act – SBC 2010, Chapter 22. <http://www.bclaws.ca>. [Accessed: Jun. 5, 2021].
- [117] NPCC. Renewable Portfolio Standard. Technical report, Northwest Power and Conservation Council, Jul. 2017. [Accessed: Jun. 5, 2021].
- [118] Northwest Power and Conservation Council. Existing and New/Proposed Power Plants. <https://www.nwcouncil.org>. [Accessed: Jun. 5, 2021].

- [119] Oregon State Department of Energy. 2018 Biennial Energy Report. <https://energyinfo.oregon.gov>. [Accessed: Jun. 5, 2021].
- [120] Washington State Department of Commerce. 2019 Biennial Energy Report. <http://www.commerce.wa.gov>, Dec. 2018. [Accessed: Jun. 5, 2021].
- [121] Canada Energy Regulator. Provincial and Territorial Energy Profiles — British Columbia. <https://https://www.cer-rec.gc.ca>. [Accessed: Jun. 5, 2021].
- [122] J. D. Glover, T. J. Overbye, and M. S. Sarma. *Power System Analysis and Design*. Boston MA: Cengage Learning, 6 edition, 2015.
- [123] A. Robb. Grid Inertia: Why it Matters in a Renewable World. <https://www.renewableenergyworld.com>, Oct. 2019. [Accessed: Jun. 5, 2021].
- [124] M. N. I. Sarkar, L. G. Meegahapola, and M. Dotta. Reactive Power Management in Renewable Rich Power Grids. *IEEE Access*, 6:41458–41489, May 2018.
- [125] D. Saleem and R. Majeed. Reactive Power Management in Distributed Generation. In *Proceedings of the 2019 IEEE International Conference on Engineering and Emerging Technologies*, Feb. 2019.
- [126] A. Ellis, R. Nelson, E. Von Engeln, R. Walling, J. MacDowell, L. Casey, E. Seymour, W. Peter, C. Barker, B. Kirby, and J. R. Williams. Reactive Power Performance Requirements for Wind and Solar Plants. In *Proceedings of the 2012 IEEE Power and Energy Society General Meeting*, Jul. 2012.
- [127] F. O. Igbinoia, G. Fandi, Z. Muller, J. Svec, and J. Tlustý. Cost implication and reactive power generating potential of the synchronous condenser. In *Proceedings of the 2016 IEEE International Conference on Intelligent Green Building and Smart Grid*, Jun. 2016.
- [128] BPA. BP-20 Rate Proceeding. Technical report, Bonneville Power Administration, Sep. 2019. [Accessed: Jun. 5, 2021].
- [129] A. Ellis, R. Nelson, E. Von Engeln, R. Walling, J. MacDowell, L. Casey, E. Seymour, W. Peter, C. Barker, B. Kirby, and J. R. Williams. Review of Existing Reactive Power Requirements for Variable Generation. In *Proceedings of the 2012 IEEE Power and Energy Society General Meeting*, Jul. 2012.
- [130] M. Hunyar and K. Veszpremi. Reactive Power Control of Wind Turbines. In *Proceedings of the 2014 IEEE International Power Electronics and Motion Control Conference and Exposition*, Sep. 2014.
- [131] A. G. Exposito, J. L. M. Ramos, and J. R. Santos. Slack Bus Selection to Minimize the System Power Imbalance in Load-Flow Studies. *IEEE Transactions on Power Systems*, 19(2):987–995, May 2004.
- [132] S. Tong and K. N. Miu. A Network-Based Distributed Slack Bus Model for DGs in Unbalanced Power Flow Studies. *IEEE Transactions on Power Systems*, 20(2):835–842, May 2005.

- [133] M. Okamura, Y. O-ura, S. Hayashi, K. Uemura, and F. Ishiguro. A New Power Flow Model and Solution Method. *IEEE Transactions on Power Apparatus and Systems*, 94(3):1042–1050, May 1975.
- [134] J. Meisel. System Incremental Cost Calculations Using the Participation Factor Load-Flow Formulation. *IEEE Transactions on Power Systems*, 8(1):357–363, Feb. 1993.
- [135] F. Miao and Z. Guo. A Method of Real-Time Load Flow Without Benchmark Buss. In *Proceedings of the 2018 IEEE TENCN*, Nov. 2008.
- [136] A. Zobian and M. D. Ilic. Unbundling of Transmission and Ancillary Services. *IEEE Transactions on Power Systems*, 12(2):539–558, May 1997.
- [137] K. Chayakulkheeree. Application of Distributed Slack Bus Power Flow to Competitive Environments. In *Proceedings of the 2007 Australasian Universities Power Engineering Conference*, Dec. 2007.
- [138] L. Reyes-Chamorro, W. Saab, R. Rudnik, A. M. Kettner, M. Paolone, and J. Y. Le Boudec. Slack Selection for Unintentional Islanding. In *Proceedings of the 2018 Power Systems Computation Conference*, Jun. 2018.
- [139] L. L. Freris and A. M. Sasson. Investigations on the Load-Flow Problem. *Proceedings of IEEE*, 114(12):1960, Dec. 1967.
- [140] MathWorks. MATLAB R2019b Documentation. <https://www.mathworks.com>, 2019. [Accessed: Jun. 5, 2021].
- [141] The U.S. Energy Information Administration. What is the Efficiency of Different Types of Power Plants? <https://www.eia.gov>. [Accessed: Jun. 5, 2021].
- [142] The U.S. Energy Information Administration. EIA Offers Two Approaches to Compare Renewable Electricity Generation with Other Sources. <https://www.eia.gov>. [Accessed: Jun. 5, 2021].
- [143] S. Kucuk. Intelligent Electrical Load Shedding in Heavily Loaded Industrial Establishments with a Case Study,. In *Proceedings of the 2018 IEEE International Conference on Electrical and Electronic Engineering*, May 2018.
- [144] G. H. Reddy, P. Chakrapani, A. K. Goswami, and N. B. D. Choudhury. Prioritization of Load Points in Distribution System Considering Multiple Load Types using Fuzzy Theory. In *Proceedings of the 2017 IEEE International Conference on Fuzzy Systems*, Jul. 2017.
- [145] X. Huang, Y. Yang, and G. A. Taylor. Service Restoration of Distribution Systems Under Distributed Generation Scenarios. *CSEE Journal of Power and Energy Systems*, 2(3):43–50, Sep. 2016.
- [146] A. Mondal, M. S. Illindala, A. S. Khalsa, D. A. Klapp, and J. H. Eto. Design and Operation of Smart Loads to Prevent Stalling in a Microgrid. *IEEE Transactions on Industry Applications*, 52(2):1184–1192, Mar. 2016.

- [147] M. AlOwaifeer and M. AlMuhaini. Load Priority Modeling for Smart Service Restoration. *Canadian Journal of Electrical and Computer Engineering*, 40(3):217–228, Jun. 2017.
- [148] R. Silva, A. Ferreira, A. Ferreira, and P. Leitao. Increasing Self-Sustainability in Micro Grids Using Load Prioritization and Forecasting Mechanisms. In *Proceedings of the 2015 IEEE Conference on Industrial Electronics and Applications*, Jun. 2015.
- [149] A. Safdarian, M. Fotuhi-Firuzabad, Y. Tohidi, and F. Aminifar. A Fast Load Shedding Algorithm to Relieve Transmission System Overloads. In *Proceedings of the 2011 IEEE International Conference on Environment and Electrical Engineering*, May 2011.
- [150] H. Gao, Y. Chen, Y. Xu, and C.-C. Liu. Resilience-Oriented Critical Load Restoration Using Microgrids in Distribution Systems. *IEEE Transactions on Smart Grid*, 7(6):2837–2848, Nov. 2016.
- [151] B. Moran. Microgrid Load Management and Control Strategies. In *Proceedings of the 2016 IEEE/PES Transmission and Distribution Conference and Exposition*, May 2016.
- [152] A. J. Wood, B. F. Wollenberg, and G. B. Sheble. *Power Generation, Operation, and Control*. New York NY: John Wiley & Sons, Inc., 3 edition, 2013.
- [153] R. C. Johnson, H. H. Happ, and W. J. Wright. Large Scale Hydro-Thermal Unit Commitment-Method and Result. *IEEE Transactions on Power Apparatus and Systems*, 90(3):1373–1384, May 1971.
- [154] G. B. Sheble and G. N. Fahd. Unit Commitment Literature Synopsis. *IEEE Transactions on Power Systems*, 9(1):128–135, Feb. 1994.
- [155] A. I. Cohen and V. R. Sherkat. Optimization-Based Methods for Operations Scheduling. *Proceedings of the IEEE*, 75(12):1574–1591, Dec. 1987.
- [156] S. Sen and D. P. Kothari. Optimal Thermal Generating Unit Commitment. *International Journal of Electrical Power & Energy Systems*, 20(7):443–451, Oct. 1998.
- [157] K. R. Voorspools and W. D’haeseleer. Long-term Unit Commitment Optimisation for Large Power Systemss. *Applied Energy*, 76(1):157–167, Sep. 2003.
- [158] N. P. Padhy. Unit Commitment - A Bibliographical Survey. *IEEE Transactions on Power Systems*, 19(2):1196–1205, May 2004.
- [159] T. Logenthiran and D. Srinivasan. Formulation of Unit Commitment Problems and Analysis of Available Methodologies Used for Solving the Problems. In *Proceedings of the 2010 IEEE International Conference on Sustainable Energy Technologies*, Dec. 2010.
- [160] M. Tahanan, W. van Ackooij, A. Frangioni, and F. Lacalandra. Large-Scale Unit Commitment Under Uncertainty. *4OR-Q*, 13(2):115–171, Jun. 2015.

- [161] IBM Corp. CPLEX User's Manual. <https://www.ibm.com>, 2019. [Accessed: Jun. 5, 2021].
- [162] Gurobi Optimization LLC. Gurobi Optimizer Reference Manual. <http://www.gurobi.com>, 2020. [Accessed: Jun. 5, 2021].
- [163] T. Senjyu, K. Shimabukuro, K. Uezato, and T. Funabashi. A Fast Technique for Unit Commitment Problem by Extended Priority List. *IEEE Transactions on Power Systems*, 18(2):882–888, May 2003.
- [164] Y. Tingfang and T. O. Ting. Methodological Priority List for Unit Commitment Problem. In *Proceedings of the 2008 IEEE International Conference on Computer Science and Software Engineering*, Dec. 2008.
- [165] S. Y. I. Abujarad, M. W. Mustafa, and J. J. Jamian. Unit Commitment Problem Solution in the Presence of Solar and Wind Power Integration by an Improved Priority List Method. In *Proceedings of the 2016 IEEE International Conference on Intelligent and Advanced Systems*, Aug. 2016.
- [166] M. Govardhan and R. Roy. An Application of Differential Evolution Technique on Unit Commitment Problem Using Priority List Approach. In *Proceedings of the 2012 IEEE International Conference on Power and Energy*, Dec. 2012.
- [167] D. Srinivasan and J. Chazelas. A Priority List-Based Evolutionary Algorithm to Solve Large Scale Unit Commitment Problem. In *Proceedings of the 2004 IEEE International Conference on Power System Technology*, Nov. 2004.
- [168] V. M. Raj and S. Chanana. Analysis of Unit Commitment Problem Through Lagrange Relaxation and Priority Listing Method. In *Proceedings of the 2014 IEEE Power India International Conference*, Dec. 2014.
- [169] D. P. Kadam, S. S. Wagh, and P. M. Patil. Thermal Unit Commitment Problem by Using Genetic Algorithm, Fuzzy Logic and Priority List Method. In *Proceedings of the 2007 IEEE International Conference on Computational Intelligence and Multimedia Applications*, Dec. 2007.
- [170] M. S. Alam, B. D. H. Kiran, and M. S. Kumari. Priority List and Particle Swarm Optimization Based Unit Commitment of Thermal Units Including Renewable Uncertainties. In *Proceedings of the 2016 IEEE International Conference on Power System Technology*, Sep. 2016.
- [171] W. Ge. Ramp Rate Constrained Unit Commitment by Improved Priority List and Enhanced Particle Swarm Optimization. In *Proceedings of the 2010 IEEE International Conference on Computational Intelligence and Software Engineering*, Dec. 2010.
- [172] A. B. M. Sarjiya and A. Sudiarso. Optimal Solution of Reliability Constrained Unit Commitment Using Hybrid Genetic Algorithm-Priority List Method. In *Proceedings of the 2014 IEEE International Conference on Information Technology and Electrical Engineering*, Oct. 2014.

- [173] X. Ke, D. Wu, N. Lu, and M. Kintner-Meyer. A Modified Priority List-Based MILP Method for Solving Large-Scale Unit Commitment Problems. In *Proceedings of the 2015 IEEE Power & Energy Society General Meeting*, Jul. 2015.
- [174] A. M. Elsayed, A. M. Maklad, and S. M. Farrag. A New Priority List Unit Commitment Method for Large-Scale Power Systems. In *Proceedings of the 2017 IEEE Nineteenth International Middle East Power Systems Conference*, Dec. 2017.
- [175] E. R. Bixby, M. Fenelon, Z. Gu, E. Rothberg, and R. Wunderling. *MIP: Theory and Practice – Closing the Gap*. Boston, MA: Springer, 1999.
- [176] T. Li and M. Shahidehpour. Price-Based Unit Commitment: A Case of Lagrangian Relaxation Versus Mixed Integer Programming. *IEEE Transactions on Power Systems*, 20(4):2015–2025, Nov. 2005.
- [177] MathWorks. MATLAB Examples – Script 9: Unit Commitment. <https://www.mathworks.com>. [Accessed: Jun. 5, 2021].
- [178] J. O. Lee, Y. S. Kim, E. S. Kim, and S. I. Moon. Generation Adjustment Method Based on Bus-Dependent Participation Factor. *IEEE Transactions on Power Systems*, 33(2):1959–1969, Mar. 2018.
- [179] R. A. Ramos, A. G. M. Moraco, T. C. C. Fernandes, and R. V. de Oliveira. Application of Extended Participation Factors to Detect Voltage Fluctuations in Distributed Generation Systems. In *Proceedings of the 2011 IEEE Power and Energy Society General Meeting*, Jul. 2011.
- [180] D. Bedoya, M. F. Bedrinana, C. A. Castro, and L. C. Pereira da Silva. Power System Critical Areas by Using Sensitivities and Participation Factors for Online Applications. In *Proceedings of the 2008 IEEE PES Transmission and Distribution Conference and Exposition*, Aug. 2008.
- [181] L. C. Pereira da Silva, Y. Wang, V. F. da Costa, and W. Xu. Assessment of Generator Impact on System Power Transfer Capability Using Modal Participation Factors. *IEEE TXplore*, 149(5):564–570, Oct. 2002.
- [182] L. C. Pereira da Silva, Y. Wang, V. F. da Costa, and W. Xu. Preliminary Results on Improving the Modal Analysis Technique for Voltage Stability Assessment. In *Proceedings of the 2000 IEEE Power Engineering Society Summer Meeting*, Jul. 2000.
- [183] B. Gao, G. K. Morison, and P. Kundur. Voltage Stability Evaluation Using Modal Analysis. *IEEE Transactions on Power Systems*, 7(4):1529–1542, Nov. 1992.
- [184] X. F. Wang, Y. Song, and M. Irving. *Modern Power Systems Analysis*. Springer Science Business Media LLC, 2008.
- [185] A. B. Birchfield, T. Xu, and T. J. Overbye. Power Flow Convergence and Reactive Power Planning in the Creation of Large Synthetic Grids. *IEEE Transactions on Power Systems*, 33(6):6667–6674, Nov. 2018.

- [186] M. B. Cain, R. P. O'Neill, and A. Castillo. History of Optimal Power Flow and Formulations. Technical report, Federal Energy Regulatory Commission, Dec. 2012.
- [187] T. Faulwasser, A. Engelmann, T. Muhlfordt, and V. Hagenmeyer. Optimal Power Flow: An Introduction to Predictive, Distributed and Stochastic Control Challenges, Nov. 2018. [Accessed: Jun. 5, 2021].
- [188] C. Coffrin, H. L. Hijazi, and P. Van Hentenryck. The QC Relaxation: A Theoretical and Computational Study on Optimal Power Flow, Jul. 2015. [Accessed: Jun. 5, 2021].
- [189] National Centers for Environmental Information. Remembering the Great Halloween Solar Storm. <https://www.ncei.noaa.gov>, Oct. 2017. [Accessed: Jun. 5, 2021].

APPENDICES

Appendix

The contents of *Appendix A* and *Appendix B* are both electronically accessible at:

<https://github.com/adammate/PHD-DISSERTATION>